Mechanistic Studies of the Vapor-Phase Beckmann Rearrangement on Solid Catalysts by *In Situ* Solid-State NMR Spectroscopy

Von der Fakultät Chemie der Universität Stuttgart
zur Erlangung der Würde eines
Doktors der Naturwissenschaften (Dr. rer. nat.)
genehmigte Abhandlung

vorgelegt von

Venkata Ramana Reddy Marthala
aus Peddakottala-Andhra Pradesh (Indien)

Hauptberichter: Prof. Dr. Michael Hunger
Mitberichter: Prof. Dr. Klaus Müller

Tag der mündlichen Prüfung: 28.05.2009

Institut für Technische Chemie
der Universität Stuttgart
2009

Dedicated to my parents

Acknowledgement

This work was performed at the Institute of Chemical Technology, University of Stuttgart, Germany. It would have been rather difficult to accomplish this thesis without the support and cooperation from the following people.

First and foremost, I would like to express my deepest gratitude to Prof. Dr. Michael Hunger for giving me the research topic to pursue my PhD, for his excellent supervision, constant encouragement, and fruitful discussions.

Special thanks to Prof. Dr.-Ing. Jens Weitkamp, Head of our Institute, for his support to access the facility at our Institute and for giving me the opportunity to attend International workshops (INSIDE PORes) and South German Catalysis Course in Ulm.

I am very grateful to Prof. Dr. Klaus Müller and Prof. Dr. Thomas Schleid for their readiness to be my co-examiners.

I would like to convey thanks to Prof. Dr. Wei Wang for his guidance and fruitful discussions in the initial months of my PhD work. I am also very thankful to Dipl.-Chem. Sandra Rabl for her research contribution as a Diploma (Diplomarbeit) student.

I would like to express my special thanks to all colleagues and employers of our Institute: Mrs. U. Albrecht, Mrs. B. Gehring, Mrs. H. Fingerle, Prof. Dr. R. Gläser, Dr. Y. Traa, Dr. T. Donauer, Dr. M. Schmidt, Dr. S. Laha, Dr. S. Dapurkar, Dr. Y.S. Ooi, Dr. B. Thomas, Dr. J. Jiao, Dr. J. Huang, Dr. Y. Jiang, Mr. S.A.S. Rezai (particularly for his friendship and discussion on many topics), Dipl.-Chem. J. Frey, Dipl.-Chem. A. Bressel, Mr. I. Nägele, Mr. A. Stieber, Mr. M. Scheibe, Mr. W. Röhm, Dipl.-Chem. T. Holl, Dipl.-Chem. F. Salzbauer, Dipl.-Chem. A. Haas, Dr. S. Altwasser, Dr. P. De Cola, Dipl.-Ing. F. Demir, Dr. D. Pufky, Dipl.-Chem. T. Schreiber, Dipl.-Chem. D. Singer, for their help and cooperation in any way.

I would also like to acknowledge Deutsche Forschungsgemeinschaft (DFG) for financial support.

Finally, I would like to thank my dearest wife Sujatha and all my family relatives for their continuous encouragement and support through out my PhD.

Abbreviations and Symbols i
1 Zusammenfassung 1
2 Abstract 6
3 Introduction and state-of-the-art 11
3.1 Introduction to zeolites 11
3.2 Introduction to mesoporous materials 13
3.3 Acid sites in zeolites and mesoporous materials 15
3.4 Methods for the production of ε-caprolactam 17
3.5 Production of ε-caprolactam by heterogeneous catalysis 20
3.6 Vapor-phase Beckmann rearrangement of cyclohexanone oxime on solid catalysts (state-of-the-art) 22
3.6.1 Nature and location of active sites of solid catalysts in the vapor-phase Beckmann rearrangement reaction 22
3.6.2 Reaction mechanisms of the Beckmann rearrangement reaction 25
3.6.3 Influence of additives in the vapor-phase Beckmann rearrangement on solid catalysts 28
4 Experimental section 32
4.1 Preparation of materials 32
4.1.1 Synthesis of silicalite-1 32
4.1.2 Synthesis of H-[B]ZSM-5 32
4.1.3 Synthesis of H-ZSM-5 32
4.1.4 Synthesis of siliceous SBA-15 material 33
4.1.5 Synthesis of [Al]SBA-15 material 34
4.1.6 Synthesis of H-[Si]MCM-41 material 34
4.1.7 Synthesis of H-[Al]MCM-41 material 34
4.1.8 Dehydration 35
4.1.9 Preparation of H/D-exchanged catalysts 35
4.1.10 Preparation of H/D-exchanged catalyst/oxime mixtures 35
4.1.11 Organic synthesis of cyclohexanone oxime-D_{11} 36
4.1.12 Preparation of cyclohexanone oxime-D_{11}/catalyst mixtures 36
4.1.13 Organic synthesis of ^{15}N-cyclohexanone oxime 36

4.1.14 Preparation of ^{15}N-cyclohexanone oxime/catalyst mixtures 37
4.1.15 Loading of ^{13}C-methanol 37
4.2 Physicochemical characterization techniques 38
4.2.1 Powder X-ray diffraction (XRD) 38
4.2.2 Elemental analysis and BET surface measurements 41
4.2.3 Scanning electron microscopy (SEM) 42
4.3 Introduction to solid-state NMR spectroscopy 44
4.3.1 Principles of solid-state NMR spectroscopy 44
4.3.2 Dipolar interactions 44
4.3.3 Chemical shift anisotropy 45
4.3.4 Quadrupolar interaction 46
4.4 High-resolution solid-state NMR techniques 46
4.4.1 Magic Angle Spinning 47
4.4.2 Cross polarization (CP) 48
4.5 Characterization by solid-state MAS NMR spectroscopy 49
4.5.1 ^{1}H MAS NMR measurements 49
4.5.2 ^{2}H MAS NMR measurements 49
4.5.3 *In situ* and *ex situ* solid-state ^{11}B MAS NMR measurements 49
4.5.4 *In situ* solid-state ^{15}N NMR measurements 51
4.5.5 *In situ* ^{13}C CP/MAS NMR measurements 51
4.5.6 ^{29}Si HPDEC MAS NMR measurements 52
5 Characterization of zeolite H-[B]ZSM-5 upon the adsorption of probe molecules studied by ^{11}B and ^{1}H MAS NMR spectroscopy 53
5.1 Introduction 53
5.2 *In situ* MAS NMR investigations of dehydrated zeolite H-[B]ZSM-5 upon adsorption of pyridine 55
5.3 *In situ* MAS NMR investigations of dehydrated zeolite H-[B]ZSM-5 upon adsorption of ammonia 58
5.4 MAS NMR investigations of dehydrated zeolite H-[B]ZSM-5 upon adsorption of dimethyl sulfoxide, acetamide, tetrahydrothiophene, and acetone 60

5.5 Effect of probe molecules with different proton affinities on the acid sites and framework boron atoms in dehydrated zeolite H-[B]ZSM-5 62
5.6 Conclusions..... 65
6 Study of surface sites and their interactions with reactant molecules by solid-state ^{2}H and ^{1}H NMR spectroscopy..... 66
6.1 Introduction..... 66
6.2 Characterization of catalysts by ^{1}H MAS NMR spectroscopy 67
6.3 Location of acid sites on H/D-ZSM-5, H/D-[Al]SBA-15, and H/D-SBA-15 catalysts studied by ^{2}H MAS NMR spectroscopy 68
6.4 Vapor-phase Beckmann rearrangement of cyclohexanone oxime-D_{11} on silicalite-1 and H-ZSM-5 studied by *in situ* ^{1}H MAS NMR spectroscopy..... 74
6.5. Conclusions..... 79
7 Vapor-phase Beckmann rearrangement of ^{15}N-cyclohexanone oxime on MFI-type zeolites and mesoporous catalysts studied by *in situ* ^{15}N MAS NMR spectroscopy 81
7.1 Introduction..... 81
7.2 Characterization of ^{15}N-cyclohexanone oxime by MAS NMR spectroscopy .. 82
7.3 Vapor-phase Beckmann rearrangement of cyclohexanone oxime on weakly acidic silicalite-1 83
7.4 Vapor-phase Beckmann rearrangement of ^{15}N-cyclohexanone oxime on mesoporous siliceous SBA-15 and MCM-41 materials..... 86
7.5 Vapor-phase Beckmann rearrangement of ^{15}N-cyclohexanone oxime on strongly acidic H-ZSM-5 zeolite 89
7.6 Vapor-phase Beckmann rearrangement of ^{15}N-cyclohexanone oxime on aluminum-containing mesoporous SBA-15 and MCM-41 materials 91
7.7 Vapor-phase Beckmann rearrangement of ^{15}N-cyclohexanone oxime on mediumly acidic H-[B]ZSM-5 zeolite 94
7.8 Establishing the reaction mechanism of Vapor-phase Beckmann rearrangement on solid catalysts..... 97
7.9 Conclusions..... 102

8 Influence of ^{13}C-methanol as an additive in the vapor-phase Beckmann rearrangement of ^{15}N-cyclohexanone oxime on MFI-type zeolites and mesoporous SBA-15 materials studied by *in situ* ^{15}N and ^{13}C MAS NMR spectroscopy 104

8.1 Introduction 104

8.2 Influence of ^{13}C-methanol as an additive in the vapor-phase Beckmann rearrangement of ^{15}N-cyclohexanone oxime on silicalite-1 105

8.3 Influence of ^{13}C-methanol as an additive in the vapor-phase Beckmann rearrangement of ^{15}N-cyclohexanone oxime on H-ZSM-5 108

8.4 Influence of ^{13}C-methanol as anadditive in the vapor-phase Beckmann rearrangement of ^{15}N-cyclohexanone oxime on mesoporous siliceous SBA-15 and [Al]SBA-15 catalysts 111

8.5 Conclusions 114

References 115

Publications

Curriculum vitae

Abbreviations and Symbols

Abbreviations

BET	S. Brunauer, P.H. Emmet, E. Teller
BP	British Petroleum
CP	Cross Polarization
CSA	Chemical Shift Anisotropy
CTMA Br	Cetyltrimethylammonium Bromide
DEE	Diethyl ether
DME	Dimethyl ether
DMSO	Dimethyl Sulfoxide
EFG	Electric Field Gradient
FID	Free Induction Decay
FT IR	Fourier Transformed Infrared Spectroscopy
HPDEC	High Power Decoupling
ICP-OES	Inductively Coupled Plasma Optical Emission Spectrometry
IUPAC	International Union of Pure and Applied Chemstry
IZA	International Zeolite Association
MAS	Magic Angle Spinning
MCM	Mobil Composition of Matter
NMR	Nuclear Magnetic Resonance
rf	Radio Frequency
SEM	Scanning Electron Microscopy
SBA	Santa Barbara Amorphous Silica
TPD	Temperature-Programmed Desorption
UCC	Union Carbide Corporation
UV/Vis	Ultraviolet-visible Spectroscopy
XAFS	X-ray Absorption Fine-Structure Spectroscopy
XRD	X-ray Diffraction
ZSM	Zeolite Socony Mobil

Symbols

A	$m^2\ g^{-1}$	Specific Surface Area
$\boldsymbol{B}$	T	Magnetic Induction
c	mol^{-1}	Concentration
C_{QCC}	MHz	Quadrupole Coupling Constant
d	m	Diameter
e	C	Charge (1.602176×10^{-19} C)
eQ	$C\ m^{-2}$	Electric Quadrupole Moment
eq	$C\ V\ m^{-2}$	z-component of Electric Field Gradient
E	J	Energy
h	J-s	Planck Constant (6.62×10^{-34} J-s)
$\hat{H}$	-	Hamiltonian Operator
$\hat{I}$	-	Angular Momentum Operator
I,S	-	Nuclear Spins
$\boldsymbol{M}$	$A\ m^{-1}$	Magnetization
m	-	Magnetic Quantum Number
n_H	$mmol\ g^{-1}$	Concentration of Protons
n_{Si} / n_{Al}	-	Silicon/Aluminum (atom ratio)
PA	$kJ\ mol^{-1}$	Proton Affinity
q	$V\ m^{-2}$	Field Gradient
r	m	Internuclear Vector
t	s, min, h	Time
V	V	Electric Potential
α	-	Adiabacity Parameter
γ	$s^{-1}\ A^{-1}\ m$	Magnetogyric Ratio
Δ	-	Difference
δ	ppm	Chemical Shift
η	-	Asymmetry Parameter
μ	$J\ m\ A^{-1}$	Magnetic Momentum
v	Hz or s^{-1}	Frequency

σ	-	Chemical Shielding Tensor
θ	°	Angle
τ_{CP}	s	Contact Time
ω	s^{-1}	Angular Frequency

1 Zusammenfassung

ε-Caprolactam, das Hauptprodukt der Beckmann-Umlagerung von Cyclohexanonoxim, ist ein Zwischenprodukt in der Herstellung von Nylon-6. Zurzeit wird *ε*-Caprolactam industriell durch die Beckmann-Umlagerung von Cyclohexanonoxim unter Verwendung von Schwefelsäure oder Oleum als homogener Katalysator hergestellt. Dieser Prozess hat zwei grundsätzliche Nachteile: (i) Die Produktion des unwirtschaftlichen Nebenprodukts Ammoniumsulfat und (ii) das umweltgefährdende, korrosive Reaktionsmedium. In den letzten Jahren ist die Nachfrage nach umweltfreundlichen Herstellungsverfahren aufgrund strengerer Umweltgesetze gestiegen. Daher hat die Beckmann-Umlagerung von Cyclohexanonoxim in der Gasphase an Festkörperkatalysatoren ein stark zunehmendes Interesse erfahren, da dies ein umweltfreundlicher, ökonomischer und energetisch bevorzugter Prozess ist. Im Jahr 2003 wurde zum ersten Mal die katalytische Beckmann-Umlagerung von Cyclohexanonoxim in der Gasphase an *High-silica*-Zeolithen des MFI-Typs industriell von Sumitomo Chemical Company Ltd. in Japan realisiert. Trotz der Kommerzialisierung dieses Prozesses sind wichtige Aspekte unklar und werden kontrovers diskutiert. Die hauptsächlichen Fragen sind: (i) Die Natur und Lokalisierung der aktiven Zentren des Katalysators, (ii) die Chemie der Beckmann-Umlagerung von Cyclohexanonoxim in der Gasphase (Adsorptions- und Desorptionsverhalten der Reaktanten, Intermediate, Produkte und Nebenprodukte der Reaktion), (iii) die Ursache der Deaktivierung des Katalysators und (iv) der Einfluss von Additiven während der Beckmann-Umlagerung in der Gasphase.

Die vorliegende Arbeit fokussiert hauptsächlich auf die oben erwähnten Fragestellungen. Zum besseren Verständnis der Reaktion wurden mechanistische Aspekte der Beckmann-Umlagerung in der Gasphase an Festkörperkatalysatoren mittels *In-situ*-MAS-NMR-Spektroskopie untersucht. Hierzu wurden verschiedene Festkörperkatalysatoren, wie Zeolithe des MFI-Typs (Silicalit-1, H-[B]ZSM-5 und H-ZSM-5) und mesoporöse Materialien (SBA-15, [Al]SBA-15, H-[Si]MCM-41, und H-[Al]MCM-41) nach in der Literatur beschriebenen Vorschriften präpariert. Die Katalysatoren wurden mittels Pulverdiffraktometrie, ICP-OES, N_2-

Adsorptionsmessungen (BET Oberfläche), REM und Festkörper ^{1}H-, ^{2}H- und ^{29}Si-MAS-NMR-Spektroskopie charakterisiert.

Es wurde berichtet, dass borhaltige ZSM-5-Zeolithe (H-[B]ZSM-5) hoch selektiv in der Beckmann-Umlagerung von Cyclohexanonoxim in der Gasphase sind. Jedoch wurde in der Literatur nichts über die Natur der aktiven Zentren in diesem Zeolith und dem Einfluss der Reaktanden auf die Bor-Atome im Gerüst berichtet. In der vorliegenden Arbeit wurden die Natur der aktiven Zentren und der Koordinationswechsel von Bor-Atomen im Gerüst, hervorgerufen durch die Adsorption des Reaktanden an dem H-[B]ZSM-5-Zeolith (n_{Si} / n_B = 38) durch simultane ^{1}H- und ^{11}B-MAS-NMR-Spektroskopie untersucht. Für diesen Zweck wurden einige Sondenmoleküle, gekennzeichnet durch verschiedene Protonenaffinitäten (*PA*), am Zeolith adsorbiert. Die Sondenmoleküle Pyridin, Ammoniak und Aceton wurden mit Hilfe einer *In-situ-Flow*-Technik auf dem H-[B]ZSM-5-Zeolith adsorbiert. Das ^{1}H-MAS-NMR-Spektrum des dehydratisierten H-[B]ZSM-5-Zeoliths enthält Signale bei 1,9, 2,5 und 3,2 ppm. Durch Adsorption von Pyridin (*PA* = 930 kJ mol^{-1}) und Ammoniak (*PA* = 854 kJ mol^{-1}) am H-[B]ZSM-5-Zeolith wurde vorwiegend das Signal bei 2,5 ppm beeinflusst. Daher wurde dieses Signal den Brønsted-sauren SiOH[B]-Gruppen in Nachbarschaft von Bor-Atomen im Gerüst zugeordnet. Des Weiteren wurde durch ^{11}B-MAS-NMR-Spektroskopie der Koordinationswechsel von B$^{[3]}$-Spezies in B$^{[4]}$-Spezies im Gerüst des H-[B]ZSM-5-Zeoliths untersucht. Es wurde gefunden, dass eine Protonenaffinität von *PA* $\geq$ 854 kJ mol^{-1} für die Sondenmoleküle nötig ist, um den Koordinationswechsel der B$^{[3]}$-Spezies in B$^{[4]}$-Spezies zu bewirken. Dieser Koordinationswechsel der Bor-Atome im Gerüst war begleitet von einer Protonierung der Sondenmoleküle mit *PA* $\geq$ 854 kJ mol^{-1}. Als ein Resultat der Protonierung wurde eine Reduzierung der ^{11}B-Quadrupol-kopplungskonstante von C_{QCC} = 2,7 ± 0,1 MHz (B$^{[3]}$) auf $C_{QCC} \leq$ 0,85 MHz (B$^{[4]}$) festgestellt. Die Protonenaffinität von *PA* $\geq$ 854 kJ mol^{-1} ist geringfügig höher (*ca.* 30 kJ mol^{-1}) als der *PA*-Wert von 821 kJ mol^{-1}, der aus der Literatur für die Protonierung von Sondenmoleküle aluminiumhaltiger Zeolithe bekannt ist. Dies wird durch die geringere Säurestärke der SiOH[B]-Gruppen des H-[B]ZSM-5-Zeoliths im Vergleich mit den Brücken-OH-Gruppen (SiOH[Al]) in aluminiumhaltigen Zeolithen unterstützt.

In der vorliegenden Arbeit wurde erstmalig die *High-speed*-^{2}H-MAS-NMR-Spektroskopie bei einer Rotordrehzahl von 25 kHz verwendet. Dies diente dazu, die Oberflächenzentren von deuterierten Katalysatoren und ihre Wechselwirkung mit nicht deuterierten Reaktanden zu untersuchen. Deuterierte Katalysatoren, wie H/D-ZSM-5, H/D-[Al]SBA-15 und H/D-SBA-15, wurden erfolgreich durch einen H/D-Austausch der OH-Gruppen mit D_2O-Dampf hergestellt. Mittels ^{2}H-MAS-NMR-Spektroskopie konnte eine geeignete spektrale Auflösung der Signale der SiOH-Gruppen (*ca.* 1,8 ppm) und Brücken-OH-Gruppen (*ca.* 5,7 ppm) im ^{2}H-MAS-NMR-Spektrum des H/D-ZSM-5-Zeoliths erreicht werden. Zwei Reaktandenmoleküle, gekennzeichnet durch verschiedene molekulare Durchmesser (Cyclohexanonoxim: *ca.* 0,65 nm, Cyclododecanonoxim: *ca.* 0,9 nm), wurden an H/D-ausgetauschten Katalysatoren bei Raumtemperatur adsorbiert. Nach Adsorption der nicht deuterierten Reaktanden wurde in den ^{2}H-MAS-NMR-Spektren der H/D-ausgetauschten Katalysatoren (H/D-ZSM-5, H/D-[Al]SBA-15 und H/D-SBA-15) intensive Signale bei *ca.* 12 ppm beobachtet. Diese Ergebnisse zeigen, dass alle Arten der Oberflächenzentren des H/D-ZSM-5-Zeoliths (Silanolgruppen, Silanolnester und Brønsted-Säurezentren), die auf der äußeren Oberfläche, neben den Porenöffnungen oder im Inneren der Poren lokalisiert sind, für Cyclohexanonoxim zugänglich sind.

Die *In-situ*-^{1}H- und ^{15}N-MAS-NMR-Spektroskopie wurde zur Untersuchung der Chemie der Beckmann-Umlagerung von Cyclohexanonoxim in der Gasphase an Zeolithen des MFI-Typs und mesoporösen Materialien, wie MCM-41 und SBA-15, verwendet. Die Ergebnisse der vorliegenden Arbeit helfen, die Adsorption, die Desorption und das Reaktionsverhalten der Reaktanden, Intermediate, Produkte und Nebenprodukte, die während der Reaktion gebildet werden, zu verstehen. Zunächst wurde die *In-situ*-^{1}H-MAS-NMR-Spektroskopie dazu verwendet, den schrittweisen Umsatz von Cyclohexanonoxim-D_{11} an Silicalit-1- (n_{Si} / n_{Al} = 1700) und H-ZSM-5-Katalysatoren (n_{Si} / n_{Al} = 14) zu untersuchen. Cyclohexanonoxim-D_{11} wurde erfolgreich mit einem H/D-Austauschgrad von *ca.* 83% hergestellt. Die Beckmann-Umlagerung von Cyclohexanonoxim-D_{11} in der Gasphase wurde an nicht deuterierten Silicalit-1- und H-ZSM-5-Katalysatoren bei verschiedenen Reaktionstemperaturen durchgeführt. Die ^{1}H-MAS-NMR-Spektroskopie lieferte den Beweis, dass sich während der Reaktion

Intermediate, wie H-gebundenes Cyclohexanonoxim und N-protoniertes Cyclohexanonoxim an SiOH- und Brücken-OH-Gruppen bilden. Durch die ^{1}H-MAS-NMR-Untersuchung der Beckmann-Umlagerung von Cyclohexanonoxim-D_{11} an schwach saurem Silicalit-1 in der Gasphase konnte die Bildung von ε-Caprolactam, Hydroxylamin und 5-Cyano-1-penten als Produkte und Nebenprodukte der Reaktion beobachtet werden. Im Gegensatz hierzu wurde an stark sauren H-ZSM-5-Katalysatoren das O-protonierte ε-Caprolactam aufgrund der starken Adsorption dieser Spezies an den Brücken-OH-Gruppen identifiziert. Des Weiteren führte die Umsetzung des O-protonierten ε-Caprolactams an den Brücken-OH-Gruppen des H-ZSM-5-Zeoliths zur Bildung von N-protoniertem ε-Caprolactam und nicht- oder N-protonierten Spezies der ε-Aminocapronsäure.

Der beobachtbare Bereich der chemischen Verschiebung der ^{15}N-MAS-NMR-Signale ist größer als der Verschiebungsbereich der ^{1}H-MAS-NMR-Signale gleicher Spezies. Daher ist die *In-situ*-^{15}N-MAS-NMR-Spektroskopie eine interessante Technik zur Untersuchung des Reaktionsmechanismus. Weiterhin ist die Interpretation der ^{15}N-MAS-NMR-Signale weniger kompliziert als die der ^{1}H-MAS-NMR-Signale. Daher wurde in der vorliegenden Arbeit die Chemie der Beckmann-Umlagerung in der Gasphase an Festkörperkatalysatoren auch mit Hilfe der ^{15}N-MAS-NMR-Spektroskopie untersucht. Die Ergebnisse dieser ^{15}N-MAS-NMR-Untersuchungen deuten darauf hin, dass sowohl die SiOH- als auch die Brønsted-Säurezentren an dieser Reaktion beteiligt sind. ^{15}N-Cyclohexanonoxim wechselwirkt mit SiOH-Gruppen durch Wasserstoffbrückenbindungen. Dies wird durch ^{15}N-MAS-NMR-Signale im Bereich von -30 bis -46 ppm belegt. Hingegen ist die Wechselwirkung von N-protoniertem Cyclohexanonoxim mit den Brønsted-Säurezentren viel stärker. In diesem Fall treten ^{15}N-MAS-NMR-Signale im Bereich von -145 bis -160 ppm auf. Nebenprodukte, wie Hydroxylamine und Amine, wurden auch an silicatischen Katalysatoren beobachtet. Die hiermit verbundenen ^{15}N-MAS-NMR-Signale dieser Spezies wurden im Bereich von -269 bis -280 und -375 bis -387 ppm beobachtet. Zusätzlich wurde die O-Protonierung des Hauptprodukts ε-Caprolactam an silicatischen und Brønsted-sauren Katalysatoren gefunden, wie das ^{15}N-MAS-NMR-Signal bei -237 ppm belegt. Jedoch hängt bei silicatischen Katalysatoren die O-Protonierung des ε-Caprolactams von der Anzahl saurer

Q^3-Silanolgruppen ($Si(OSi)_3OH$), wie durch ^{29}Si-MAS-NMR-Spektroskopie gezeigt, ab. Die Umsetzung von O-protoniertem ε-Caprolactam in N-protoniertes ε-Caprolactam und in nicht- oder N-protonierte ε-Aminocapronsäure wurde ausschließlich an Brønsted-sauren Katalysatoren beobachtet.

Methanol ist ein Additiv im Reaktionssystem, das während der Beckmann-Umlagerung von Cyclohexanonoxim in der Gasphase die Selektivität in Richtung des gewünschten Produkts ε-Caprolactam verschiebt. In der vorliegenden Arbeit wurde der Einfluss von Methanol auf die gebildeten Spezies und die Umsetzung des Additivs Methanol während der Beckmann-Umlagerung in der Gasphase mit Hilfe der *In-situ*-^{15}N- und ^{13}C-MAS-NMR-Spektroskopie untersucht. An Silicalit-1 und H-ZSM-5-Zeolithen wurden Kohlenwasserstoffe mit steigenden Reaktionstemperaturen gebildet und abgeschieden (^{13}C-MAS-NMR-Signale bei 25 bis 30 ppm). Außerdem wurde die Bildung von Isopropylamin (^{13}C-MAS-NMR-Signal bei 42 ppm) an Silicalit-1 als Ergebnis der Reaktion von Isobutan (^{13}C-MAS-NMR-Signal bei 25 ppm) mit Hydroxylamin, das ein Nebenprodukt der Beckmann-Umlagerung ist, beobachtet. An stark saurem H-ZSM-5-Zeolith dehydratisiert Methanol (^{13}C-MAS-NMR-Signal bei *ca.* 50 ppm) zu Dimethylether und Wasser. Dieses Reaktionswasser bewirkt die Umwandlung von O-protoniertem ε-Caprolactam in nicht- oder N-protonierte ε-Aminocapronsäure. An mesoporösen Materialien, wie SBA-15, wurde mittles ^{15}N- und ^{13}C-MAS-NMR-Spektroskopie weder ein Einfluss noch eine Umwandlung des Additivs Methanol festgestellt.

2 Abstract

ε-Caprolactam, the main product of the Beckmann rearrangement of cyclohexanone oxime, is an intermediate in the manufacture of nylon-6. Currently, most of the industrial plants produce *ε*-caprolactam by the Beckmann rearrangement of cyclohexanone oxime using sulphuric acid or oleum as a homogeneous catalyst. This process has two main disadvantages: (i) The production of uneconomical by-product, such as ammonium sulphate, and (ii) the environmentally unfriendly corrosive reaction medium. In recent years, the demand for environmentally benign processes has been increasing due to the stringent environmental regulations. Therefore, the new route of the vapor-phase Beckmann rearrangement of cyclohexanone oxime on solid acid catalysts has gained increasing interest as an environmentally, economically and energetically favorable process. For the first time in 2003, the catalytic vapor-phase Beckmann rearrangement of cyclohexanone oxime on high-silica MFI-type zeolites has been industrialized by Sumitomo Chemical Company Ltd. in Japan. Despite the commercialization of this process, several issues are not clear and remain under debate. The main issues are: (i) The nature and location of active sites of the catalysts, (ii) the chemistry of the vapor-phase Beckmann rearrangement reaction (*i.e.* adsorption and desorption behavior of reactants, intermediates, products, and by-products of the reaction), (iii) the reasons for the catalyst deactivation, and (iv) the influence of additives during the vapor-phase Beckmann rearrangement.

The present work mainly focussed on the above-mentioned issues. In this study, for better understanding of the reaction, mechanistic aspects of the vapor-phase Beckmann rearrangement on solid catalysts have been studied by *in situ* solid-state NMR spectroscopy. To study the reaction, several solid catalysts, such as MFI-type zeolites (silicalite-1, H-[B]ZSM-5 and H-ZSM-5) and mesoporous materials (SBA-15, [Al]SBA-15, H-[Si]MCM-41, and H-[Al]MCM-41) were prepared according to the procedures described in the literature. The catalysts were characterized by various techniques, such as powder X-ray diffraction, ICP-OES, N_2 adsorption measurements (BET surface), SEM, and solid-state ^{1}H, ^{2}H, and ^{29}Si MAS NMR spectroscopy.

It has been reported that boron-containing ZSM-5 zeolite (H-[B]ZSM-5) is highly selective in the vapor-phase Beckmann rearrangement of cyclohexanone oxime.

However, the nature of the active sites in this zeolite and the influence of reactant molecules on framework boron atoms were not reported in the literature. In this study, the nature of active sites and the coordination change of framework boron atoms upon adsorption of reactant molecules in H-[B]ZSM-5 (n_{Si} / n_B = 38) zeolite were studied by simultaneous ^{1}H and ^{11}B MAS NMR spectroscopy. For this purpose, several probe molecules characterized by different proton affinities (*PA*) were adsorbed on the zeolite. Probe molecules, such as pyridine, ammonia, and acetone, were loaded on H-[B]ZSM-5 zeolites by an *in situ* flow technique. The ^{1}H MAS NMR spectrum of dehydrated zeolite H-[B]ZSM-5 consists of signals at 1.9, 2.5, and 3.2 ppm. Upon adsorption of pyridine (*PA* = 930 kJ mol^{-1}) and ammonia (*PA* = 854 kJ mol^{-1}) on H-[B]ZSM-5 zeolite, the signal at 2.5 ppm was mainly affected. Therefore, the signal at 2.5 ppm was assigned to the Brønsted acidic SiOH[B] groups in the vicinity of framework boron species. On the other hand, by ^{11}B MAS NMR spectroscopy, the coordination change of $B^{[3]}$ species into $B^{[4]}$ species was investigated. It was found that the proton affinity of $PA \geq 854$ kJ mol^{-1} is required for probe molecules to induce the coordination change of the framework $B^{[3]}$ species into $B^{[4]}$ species in H-[B]ZSM-5 zeolite. This coordination change of framework boron was accompanied by the protonation of probe molecules with $PA \geq 854$ kJ mol^{-1}. As a result of protonation, a decrease of the ^{11}B quadrupole coupling constant from C_{QCC} = 2.7 ± 0.1 MHz ($B^{[3]}$) to $C_{QCC} \leq 0.85$ MHz ($B^{[4]}$) was noticed. This *PA* value (≥ 854 kJ mol^{-1}) is slightly higher (*ca.* 30 kJ mol^{-1}) than the proton affinity of *PA* = 821 kJ mol^{-1} required for the protonation of probe molecules adsorbed on aluminum-containing zeolites reported in the literature. This is supported by the lower acid strength of SiOH[B] groups in H-[B]ZSM-5 zeolites than the bridging OH groups (SiOH[Al]) in aluminum-containing zeolites.

In the present study, for the first time, high-speed ^{2}H MAS NMR spectroscopy at the sample spinning rates of 25 kHz was applied to study the surface sites of deuterated catalysts and their interaction with non-deuterated reactant molecules. Deuterated catalysts, such as H/D-ZSM-5, H/D-[Al]SBA-15, and H/D-SBA-15, were successfully prepared by the H/D exchange of OH groups using D_2O vapor. By ^{2}H MAS NMR spectroscopy, suitable spectral resolution of the signals of SiOH groups (*ca.* 1.8 ppm) and bridging hydroxyl groups (*ca.* 5.7 ppm) in the ^{2}H MAS NMR spectrum of H/D-ZSM-5

was achieved. Two reactant molecules characterized by different molecular diameters, such as cyclohexanone oxime (*ca.* 0.65 nm) and cyclododecanone oxime (*ca.* 0.9 nm), were adsorbed on H/D exchanged catalysts at room temperature. Upon adsorption of non-deuterated reactant molecules (*i.e.* cyclohexanone and cyclododecanone oximes), a dominating signal at *ca.* 12 ppm was observed in the ^{2}H MAS NMR spectra of H/D exchanged catalysts (H/D-ZSM-5, H/D-[Al]SBA-15, and H/D-SBA-15). These results indicate that all kinds of surface sites of H/D-ZSM-5 zeolite, such as silanol groups, silanol nests, or Brønsted acid sites, which can be located on the external surface, near the pore mouth, or in the interior pores, are accessible for cyclohexanone oxime.

In situ solid-state ^{1}H and ^{15}N MAS NMR spectroscopy were utilized to study the chemistry of the vapor-phase Beckmann rearrangement of cyclohexanone oxime on MFI-type zeolites and mesoporous MCM-41 and SBA-15-type materials. The results obtained in this work help to understand the adsorption, desorption, and reaction behavior of reactants, intermediates, products, and by-products formed during the reaction. Initially, *in situ* ^{1}H MAS NMR spectroscopy was applied to study the step-wise conversion of cyclohexanone oxime-D_{11} on silicalite-1 (n_{Si} / n_{Al} = 1700) and H-ZSM-5 (n_{Si} / n_{Al} = 14) catalysts. Deuterated cyclohexanone oxime (*i.e.* cyclohexanone oxime-D_{11}) was successfully prepared with the H/D exchange degree of *ca.* 83%. The vapor-phase Beckmann rearrangement of cyclohexanone oxime-D_{11} was performed on non-deuterated silicalite-1 and H-ZSM-5 catalysts at different reaction temperatures. The ^{1}H MAS NMR spectroscopy provided the evidence on the formation of reaction intermediates, such as H-bonded cyclohexanone oxime and N-protonated cyclohexanone oxime on SiOH groups and bridging hydroxyl groups, respectively. From the ^{1}H MAS NMR studies of the vapor-phase Beckmann rearrangement of cyclohexanone oxime-D_{11} on weakly acidic silicalite-1, the formation of ε-caprolactam, hydroxylamine, and 5-cyano-1-penetene was observed as product and by-product molecules of the reaction. In contrast, on strongly acidic H-ZSM-5 catalyst, the O-protonated ε-caprolactam was identified due to the strong adsorption of this species on bridging hydroxyl groups. Furthermore, the conversion of O-protonated ε-caprolactam on bridging hydroxyl groups of H-ZSM-5 led to the formation of N-protonated ε-caprolactam, or non- or N-protonated ε-aminocapric acid species.

The observable chemical shift range of ^{15}N MAS NMR spectroscopy is larger than the observable chemical shifts range of ^{1}H MAS NMR spectroscopy. Therefore, *in situ* solid-state ^{15}N NMR spectroscopy is the most suitable technique to study the reaction mechanism. Furthermore, the interpretation of ^{15}N MAS NMR signals is less complicated than of ^{1}H MAS NMR signals. In this work, the chemistry of the vapor-phase Beckmann rearrangement on solid catalysts was thoroughly studied by *in situ* ^{15}N MAS NMR spectroscopy. The ^{15}N MAS NMR results suggest that both SiOH and Brønsted acid sites are active in this reaction. ^{15}N-cyclohexanone oxime interacts with SiOH groups *via* hydrogen bonding, which is indicated by the ^{15}N MAS NMR signal in the range of -30 to -46 ppm, while it interacts strongly with Brønsted acid sites and form N-protonated cyclohexanone oxime as represented by the ^{15}N MAS NMR signal in the range of -145 to -160 ppm. By-products, such as hydroxylamine and amines, were also observed on siliceous catalysts. The corresponding ^{15}N MAS NMR signals of these species are in the range of -269 to -280, and -375 to -387 ppm, respectively. In addition, O-protonation of the main product *ε*-caprolactam was found on both siliceous and Brønsted acidic catalysts as evidenced by the ^{15}N MAS NMR signal at -237 ppm. On siliceous catalysts, however, the O-protonation of *ε*-caprolactam depends on the number of acidic Q^3 ($Si(OSi)_3OH$) silanol groups, which is ascertained by ^{29}Si MAS NMR spectroscopy. Furthermore, the conversion of O-protonated *ε*-caprolactam into N-protonated *ε*-caprolactam, and non- or N-protoanted *ε*-aminocapric acid was exclusively observed on Brønsted acidic catalysts.

Generally, methanol as an additive in the reaction system improves the selectivity towards the desired product *ε*-caprolactam during the vapor-phase Beckmann rearrangement of cyclohexanone oxime. In this study, the influence of the methanol on the adsorbed species formed and the conversion of the additive methanol during the vapor-phase Beckmann rearrangement reaction were investigated by *in situ* ^{15}N and ^{13}C MAS NMR spectroscopy. On silicalite-1 and H-ZSM-5 zeolites, hydrocarbons (^{13}C MAS NMR signals in the range of 25 to 30 ppm) were formed and deposited at increasing reaction temperatures. Furthermore, the formation of isopropyl amine (^{13}C MAS NMR signal at 42 ppm) was observed on silicalite-1 as a result of the reaction of isobutane (^{13}C MAS NMR signal at 25 ppm) and hydroxyl amine, which is a by-product of the Beckmann rearrangement. On strongly acidic H-ZSM-5 zeolite, methanol (^{13}C MAS

NMR signal at *ca*. 50 ppm) dehydrates into dimethylether (DME) and water. This water promotes the conversion of O-protonated *ε*-caprolactam into non- or N-protonated *ε*-aminocapric acid. On the mesoporous SBA-15 materials, no influence and conversion of methanol was detected by ^{15}N and ^{13}C MAS NMR spectroscopy.

3 Introduction and state-of-the-art

3.1 Introduction to zeolites

According to the IUPAC definition, porous materials are classified into three main categories depending on their pore dimensions [1-4]. They are: (i) Microporous materials with pore diameters less than 2 nm, (ii) mesoporous materials with pore diameters in the range of 2 to 50 nm, and (iii) macroporous materials with pore diameters greater than 50 nm. Among these materials, microporous materials (*e.g.* zeolites) have gained great interest in heterogeneous catalysis. The term "zeolite" was originally introduced by A.F. Cronstedt, a Swedish mineralogist, who discovered the first zeolite mineral stilbite in 1756 [5-7]. He observed that the stilbite mineral started to bubble upon heating. This observation led to name such minerals as zeolites. To date, several zeolites (*e.g.*, faujasite, mordenite, chabazite *etc*.) have been found in the nature as deposits. However, the naturally occurring zeolites have some disadvantages, which limit their applications in heterogeneous catalysis. The main disadvantages of natural zeolites are: (i) The presence of undesired impurities, (ii) the variation of chemical composition from deposit to deposit, and (iii) no optimization of their properties is possible [3]. During 1940's, the era of synthetic zeolites has started as the result of Barrer's successful pioneering work in making novel zeolites [6-11]. This led to an increasing demand for synthetic zeolites due to their quality and different morphological structures. Zeolites are found to be very interesting for several industrial applications, such as in adsorption, separation, and petrochemical processes [3, 5, 12-17].

According to mineralogists, zeolites are defined as hydrated, crystalline tectoaluminosilicates with a framework based on an extensive three-dimensional network of tetrahedral (either Si^{+4} or Al^{+3}) atoms shared by oxygen atoms [3, 5-7]. This results in negative charges of the framework ($AlO_{4/2}^{-}$). Since the net charge of zeolites should be neutral, the framework charge is compensated by the extra-framework cations [3, 5, 6]. The general empirical formula of zeolites is represented by:

$$A_{y/m}{}^{m+}[(SiO_2)_x.(AlO_2^{-})_y].\ zH_2O$$

where A is a cation with a charge m, $(x + y)$ is the number of tetrahedra per crystallographic unit cell, and x / y is the framework silicon/aluminum ratio (n_{Si} / n_{Al}) [3]. However, due to the rapid evolution of zeolite science, the definition of molecular sieves was introduced to represent zeolites and other non-aluminosilicate materials, such as aluminophosphates [18, 19], silicoaluminophosphates [20], and metal aluminophosphates [21]. Until now, approximately 180 framework structures of zeolites and other related materials have been recognized by the International Zeolite Association (IZA) [22].

In the present study, MFI-type zeolites (silicalite-1, H-[B]ZSM-5 and H-ZSM-5) are used as catalysts in the vapor-phase Beckmann rearrangement of cyclohexanone oxime. MFI-type zeolites are widely known as shape selective catalysts in several reactions [23-27]. They contain unique channel structures, which differ from the other shape-selective catalysts, such as faujasite, Linde Type A, and erionite [27,28]. The framework of MFI-type zeolites consist of eight five-membered rings commonly known as a pentasil unit (Fig. 3.1). These pentasil units (*i.e.* secondary building blocks) join through the edges to form chains, sheets, and then a three-dimensional framework structure as shown in Fig. 3.1. MFI-type zeolites have characteristic configuration with ideal $4_1m2(D_{2d})$ symmetry. They have two specific types of channels, both of which have ten-membered ring openings. One channel system is sinusoidal and has a nearly circular (5.3 x 5.6 Å) cross section. The other channel system has elliptical openings (5.5 x 5.1 Å) [3]. These two intersecting channels are advantageous for molecular traffic control shape selectivity.

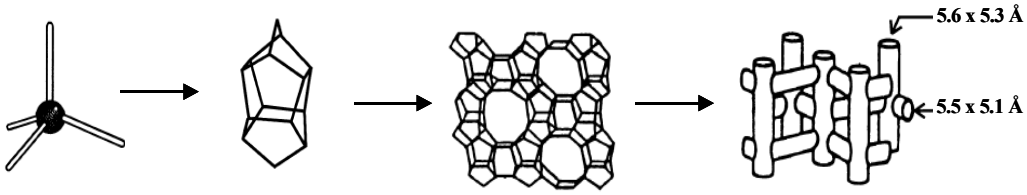

Figure 3.1. Structural units of MFI-type zeolites, their micropore, and channel system [3].

3.2 Introduction to mesoporous materials

Due to the shape selective properties and high thermal and hydrothermal stabilities, zeolites have been applied in numerous heterogeneous catalytic processes. However, because of their small pore windows (< 2 nm), they have limited catalytic applications in bulky molecule catalysis. To overcome this problem, attempts have been made to synthesize the materials with large pore diameters (> 2 nm). As a result, to date, several mesoporous materials have been synthesized [29-38]. For the first time, in 1990, Yanagisawa *et al.* [29] prepared disordered mesoporous alkyltrimethylammonium-kanemite complexes by the intercalation of kanemite with surfactant (hexadecyltrimethyl ammonium chloride) solution (pH = 8 to 9) followed by the hydrothermal treatment at 338 K. But the credit goes to Mobil researchers, who discovered the well-ordered M41S-type materials [32, 33]. Since their discovery in 1992, these materials have gained worldwide attention due to the large pore diameters, extremely high specific surface areas, and novel ordered pore structures. They are studied in a broad manner for applications in heterogeneous catalysis [4, 39], separation processes [40], and in the preparation of optical and electronic devices [41-43]. Among several mesoporous materials, the pores of M41S-type and SBA-15 materials could easily be tailored in a wide range [33, 36, 39]. M41S-type materials include the hexagonal phase ($p6m$) of MCM-41, the cubic phase ($Ia\bar{3}d$) of MCM-48, and the unstable lamellar phase of MCM-50 [39].

The general preparation method of mesoporous MCM-41 materials is relatively similar to that of zeolites excepting that surfactant molecules are used as structure directing agents (SDA) in tailoring the pores. Nevertheless, due to the presence of surfactant molecules the formation mechanism is different from that of zeolites. Two possible synthesis mechanisms are suggested for MCM-41 materials, namely: (i) Liquid crystal templating mechanism and (ii) silicate anion initiation mechanism. These two mechanisms are schematically represented in Fig. 3.2. The liquid crystal templating mechanism proposed by Beck *et al.* [32, 33] involves the formation of micelle, which are organized in such a way that they form micelle rods. These micelle rods are organised themselves to form specific hexagonal structure. Around the micelle, silicate forms an inorganic wall by condensation. The surfactant can be removed by calcination to obtain

MCM-41 materials. In the second approach, no formation of liquid crystals was proposed as indicated by path two in Fig. 3.2 [39].

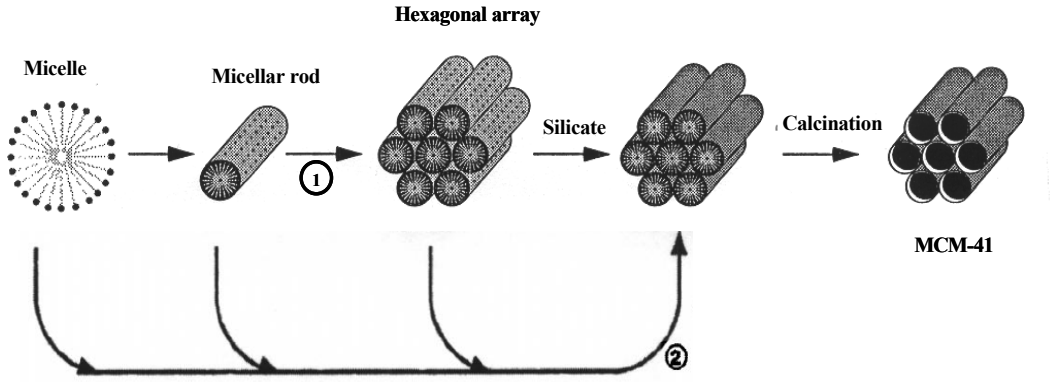

Figure 3.2. Possible synthesis mechanisms of MCM-41 materials: (1) Liquid crystal templating and (2) silicate anion initiation [39].

In 1998, Zhao *et al.* [35, 36] discovered a new type of mesoporous materials called SBA-15. The authors synthesized the SBA-15 material in acidic media using triblock copolymer as a surfactant species. By varying synthesis materials and conditions, and by the addition of different co-solvents, several morphological structures, such as noodle-like, gyroid- and discoid -like, and hard spheres, can be synthesized [35, 36, 44]. In the case of MCM-41 materials, the pore size can be tuned up to 10 nm, while for SBA-15 materials, the pore size is tuneable up to 30 nm. This results in obtaining higher specific surface areas than for MCM-41 materials. In addition, the large pores are favorable for the application of these materials in bulky molecule catalysis (*e.g.* fine chemical production). In comparison with MCM-41 materials, the SBA-15 materials have higher hydrothermal stability and thicker pore walls (3.1-6.4 nm). These properties make SBA-15 material as a versatile catalyst and catalyst support. In the present work, siliceous and aluminum-containing MCM-41 and SBA-15 materials were used as catalysts in the vapor-phase Beckmann rearrangement reaction.

3.3 Acid sites in zeolites and mesoporous materials

The most important properties of the porous solids, which is mainly required in heterogeneous catalysis, is their acidic or basic behavior [45]. Siliceous materials contain only silanol groups, but no bridging hydroxyl groups acting as Brønsted acid sites. Therefore, they exhibit neither acidic nor basic behavior. Nevertheless, such siliceous materials may contain different types of silanol groups, such as terminal, geminal, vicinal, and nests as shown in Fig. 3.3 [46]. Among these silanol groups, nest silanols (Fig. 3.3d) generated at defect sites (located near the pore mouth or in the pores) are formed by removing silicon atoms from the framework. Though nest silanols are weakly acidic, they can be very active and selective in the vapor-phase Beckmann rearrangement of cyclohexanone oxime [46, 47].

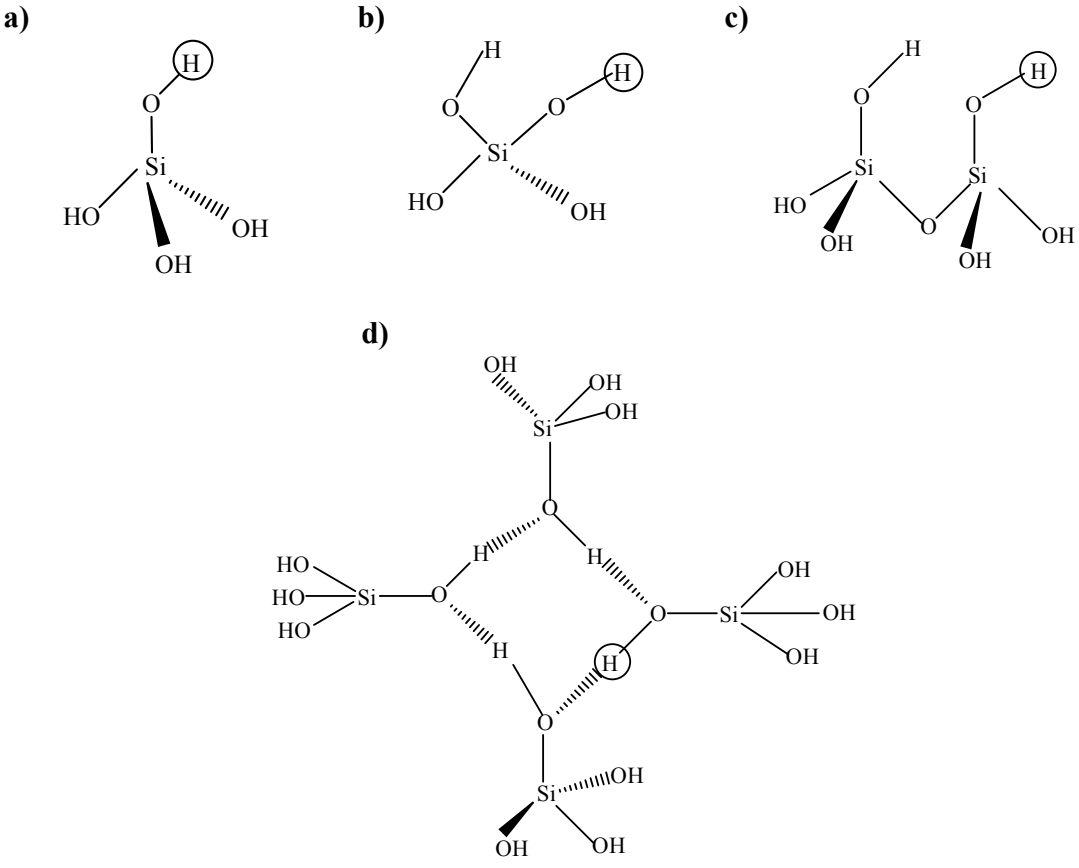

Figure 3.3. Terminal (a), geminal (b), vicinal (c), and nest (d) silanol groups in zeolites and mesoporous materials [46].

Although siliceous materials are non- or weakly acidic, incorporation of aluminum atom into the framework of zeolites or mesoporous materials creates bridging hydroxyl groups or Brønsted acid sites, respectively. These bridging hydroxyl groups or Brønsted acid sites act as proton donors in heterogeneous catalysis. Incorporation of aluminum atoms at T site into the framework induces negative framework charges, which are compensated by extra-framework cations, such as Na^+ ions. The Na-form of catalysts is then ion-exchanged by ammonium ions. Upon heating the NH_4-form catalysts, Brønsted acid sites are created as shown in Scheme 3.1. In aluminum-containing zeolites, Brønsted acid sites exist in the form of bridging hydroxyl groups. On the other hand, in aluminum-containing mesoporous materials, due to their weak Brønsted acidity, no well defined bridging hydroxyl groups could be identified. However, the presence of Brønsted acid sites in mesoporous materials can be identified by the adsorption of basic probe molecules as shown in Scheme 3.2. [48]. In addition, SiOH groups in the neighborhood of strong Lewis acid sites also cause a weak Brønsted acidity by synergistic effect as indicated in Scheme 3.3 [49].

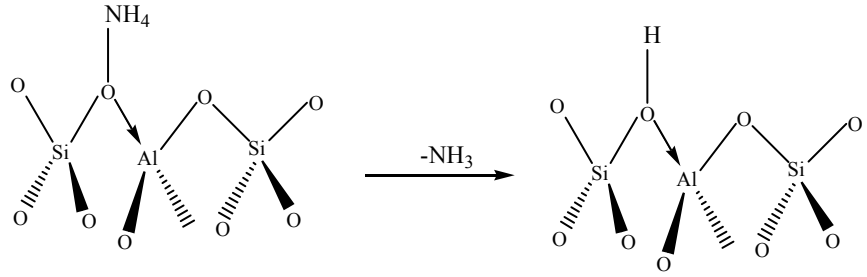

Scheme 3.1. Creation of bridging hydroxyl groups from NH_4-form of zeolites upon thermal decomposition.

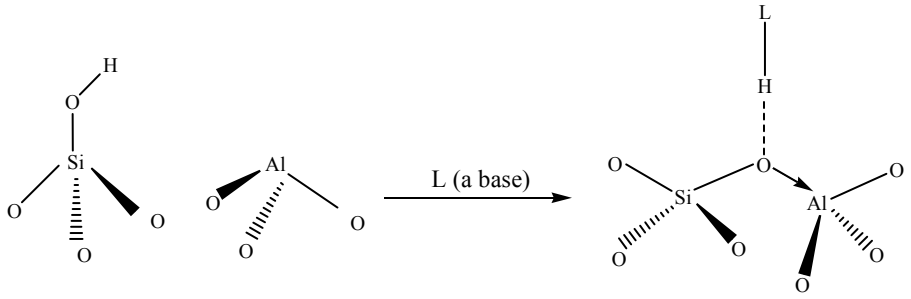

Scheme 3.2. Creation of Brønsted acid sites in aluminum-containing mesoporous materials upon adsorption of base molecules [48].

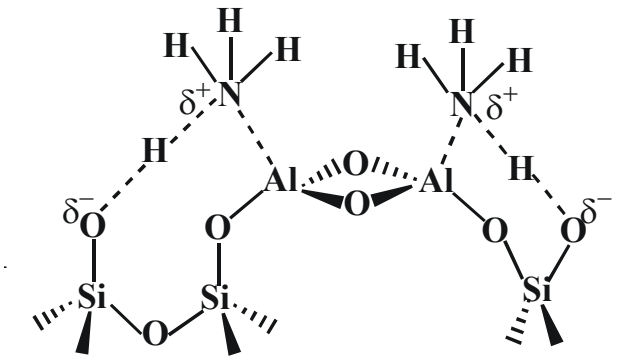

Scheme 3.3. Creation of weak Brønsted acidity in the neighbored Lewis acid sites due to the synergistic effect in mesoporous H-MCM-41 material [49].

To date, various characterization techniques have been applied to study the acidity of zeolites [45]. The techniques include test reactions, titration, temperature-programmed desorption (TPD), microcalorimetry, FT IR, and magic-angle spinning (MAS) NMR spectroscopy [45]. Among these techniques, ^{1}H MAS NMR spectroscopy has been widely used to study the hydroxyl groups, such as bridging hydroxyls or Brønsted acid sites, in zeolites, [45]. Freude and co-workers [50, 51] were the first in studying the Brønsted acidity of zeolites using high-resolution ^{1}H MAS NMR spectroscopy.

3.4 Methods for the production of ε-caprolactam

ε-Caprolactam is the monomer in the manufacture of nylon-6. Nylon-6 is a poly amide and exhibits excellent properties, such as high-strength-to-weight ratio, durability, good chemical and thermal stability. Owing to these properties, nylon-6 has numerous applications. The major applications include the manufacture of fibres, resins, industrial yarns, and engineering plastics *etc.* Due to the industrial advantages of nylon-6, the production of the monomer, *i.e.* ε-caprolactam, has gained great demand in the industrial sector. Therefore, the demand of ε-caprolactam mainly depends on the demand of nylon-6 fibres and resins. It has been reported that global production of ε-caprolactam was amounted to 3.7 and 4.9 million tonnes in 2002 and 2006, respectively [52-55]. Globally, Eastern and Western Europe are the largest producers of ε-caprolactam (*ca*. 50% of the

global caprolactam production), while Asia is the largest consumer of ε-caprolactam [52, 53].

In 1886, Ernst Beckmann discovered the rearrangement reaction in which ketoximes were transformed into acid amides [56]. Followed by this success, several Beckmann rearrangement reactions have been discovered [57-59]. Among these reactions, the transformations of cyclohexanone and cyclododecanone oximes into their respective lactams *via* the Beckmann rearrangement have gained significant interest. These lactams are used in the manufacture of nylon-6 and nylon-12, respectively [60]. In a conventional method, ε-caprolactam is mainly produced by using cyclohexanone oxime as an intermediate. However, it can also be produced by other methods without the use of cyclohexanone oxime. The other routes are: The Snia Vicosa Process, the UCC process, the TechniChem Nitrocyclohexanone process, and the BP hydrogen peroxide process [61]. Nevertheless, except a few processes, many industrial plants currently produce ε-caprolactam *via* cyclohexanone oxime as an intermediate [61].

The classical production of ε-caprolactam comprises two steps: (i) The production of cyclohexanone oxime and (ii) the Beckmann rearrangement of cyclohexanone oxime into ε-caprolactam. But in many cases, the synthesis of cyclohexanone oxime involves different paths as shown in Scheme 3.4. Cyclohexanone oxime is originally produced from cyclohexanone, which in turn is produced from either benzene or phenol. However, the Toray's PNC (Photonitrosation of cyclohexane) process is an exception, in which cyclohexanone oxime is produced by the reaction of cyclohexane and nitrosyl chloride under the presence of UV radiation [61, 62]. In the process using benzene as starting material, benzene initially is hydrogenated to produce cyclohexane or cyclohexene. Subsequently, cyclohexane is further oxidized to yield cyclohexanone. In the other route, cyclohexene is hydrolyzed to cyclohexanol, which is further dehydrogenated over Cu- or Zn- catalysts with a conversion of 90% and a selectivity of 95% [61, 63]. However, cyclohexanone is formed in a single step *via* phenol hydrogenation (Fig.3.7) over carried Pd-catalysts (*e.g.* Pd-CaO/Al_2O_3) with a selectivity of more than 95% [61].

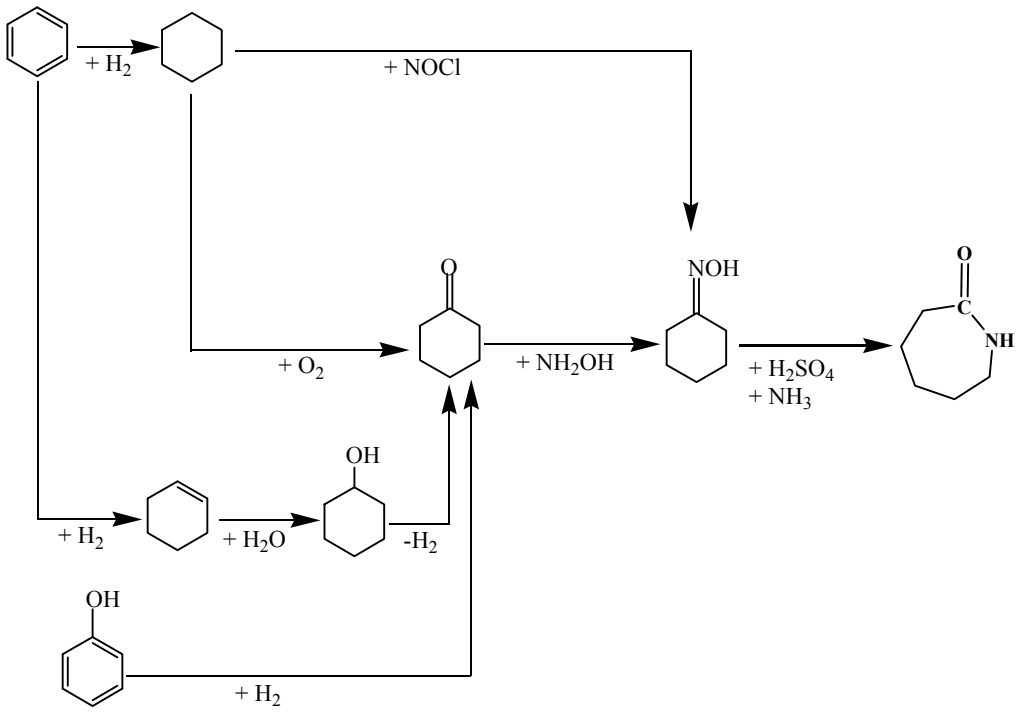

Scheme 3.4. Several pathways for the production of ε-caprolactam [62].

Step 1:

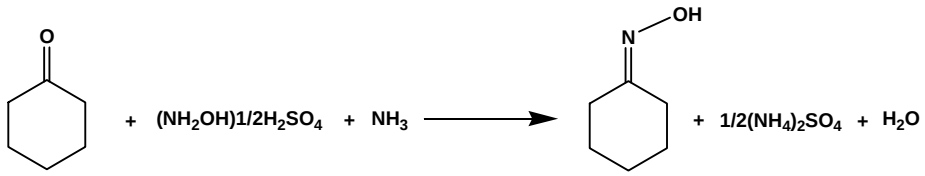

Step 2:

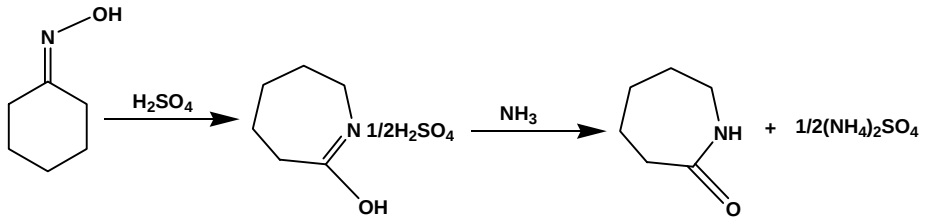

Scheme. 3.5. Homogeneous ammoximation (step 1) and the Beckmann rearrangement (step 2) processes [46, 62].

The production of cyclohexanone oxime from cyclohexanone and hydroxylamine is known as oximation process, and the conversion of cyclohexanone oxime into ε-caprolactam is referred as Beckmann rearrangement [61-63]. In the oximation process, many companies use hydroxylamine in its sulphate or phosphate form, while in the Beckmann rearrangement process sulphuric acid or oleum is used as homogeneous catalysts. Therefore, ammonia is required in both processes to neutralize the reaction mixture and to separate the product [46, 61-63]. This leads to a formation of large amount of by-products (*i.e.* ammonium sulphate) as shown by steps 1 and 2 in Scheme 3.5. The amount of by-products depends on the process and it is estimated to be *ca.* 1.6-4.4 tonnes per ton of ε-caprolactam [46, 61-63].

3.5 Production of ε-caprolactam by heterogeneous catalysis

Due to the large amount of by-products (*i.e.* ammonium sulphate) and hazardous working conditions, the conventional method became economically and environmentally unfriendly process. Therefore, the demand for economically favorable and green processes has been increasing [61-67]. For the past few decades, much effort has been devoted by researchers to replace the homogeneous catalytic process by a heterogeneous catalytic process. As a result, for the first time in 2003, a heterogeneous catalytic process using zeolites has been successfully industrialized by Sumitomo Chemical Company Ltd. in Japan [62]. Like in the conventional method, the new heterogeneous process for the production of ε-caprolactam also comprises two steps: (i) The ammoximation of cyclohexanone and (ii) the vapor-phase Beckmann rearrangement of cyclohexanone oxime.

In 1967, the first catalytic ammoximation of cyclohexanone with NH_3/H_2O_2 using tungsten phosphate as catalyst was reported [61]. However, further research studies proved that titanium silicalite-1 (TS-1) is a very good catalyst in the ammoximation process [61]. Two possible ammoximation reaction routes are represented by Scheme 3.6. According to the first route, cyclohexanone reacts with ammonia and yield cyclohexylimine, which is further oxidized to cyclohexanone oxime with hydrogen peroxide on TS-1 catalyst [68, 69]. Zecchina *et al.* [70, 71], by means of spectroscopic methods (IR, Raman, UV/Vis, and XAFS), suggested that the second route is more

favorable. According to this route, initially ammonia is oxidized to hydroxylamine with hydrogen peroxide on TS-1 catalyst. Subsequently, hydroxylamine reacts with cyclohexanone and converts into cyclohexanone oxime [70, 71]. In comparison to the homogeneous process, the major advantage of this catalytic ammoximation process is that only water is produced as a by-product in the reaction. But the main drawback of this process is the high costs of catalyst and hydrogen peroxide [61]. Nevertheless, this process seems to be more economical and environmentally friendly than the conventional process.

Route 1:

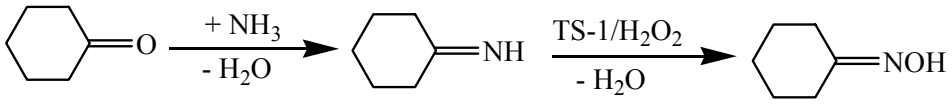

Route 2:

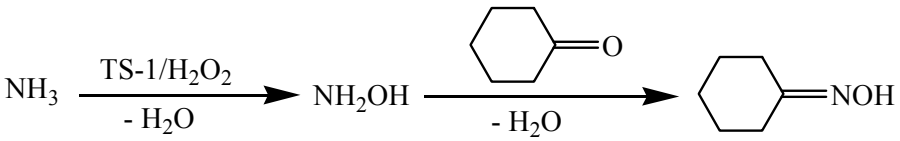

Scheme 3.6. Possible reaction pathways in the heterogeneous catalytic ammoximation process [68-71].

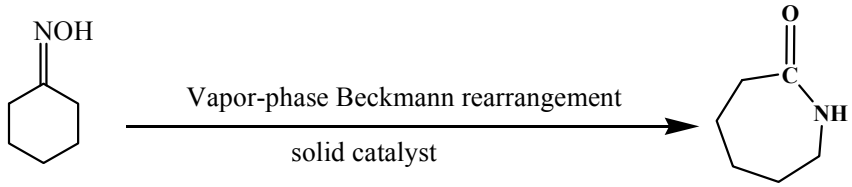

Scheme 3.7. Catalytic vapor-phase Beckmann rearrangement on solid catalyst.

The second step of new catalytic process is the vapor-phase Beckmann rearrangement process (Scheme 3.7) in which cyclohexanone oxime is transformed into ε-caprolactam on a solid catalyst. To date, several solid catalysts including non-zeolitic, zeolitic, and mesoporous materials were studied in the vapor-phase Beckmann rearrangement reaction [61]. Non-zeolitic catalysts, such as silica gel, alumina, magnesia, thoria, and heteropoly acids, were reported to catalyze the cyclohexanone oxime conversion [72, 73]. However, the selectivity to ε-caprolactam on these catalysts was very low because of the undesired side-reactions [61]. The use of other non-zeolitic catalysts was also reported by many other researchers (see Ref. [61]). For the first time, in 1966, Landis and Venuto [74] used X-, Y-, and mordenite zeolites in the H-form or doped with rare-earth or transition metals. Since then, the vapor-phase Beckmann rearrangement has been performed on a wide variety of zeolites, such as FAU (Y-type zeolites) [74-77], MFI (*e.g.* TS-1, silicalite-1, [B]ZSM-5, ZSM-5) [78-98], MEL [98, 99], MTW [98], SAPO-11 [100], *BEA (Beta zeolites) [101-103], H-LTL [104], H-OFF-ERI [104], MCM-22 [105], FER, and LTA [83, 84, 106]. In addition, mesoporous materials, such as MCM-41, SBA-15, and MCM-48, have been applied in the vapor-phase Beckmann rearrangement reaction [107-118]. Nevertheless, high conversion of cyclohexanone oxime and high ε-caprolactam selectivity were obtained on the zeolites with MFI topology [78-98]. In particular, high-silica MFI zeolites (*e.g.* silicalite-1) and boron-containing MFI zeolites (*e.g.* [B]ZSM-5) showed excellent performance in the vapor-phase Beckmann rearrangement of cyclohexanone oxime [78-98]. Despite the great efforts on the catalytic investigations, some issues remain under debate. In Section 3.6, the state-of-the-art vapor-phase Beckmann rearrangement is presented.

3.6 Vapor-phase Beckmann rearrangement of cyclohexanone oxime on solid catalysts (state-of-the-art)

3.6.1 Nature and location of active sites of solid catalysts in the vapor-phase Beckmann rearrangement reaction

In the liquid-phase Beckmann rearrangement reaction using sulfuric acid as homogeneous catalyst, strong Brønsted acid sites are thought to be the active sites of the catalysts. In 1986, Sato *et al.* [119] studied the vapor-phase Beckmann rearrangement

reaction on silica supported boria catalyst (B_2O_3/SiO_2). They proposed that the strong acidic sites are active in the reaction. In contrast, Sato *et al.* [79-81, 85, 120] concluded that neutral silanol groups present on the external surface are highly active and selective in the vapor-phase Beckmann rearrangement of cyclohexanone oxime. The authors studied the reaction on pentasil (MFI-type) zeolites with different n_{Si} / n_{Al} ratios and in the presence of organic bases [80]. They found no significant influences on the selectivity to ε-caprolactam with the use of organic bases. Nevertheless, from the catalytic investigations, a high lactam selectivity and long catalyst life time were obtained on highly siliceous (n_{Si} / $n_{Al} \geq$ 500) MFI-type zeolites [80]. By FT IR spectroscopic analysis, the same group [81, 85] found that highly siliceous MFI-type zeolites (n_{Si} / $n_{Al} \geq$ 30000) exhibits a better lactam selectivity than the zelite with n_{Si} / n_{Al} = 1640. These results indicate that silanols present on the external surface are active in the Beckmann rearrangement reaction. These studies are further supported by the adsorption and catalytic investigations of Yashima *et al.* [82, 83].

Yashima *et al.* [82, 83] studied the reaction on several catalysts, such as H-ZSM-5, H-ferrierite, H-mordenite, H-borosilicate, silicalite-1, Na-A, Ca-A, Na-, K-clinoptilolite, silica gel, and MgO. The catalysts are characterized by different acidities, pore dimensions, and topologies. The investigations showed high selectivities towards ε-caprolactam on zeolites having smaller pore window size, such as silicalite-1, Na-A, and Na-, K-clinoptilolite, than the size of cyclohexanone oxime molecule. From these results, the authors concluded that the vapor-phase Beckmann rearrangement of cyclohexanone oxime to ε-caprolactam proceeds selectively on the weakly acidic active sites located on the external surface of zeolites crystals. Furthermore, they observed side-reactions, like ring-openings, decomposition, and polymerization on strongly acidic bridging hydroxyl groups in H-ZSM-5 zeolite.

To understand the nature and location of active sites, Hölderich and his co-workers [47, 88, 90, 121] studied the vapor-phase Beckmann rearrangement reaction on MFI-type zeolites. To confirm the location, where the reaction takes place, the authors studied the reaction on [B]MFI zeolites with different crystal sizes. They found a high conversion of cyclohexanone oxime on the zeolites having high external surface areas (*i.e.* small crystal size). According to these results, they concluded that the Beckmann

rearrangement do not take place inside the micropores of MFI-type zeolites, but rather on the outer surface [47, 121, 90]. Furthermore, the authors extended their catalytic investigations on a variety of zeolites modified by different methods, such as acid and base treatment, chemical vapor deposition (CVD), deboration, and steaming procedures. From the physiochemical characterization of the modified zeolites by FT IR, NMR, NH_3-TPD, and pyridine adsorption techniques, the results specify that weakly acidic vicinal silanol groups and silanol nests are the most favorable sites for the vapor-phase Beckmann rearrangement [47, 88-90, 121]. Dai *et al.* [77] also made a similar conclusion by studying the reaction on H-USY zeolite modified by steaming and acidic treatment. They concluded that moderately dealuminated USY zeolites show excellent catalytic performance due to the creation of weakly hydrogen-bonded silanol groups. O'Sullivan *et al.* [122] investigated the Beckmann rearrangement reaction on several catalysts including Beta zeolite, mordenite, ZSM-5, Y-zeolite, mesoporous alumino silicate, and amorphous silica-alumina with different n_{Si} / n_{Al} ratios. From the FT IR spectroscopic analysis of pyridine adsorption and catalytic investigations, they concluded that a low ratio of strong/weak acid sites is important in achieving a high yield of ε-caprolactam.

On the other hand, Camblor *et al.* [102] studied the liquid-phase Beckmann rearrangement of different oximes (cyclohexanone, acetophenone, and cyclododecanone oximes) on Beta and H-ZSM-5 zeolites. In contrast to the above-mentioned results, these studies concluded that internal silanols are active and selective for performing the Beckmann rearrangement inside the pores. Furthermore, they concluded that external silanol groups are also active but promote the side-reactions, like hydrolysis of oxime to ketones. In 2001, Kath *et al.* [92] conducted adsorption and catalytic investigations of the vapor-phase Beckmann rearrangement on MFI-type zeolites (*e.g.* silicalite-1). From the adsorption breakthrough curves of cyclohexanone oxime and ε-caprolactam on MFI-type zeolites, they confirmed that the reactant is able to penetrate into the pores of the catalysts, while it is difficult for ε-caprolactam to enter into the pores of MFI-type zeolites. According to the adsorption and catalytic studies, the authors concluded that the Beckmann rearrangement of cyclohexanone oxime either proceeds completely inside the pores of silicalite-1 or takes place simultaneously inside the micropores and at the external surface of the crystals. Many other groups also reported that the weakly acidic

silanol nests, located near the pore mouth of MFI-type zeolites, are the active sites in the Beckmann rearrangement of cyclohexanone oxime [46, 62, 123]. Theoretical studies also indicated that a part of cyclohexanone oxime is able to enter into the pores of MFI-type zeolites, and therefore the active sites are located near the pore mouth of MFI-type zeolites [46, 62, 123].

Recently, Fernández *et al.* [124], studied the Beckmann rearrangement of acetophenone and cyclododecanone oximes on porous solids (Beta, MFI-type, and MCM-41 materials) by *in situ* FT IR spectroscopy. Their results indicated that Brønsted acid sites as well as silanol nests located in the pores of zeolites and MCM-41 materials are active in the reaction. Furthermore, Fernández *et al.* [125] studied the vapor-phase Beckmann rearrangement of cyclohexanone and cyclododecanone oximes on MFI-type zeolites by solid-state ^{15}N NMR spectroscopy and concluded that the reaction occurs inside the pores of MFI zeolites. In conclusion, the literature on the nature and location of active sites is still controversial and merits further investigations. Therefore, the solid-state NMR studies described in Chapters 6 and 7 address these points.

3.6.2 Reaction mechanisms of the Beckmann rearrangement reaction

It is certain that the understanding of the reaction mechanism is very important for the development of a new process. Since the discovery of the Beckmann rearrangement reaction in 1886 [56], the reaction mechanism has been the matter of debate. According to the liquid-phase Beckmann rearrangement using sulfuric acid as homogeneous catalyst, the mechanism is understood to be a typical concerted intramolecular hydride transfer reaction [57]. On the other hand, the mechanism of the vapor-phase Beckmann rearrangement reaction on different solid catalysts is poorly understood. In 1966, Landis and Venuto [74] studied the Beckmann rearrangement on crystalline aluminosilicates (*e.g.* Y-zeolites) and proposed the reaction mechanism 1 described in Scheme 3.8. According to these authors [74], the adsorption of ketoxime on a acid site leads to the formation of O-protonated oxime. In the next stage, intramolecular migration of alkyl group *anti* to the departing hydroxyl group occurs followed by the loss of water molecule. This causes electron deficiency at the nitrogen atom and forms a nitrilium cation as migration of alkyl group occurs. Finally, the resulting imine derivatives may

then rearrange to the amide. In addition to the mechanism proposed by Landis and Venuto [74], other mechanisms have been reported by Murakami *et al.* [126] and Nguyen *et al.* [127-129].

Mechanism 1:

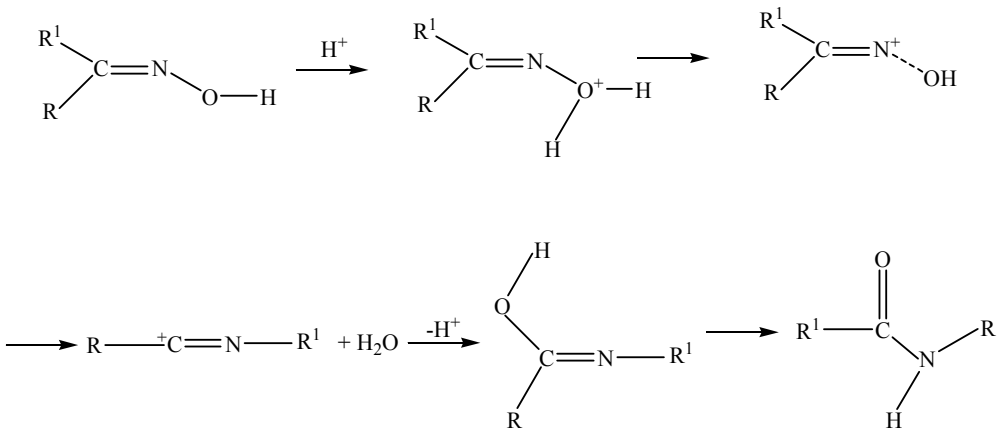

Mechanism 2:

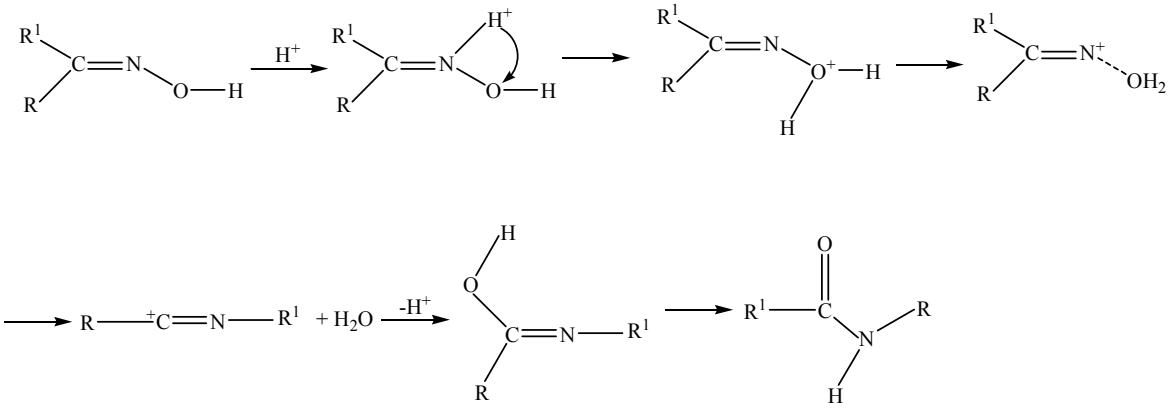

Scheme 3.8. Possible reaction mechanisms of the Beckmann rearrangement of oxime into an acid amide [74, 126-129].

On the basis of *ab initio* molecular orbital (MO) calculations, Nguyen *et al.* [127-129] proposed a slightly different reaction mechanism as represented by the mechanism 2 in Scheme 3.8. According to this mechanism, initially N-protonated oxime is formed and

then O-protonated oxime is formed on a active site. This is supported by the energy difference between the N- and O-protonated forms of the oxime molecule. An energy difference of *ca.* 77 kJ mol^{-1} was found in favor of the N-protonated oxime. Nguyen *et al.* [127-129] further concluded that the 1,2-H shift from the N-protonated oxime to the O-protonated oxime is the rate-determining step.

In 2000, by using quantum chemical methods, Sinhora *et al.* [130] investigated the mechanistic aspects of the vapor-phase Beckmann rearrangement on SiO_2-Al_2O_3, SiO_2, γ-Al_2O_3, and ZnO. Based on these calculations, Brønsted acid site first attacks the nitrogen atom of the oxime molecule (N-protonation) followed by a proton transfer to the oxygen atom (O-protonation). Simultaneously, the transfer of alkyl group and an elimination of the hydroxyl group of the oxime as water occur (supports mechanism 2). In contrast to the studies of Nguyen *et al.* [127-129], Sinhora *et al.* [130] concluded that the transfer and elimination of water is the rate-determining step of the reaction. These studies are further supported by the studies of Sirijaraensre *et al.* [131] in 2005, who investigated the mechanism of the Beckmann rearrangement on H-ZSM-5 zeolite by theoretical calculations. Sirijaraensre *et al.* [131] also concluded that formation of N-protonated oxime is preferred in comparison with the formation of O-protonated oxime in the initial step of the reaction. Furthermore, they concluded that the rate-determining step of the reaction is either the rearrangement or tautomerization.

On the other hand, using *ab intio* calculations, Šimunić-Mežnarić *et al.* [132] investigated the structures and stabilities of possible reaction intermediates in the Beckmann rearrangement of several cyclic oximes (cyclobutanone, cyclopentanone, cyclohexanone, and cyclopropylethanone oximes) on solid superacids (*i.e.* SbF_5). They found that under superacid conditions, the Beckmann rearrangement proceeds *via* the formation of a seven-membered cyclic nitrylium ion intermediate. More recently, solid-state NMR spectroscopy was utilized to study the mechanism of the vapor-phase Beckmann rearrangement reaction [125, 133, 134].

In conclusion, the majority of the studies reveal the formation of N-protonated oxime on strong Brønsted acid sites as the initial reaction intermediate, followed by the formation of O-protonated oxime. However, the adsorption state and the reaction behavior of reactants, intermediates, products, and by-products of the vapor-phase

Beckmann rearrangement on solid catalysts characterized by different acidities and topologies have been not reported in the literature. In the present work, the mechanistic aspects of the vapor-phase Beckmann rearrangement reaction are mainly studied by *in situ* ^{1}H and ^{15}N MAS NMR spectroscopy (see Chapters 6-8).

3.6.3 Influence of additives in the vapor-phase Beckmann rearrangement on solid catalysts

It has been reported that under the presence of solvents or additives the selectivity towards ε-caprolactam is significantly improved. Landis and Venuto [74], in 1966, studied the influences of polar and non-polar solvents in the vapor-phase Beckmann rearrangement of cyclohexanone oxime on REX zeolites (rare earth zeolites X). With the use of non-polar solvents (cyclohexane and benzene), moderate conversions of cyclohexanone oxime (30-40%) and a fair selectivities towards ε-caprolactam (60-45%) were obtained. In contrast, with the use of a polar solvent, such as methanol, a low conversion (38%) and selectivity (26%) were obtained. They suggested that the polar solvent (methanol) could be strongly adsorbed on the acid sites and block the active sites of the catalyst for the reactant molecules (*i.e.* cyclohexanone oxime).

In 1994, Kitamura and Ichihashi [135] studied the role of different solvents, such as benzene, methanol, ethanol, propanol, iso-propanol, hexane, acetaldehyde, and acetic acid, in the vapor-phase Beckmann rearrangement on highly siliceous zeolites. In result of the catalytic investigations, the authors noticed that methanol greatly improved the catalytic performance. Upon the sufficient addition of methanol to the reaction system, the selectivity towards ε-caprolactam was improved from 85% up to 95% [46, 62, 93]. This could be due to the modification of the zeolite surface in the presence of alcohols. This explanation was further supported by FT IR studies [46, 62, 93]. The FT IR studies indicated that methanol reacts with terminal silanols on the crystal surface of high-silica MFI zeolites and forms methylsilylether species. In contrast, nest silanols located near the pore mouth remain in the zeolites and are responsible for the Beckmann rearrangement [46, 62, 93].

Dai *et al.* [101] published the influences of different diluents (benzene, methanol, ethanol, propan-1-ol, butan-1-ol, pentan-1-ol, hexan-1-ol, butan-2-ol, 2-methylpropan-2-

ol) in the vapor-phase Beckmann rearrangement on H-Beta and silicalite-1. From the catalytic studies, these authors found that, among the solvents used, the application of hexan-1-ol showed the highest selectivity towards ε-caprolactam on both H-Beta and silicalite-1 catalysts. However, at higher time on stream, the catalyst life of silicalite-1 was decreased, which was evidenced by the decrease of catalytic activity from *ca.* 95% after 1 h to 80% after 4 h. From these studies, the authors pointed out that the effect of solvent on the Beckmann rearrangement also depends on the type of zeolites and reaction conditions. Dai *et al.* [77, 101, 104] extended their investigations to study further the influence of different solvents in the vapor-phase Beckmann rearrangement on various zeolites (H-Beta, H-LTL, H-OFF-ERI, H-USY, H-MOR, and silicalite-1). Again, they confirmed that hexanol-1 shows the best selectivity towards ε-caprolactam, especially on large-pore zeolites, like H-LTL, H-OFF-ERI, and H-USY. Furthermore, the studies of Dai *et al.* [77, 101, 104] were supported by Chang and Ko [114, 115], who also reported that the selectivity to ε-caprolactam depends on the type of solvent in the reaction. From their studies of the vapor-phase Beckmann rearrangement on mesoporous SBA-15 and MCM-48 catalysts, the selectivity to ε-caprolactam in the presence of solvents follows the order hexanol-1 > ethanol ≥ benzene > toluene.

The group of Hölderich [47, 86] studied the influence of polar and non-polar solvents in the vapor-phase Beckmann rearrangement of cyclohexanone oxime on B-MFI zeolites. Their investigations showed much higher yields and lower deactivation rates in the presence of polar solvents, such as methanol and ethanol, than in the presence of non-polar solvents, such as benzene and toluene. According to these authors, the reason might be the capability of alcohols to dehydrate to ether and olefins by eliminating water under reaction conditions of 573 K and 0.1 bar. In addition, they reported that the formed water and the polar nature of the solvents are responsible to supersede polymers and coke precursors from the catalyst surface.

Yashima *et al.* [83] studied the influence of various solvents on the conversion of cyclohexanone oxime and selectivity to ε-caprolactam in the vapor-phase Beckmann rearrangement on H-mordenite, H-ZSM-5, silicalite-1, H-ferrierite, and Ca-A zeolites. The solvents used for the study are benzene, ethanol, acetone, cyclohexane, tetrahydrofuran (THF), and chloroform. They found ethanol is the most suitable solvent

in the reaction on MFI-type zeolites, especially on silicalite-1. With the use of ethanol as solvent, 98% selectivity to ε-caprolactam was achieved on silicalite-1. However, they could not observe the influence of the polarity of the solvents in the vapor-phase Beckmann rearrangement. In 2000, the same group [136] performed kinetic investigations to study the effect of solvents in the vapor-phase Beckmann rearrangement of cyclohexanone oxime on silicalite-1. The solvents used in this study are characterized by different polarities. The polarities of benzene, cyclohexane, toluene, diethylether (DEE), ethanol, methanol, pyridine, acetone, and acetonitrile are 0.0, 0.33, 0.38, 1.25, 1.44, 1.66, 2.15, 2.90, and 3.92, respectively. From the kinetic studies, the authors found that ethanol with medium polarity (1.44) showed the best performance in the reaction. Furthermore, they concluded that the alcohols with short hydrocarbon chains, such as ethanol and methanol, are the most effective solvents in the reaction. In the presence of these solvents, ε-caprolactam can be simply desorbed from the active sites in order to accelerate the Beckmann rearrangement without forming a hydrophobic layer. Also, Forni *et al.* [112] observed best results when ethanol was used as an additive in the feed.

Some other research groups [67, 106, 137] found that polar solvents, such as acetonitrile, are the best solvent in the Beckmann rearrangement. According to Mao *et al.* [137], a ε-caprolactam selectivity of 98.6% was achieved when acetonirile was used as a solvent in the vapor-phase Beckmann rearrangement of cyclohexanone oxime on B_2O_3/TiO_2-ZrO_2 catalyst. Kob and Drago [138] also showed acetonitrile as a good solvent in the Beckmann rearrangement reaction on tungsten oxide. However, they noticed that methanol has slightly better performance in the reaction than acetonitrile. On the other hand, recently, Ngamcharussrivichai *et al.* [113] studied the influences of different solvents in the liquid-phase Beckmann rearrangement on Al-MCM-41 catalyst. A series of solvents, such as chlorobenzene (PhCl), benzonitrile (PhCN), acetophenone (MPK), acetonitrile (MeCN), dimethyl sulfoxide (DMSO), and N, N-dimethylformamide (DMF), were used in the reaction. According to their studies, benzonitrile is found to be a suitable solvent for improving the lactam yield. In addition, this solvent reduced the formation of by-products (*e.g.* cyclohexanone) and polymerization products. Nevertheless, the conversion and selectivity obtained by using benzonitrile as solvent were only 50% and 89%, respectively.

In conclusion, the above-mentioned literature on the effect of solvents or additives suggest that alcohols, such as methanol or ethanol, are the suitable solvents in the vapor-phase Beckmann rearrangement on highly siliceous MFI zeolites, while hexanol-1 is the best solvent in the reaction on large-pore zeolites. However, the above-mentioned studies do not provide clear mechanistic evidences of the solvent effect on the formation of reactants, intermediates, products, and by-products in the vapor-phase Beckmann rearrangement reaction. Therefore, to evaluate the reasons, in the present work, the influence of the additive ^{13}C-methanol in the vapor-phase Beckmann rearrangement of ^{15}N-cyclohexanone oxime on solid catalysts was studied by *in situ* ^{13}C and ^{15}N CP/MAS NMR spectroscopy (see Chapter 8).

4 Experimental section

4.1 Preparation of materials

4.1.1 Synthesis of silicalite-1

Silicalite-1 [92] was synthesized according to the following procedure. Initially, 31.50 g of demineralized water and 10.83 g of ammonium hydroxide were taken in a beaker, and 12.00 g of silicic acid hydrate powder (≥ 99%, Fluka) was slowly added to the mixture in a beaker under strong stirring conditions. Finally, 22.77 g of tetrapropylammonium hydroxide (1.0 M, Aldrich) was added and stirred for 3 h. The synthesis solution was then transferred into a 0.30 l stainless steel autoclave containing a Teflon insert and heated at 448 K under permanent shaking for 28 h. The product was recovered by filtration, washed thoroughly with demineralized water, dried at 353 K for 24 h, and then calcined for 6 h at 823 K in a flow of synthetic air (20 vol.% oxygen, 60 l/h).

4.1.2 Synthesis of H-[B]ZSM-5

The synthesis of [B]ZSM-5 (n_{Si} / n_B = 38) was carried out according to Ref. [139]. Initially, 12.42 g of tetrapropylammonium hydroxide (1.0 M, Aldrich) was added to a beaker containing 70.96 g of demineralized water, and stirred for 10 min. To this mixture, 0.66 g of H_3BO_3 (> 99.5%, Fluka) was added and stirred for 30 min. Finally, 7.60 g of Cab-o-Sil (Riedel-de Haën) was slowly added to the above mixture under stirring. This solution was stirred for one hour and transferred to 0.30 l stainless steel autoclave containing a Teflon insert, and heated at 423 K for 5 days. The product was recovered by filtration, washed thoroughly with demineralized water, dried at 353 K, and calcined at 823 K. In order to obtain H-[B]ZSM-5, the calcined material was ion-exchanged with 1.0 M ammonium acetate solution for 12 h at 353 K. After ion exchange, the material was calcined at 773 K.

4.1.3 Synthesis of H-ZSM-5

H-ZSM-5 (n_{Si} / n_{Al} = 14) zeolite was synthesized according to the procedure described in Ref. [140]. The typical procedure consists of two steps: (i) Seed gel preparation and (ii) synthesis gel preparation. The seed gel was prepared by dissolving

and thorough mixing of 1.38 g of sodium hydroxide (99%, Merck) and 11.70 g of tetrapropylammonium hydroxide (1.0 M, Aldrich) in 71.03 g of demineralized water. Then, 15.89 g of silicic acid hydrate (≥ 99%, Fluka) was added to the above mixture in portions under strong stirring conditions. When all the silicic acid was added, the mixture was stirred for 1 h at ambient temperature. Finally, the mixture was stirred at 373 K for 16 h. For the synthesis gel preparation, 0.88 g of sodium hydroxide and 1.03 g of sodium aluminate (Riedel-de Haën) were dissolved and mixed thoroughly in 86.78 g of demineralized water. To this mixture, 11.31 g of silicic acid was added in portions under stirring. When all the silicic acid was added, the mixture was stirred vigorously for 1 h at ambient temperature. Subsequently, 5.00 g of seed gel from step (i) was added to the mixture and stirred for another 1 h. The mixture was then transferred into a 0.30 l stainless steel autoclave containing a Teflon insert and heated at 453 K for 40 h. The product was recovered by filtration, washed thoroughly with demineralized water, dried at 353 K for 24 h, and then calcined for 6 h at 823 K in a flow of synthetic air (20 vol.% oxygen, 60 l/h). In order to obtain H-ZSM-5 zeolite, the calcined material was ion-exchanged with 0.40 M ammonium nitrate solution for 6 h, and then with 0.10 M ammonium nitrate solution for 12 h at 353 K. After ion exchange, the material was calcined at 773 K.

4.1.4 Synthesis of siliceous SBA-15 material

Typical synthesis procedure of the siliceous SBA-15 material [35] is as follows: 6.00 g of triblock copolymer ($EO_{20}PO_{70}EO_{20}$) was dissolved in 29.40 g of hydrochloric acid (37 wt.%). To this mixture, 192.00 g of demineralized water was added. Subsequently, 13.20 g of tetraethylortho silicate (98%, Aldrich) was added drop by drop under stirring. This mixture was stirred at room temperature for 10 min and then at 313 K for 24 h. Finally, the mixture was transferred into a 0.30 l stainless steel autoclave and heated at 373 K for 24 h. The product was recovered by filtration, washed thoroughly with demineralized water, dried at 353 K for 24 h, and then calcined for 6 h at 823 K in a flow of synthetic air (20 vol.% oxygen, 60 l/h).

4.1.5 Synthesis of [Al]SBA-15 material

To synthesize aluminum-containing SBA-15 material ([Al]SBA-15) [141, 142], 4.40 g of triblock copolymer ($EO_{20}PO_{70}EO_{20}$) was dissolved in 118.00 g of hydrochloric acid (0.1 wt.%). To this mixture, 7.00 g of tetramethylortho silicate (> 99%, Fluka) was added drop by drop under stirring. In addition, 1.00 g of aluminumtriisopropylate (> 98%, Merck) in 10.00 g of hydrochloric acid was added to the above mixture. Subsequently, the mixture was stirred at 313 K for 24 h. Then the *pH* value of the mixture was adjusted to 7.00 *via* the addition of ammonium hydroxide solution. Finally, the mixture was transferred into a 0.30 l stainless steel autoclave and heated at 373 K for 24 h. The product was recovered by filtration, washed thoroughly with demineralized water, dried at 353 K for 24 h, and then calcined for 6 h at 823 K in a flow of synthetic air (20 vol.% oxygen, 60 l/h).

4.1.6 Synthesis of siliceous MCM-41 (H-[Si]MCM-41) material

In a typical synthesis, 4.80 g of tetramethylammonium hydroxide (TMAOH) was added to 4.3 g of sodium silicate diluted with 100.00 g demineralized water (solution A). In another beaker, solution B was prepared by dissolving 5.00 g of CTMABr in 12.50 g of water and 7.50 g of ethanol. To this mixture, 0.5 g of aqueous ammonia was then added. Followed by the addition of solution B to the solution A, 1.8 g of Cab-o-Sil was added and stirred the mixture for 1 h. The obtained gel with a *pH* value of 11.5 was transferred into a 0.30 l stainless steel autoclave and heated at 383 K for 5 days. The product was filtered, washed with demineralized water, dried at 353 K, and calcined at 823 K in a flow of synthetic air (20 vol.% oxygen, 60 l/h). In order to obtain H-[Si]MCM-41 material, the calcined Na-form of [Si]MCM-41 was ion-exchanged twice with 0.1 M ammonium nitrate solution for 3 h at 333 K. After ion exchange, the material was filtered, washed, dried at 353 K, and calcined at 773 K [143].

4.1.7 Synthesis of H-[Al]MCM-41 material

The synthesis procedure of aluminum-containing mesoporous MCM-41 ([Al]MCM-41 [143]) material was similar to that of siliceous MCM-41 material excepting that 0.025 g of sodium hydroxide dissolved in 2.00 g of water was added to the solution A, and 1.30 g of hydrated aluminum sulfate ($Al_2(SO_4)_3 \cdot 18H_2O$) dissolved in

12.50 g of water was added to the obtained gel and stirred for 90 min. The H-form of [Al]MCM-41 (H-[Al]MCM-41) was obtained by ion exchange of Na-form of [Al]MCM-41 material as described in Section 4.1.6.

4.1.8 Dehydration

For dehydration, the above-mentioned catalysts were filled into glass tubes of *ca.* 3 mm diameter, and fixed by stop cocks. The tubes were inserted in a programmable oven and connected to a vacuum line. The following programme was used for the temperature control of the oven: In the first step, the samples were heated from 298 K to 393 K at a rate of 0.5 K min^{-1} and maintained for 3 h. In the next step, the oven temperature was increased from 393 K to 723 K at a rate of *ca.* 1 K min^{-1} and maintained for 12 h. Subsequently, the glass tubes were cooled to room temperature. Finally, the glass tubes were sealed and reopened under nitrogen flow in a glove box prior to their use.

4.1.9 Preparation of H/D-exchanged catalysts

To study the interaction of reactant molecules (oximes) with surface sites of solid catalysts by ^2H MAS NMR spectroscopy (see Chapter 6), deuterated catalysts, such as H/D-ZSM-5, H/D-SBA-15, H/D-[Al]SBA-15, were prepared by the H/D exchange of OH groups using D_2O vapor. The procedure is as follows: Initially, the non-deuterated catalysts were dehydrated at 723 K as described in Section 4.1.8. After dehydration, the samples were cooled to room temperature. Subsequently, the samples were kept in contact with D_2O vapor for one hour. Then, the samples were dehydrated again at 473 K for 2 h. This procedure was repeated for 5 times. Finally, the glass tubes containing deuterated catalysts were sealed.

4.1.10 Preparation of H/D-exchanged catalyst/oxime mixtures

Mixtures of oxime (non-enriched cyclohexanone oxime or cyclododecanone oxime) and the H/D-exchanged catalysts were prepared as follows: *Ca.* 10-15 mg of non-deuterated oxime was initially evacuated at room temperature and mixed with *ca.* 20 mg of H/D-exchanged catalyst in a glove box under dry nitrogen. The mixtures were then

transferred into 2.5 mm MAS NMR rotors for ^{2}H MAS NMR measurements as described in Section 4.5.2.

4.1.11 Organic synthesis of cyclohexanone oxime-D_{11}

Typical synthesis procedure of cyclohexanone oxime-D_{11} is as follows: In a 25 ml round-bottom flask, 1.00 g of deuterated hydroxylamine-hydrochloride (ND_2OD**.**DCl, CDN Isotopes, Lot#B218P2) was dissolved in 4.28 g of deuterated water. Subsequently, 0.86 g of sodium acetate (Riedel-de Haën) was then added and the solution was warmed to 313 K. Finally, 1.00 g of cyclohexanone-D_{10} (CDN Isotopes, Lot#G126P13) was added dropwise under stirring. After the complete addition of cyclohexanone, the flask was sealed and shaken vigorously until the oxime was precipitated as a fine white powder. The solid product was collected by vacuum filtration and dried in air for 24 h at room temperature.

4.1.12 Preparation of cyclohexanone oxime-D_{11}/catalyst mixtures

To study the vapor-phase Beckmann rearrangement by *in situ* ^{1}H MAS NMR spectroscopy (see Chapter 6), the mixtures of non-deuterated catalyst and deuterated cyclohexanone oxime-D_{11} were prepared as follows: Initially, cyclohexanone oxime-D_{11} was evacuated at room temperature and mixed with dehydrated non-deuterated catalyst (silicalite-1 and H-ZSM-5) in a ratio of *ca.* 1:1 (one oxime molecule per OH group). The mixtures were then transferred into 4 mm MAS NMR rotors under dry nitrogen flow in a glove box. The mixtures in the rotors were heated at different reaction temperatures between 393 K and 523 K. To obtain a homogeneous mixture, the sample was initially heated for 30 min at 393 K, while at the higher reaction temperatures the samples were heated for 20 min only. Subsequently, the mixtures were cooled to room temperature to record the ^{1}H MAS NMR spectra at room temperature as described in Section 4.5.1.

4.1.13 Organic synthesis of ^{15}N-cyclohexanone oxime

A typical procedure for the synthesis of ^{15}N-enriched cyclohexanone oxime is as follows: In a 25 ml round-bottom flask, 1.00 g of ^{15}N-hydroxylamine-hydrochloride (^{15}N-enrichment of 98% +, Cambridge Isotope Laboratories, Lot#PR-15516) was dissolved in 4.28 g of demineralized water. Subsequently, 0.86 g of sodium acetate (Riedel-de Haën

AG) was added and the solution was heated to 313 K. Finally, 1.00 g of cyclohexanone was added dropwise under stirring. After the complete addition of cyclohexanone, the flask was sealed and shaken vigorously until the oxime was precipitated as a fine white powder. The solid product was collected by vacuum filtration and dried in air for 24 h at room temperature.

4.1.14 Preparation of ^{15}N-cyclohexanone oxime/catalyst mixtures

To study the vapor-phase Beckmann rearrangement of ^{15}N-cyclohexanone oxime into ε-caprolactam by *in situ* ^{15}N CP and HPDEC MAS NMR spectroscopy (see Chapter 7), mixtures of ^{15}N-cyclohexanone oxime and the solid catalysts were prepared. The typical procedure is as follows: *ca.* 20 mg of ^{15}N-cyclohexanone oxime was initially evacuated at room temperature and mixed with *ca.* 300 mg of dehydrated zeolite in a glove box under dry nitrogen. In the case of mixtures of ^{15}N-cyclohexanone oxime and dehydrated mesoporous catalysts, the amounts of ^{15}N-oxime and catalysts used were *ca.* 15 mg and 150 mg, respectively. The mixtures were then transferred into 7 mm MAS NMR rotors under dry nitrogen flow and heated at reaction temperatures between 393 K and 523 K as described in Section 4.1.12. Subsequently, the mixtures were cooled to room temperature to record the ^{15}N MAS NMR spectra at room temperatures as described in Section 4.5.4.

4.1.15 Loading of ^{13}C-methanol

In order to study the influence of the additive methanol in the vapor-phase Beckmann rearrangement of ^{15}N-cyclohexanone oxime (see Chapter 8), ^{13}C-methanol (^{13}C-enrichment of 99%, chemical purity of 98%+, purchased from Cambridge Isotope Laboratories, Inc.) was adsorbed on the ^{15}N-oxime/catalyst mixtures at a partial pressure of 70 mbar using a vacuum line. The methanol loadings of the ^{15}N-oxime/silicalite-1, ^{15}N-oxime/SBA-15, ^{15}N-oxime/H-ZSM-5, and ^{15}N-oxime/[Al]SBA-15 mixtures were 0.7, 1.4, 0.7, and 1.4 mmol g^{-1}, respectively. The mixtures were then transferred into 7 mm MAS NMR rotors under dry nitrogen flow and heated at reaction temperatures between 393 K and 523 K as described in Section 4.1.12. Subsequently, the mixtures were cooled to room temperature to record the ^{15}N and ^{13}C MAS NMR spectra at room temperature as described in Sections 4.5.4 and 4.5.5, respectively.

4.2 Physicochemical characterization techniques

4.2.1 Powder X-ray diffraction (XRD)

X-ray diffraction is a versatile, non-destructive, quantitative, and primary technique employed for the characterization of zeolites and mesoporous materials [144]. XRD is a fingerprint technique and it is used to identify the phase, purity, and crystallinity, and to find lattice parameters. In addition, structural properties of powder materials, such as stress, grain size, phase composition, and crystal orientation, can be studied. In this thesis, the phase identification of zeolites and mesoporous materials under study was accomplished by recording the X-ray diffractograms on Siemens D5000 and Bruker D8 instruments with the CuKα radiation (λ = 0.514 nm). The XRD patterns of zeolites were recorded in the range of 2θ = 3 to 50°, while for mesoporous materials the range of 2θ = 0 to 10° was used.

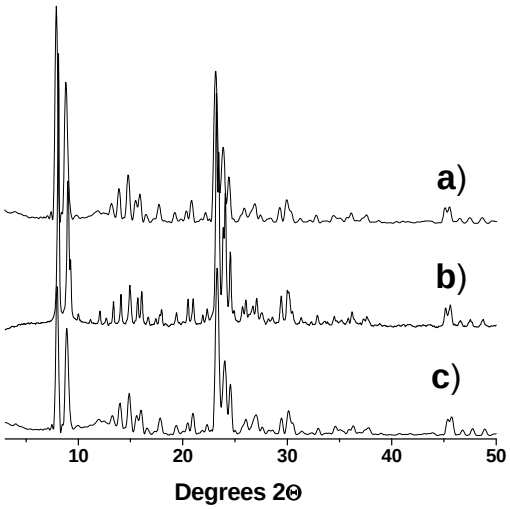

Figure 4.1. XRD patterns of calcined silicalite-1 (a), ZSM-5 (b), and [B]ZSM-5 (c).

The XRD patterns of calcined silicalite-1, ZSM-5, and [B]ZSM-5 zeolites show similar reflection lines characteristic for the MFI structure with appreciable crystallinity (Fig. 4.1). On the other hand, the XRD patterns of mesoporous SBA-15, [Al]SBA-15, Na-[Si]MCM-41, and Na-[Al]MCM-41 materials show the reflections of the (1 0 0), (1 1

0), and (2 0 0) planes, which are typical for mesoporous materials (Figs. 4.2-4.5). These three peaks indicate the well-ordered structure of mesoporous materials.

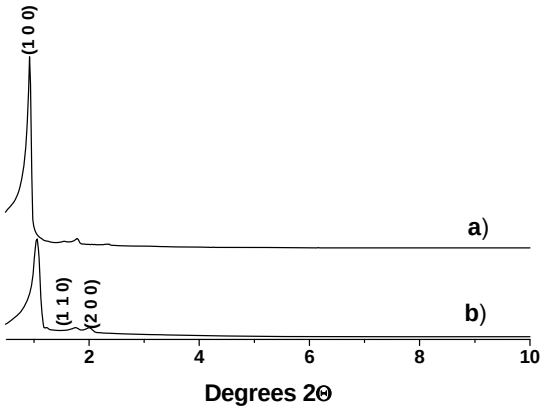

Figure 4.2. XRD patterns of as-synthesized (a) and calcined SBA-15 (b).

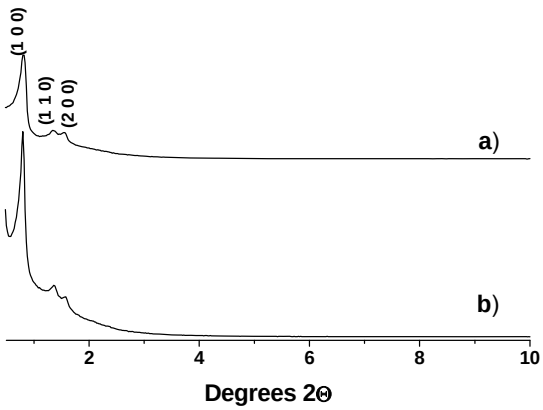

Figure 4.3. XRD patterns of as-synthesized (a) and calcined [Al]SBA-15 (b).

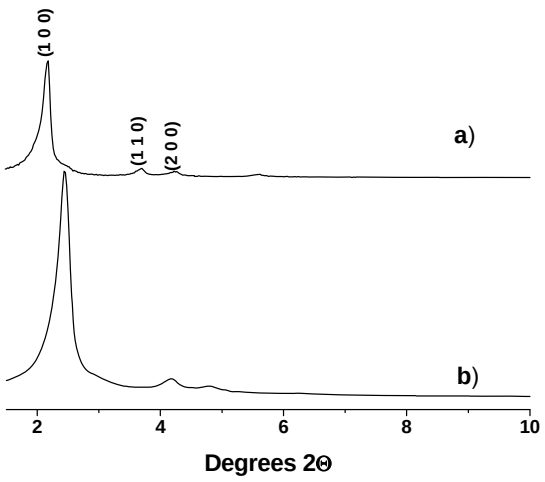

Figure 4.4. XRD patterns of as-synthesized (a) and calcined Na-[Si]MCM-41 (b).

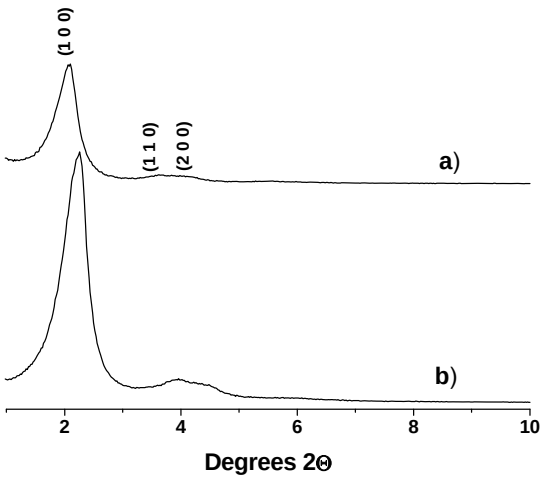

Figure 4.5. XRD patterns of as-synthesized (a) and calcined Na-[Al]MCM-41 (b).

4.2.2 Elemental analysis and BET surface measurements

Optical emission spectrometry with inductively coupled plasma (ICP-OES) is an analytical technique used for the chemical analysis of the samples. The principle of this analysis is the generation of a plasma. When samples are passed through this plasma, the atoms or ions emit the light of characteristic wavelengths. The light intensity is correlated with the concentration of the atoms under study. The BET surface area, pore volume, and average pore diameters were measured by N_2 adsorption.

Table 4.1. Physiochemical properties of the catalysts under study.

Catalyst (calcined)	n_{Si} / n_{Al}	n_H / mmol g^{-1}	BET surface area / m^2 g^{-1}	Pore volume / cm^3 g^{-1}	Average pore diameter / nm
Silicalite-1	1700	0.31	365	0.20	0.55[a]
H-ZSM-5	14	1.12	338	0.16	0.55[a]
H-[B]ZSM-5	38[b]	0.65	355	0.19	0.55[a]
SBA-15	1800	2.81	986	1.00	5.65
[Al]SBA-15	9	1.29	672	1.54	8.97
H-[Si]MCM-41	1080	2.69	998	0.91	2.95
H-[Al]MCM-41	11	2.00	914	0.86	3.09

[a]) According to Ref. [22]. [b]) n_{Si} / n_B ratio.

In the current work, a Perkin Elmer Plasma 400 spectrometer was used for the chemical analysis. Prior to this analysis, solid samples were dissolved in concentrated acids, such as HF (3 ml), HCl (2 ml), and HNO_3 (2 ml). For BET measurements an

automated nitrogen adsorption analyzer (Micromeritics, ASAP 2010) was utilized. The physiochemical properties of the catalysts under study are presented in Table 4.1.

4.2.3 Scanning electron microscopy (SEM)

Scanning electron microscopy (SEM) has been applied to study the morphology of solid specimens, such as zeolites and the other solid catalysts. SEM gives information on crystal size and shape (*e.g.* spherical, cubic, hexagonal *etc.*) of solid catalysts. The working principle of SEM is as follows: The electron gun of the SEM produces an electron beam by heating up the filament (usually made of tungsten, which act as the cathode). When the electron beam scans the sample, secondary or backscattered electrons are collected by the detector. The detector converts the secondary electrons to a signal, which is visible on the screen to produce the image of the specimen under study.

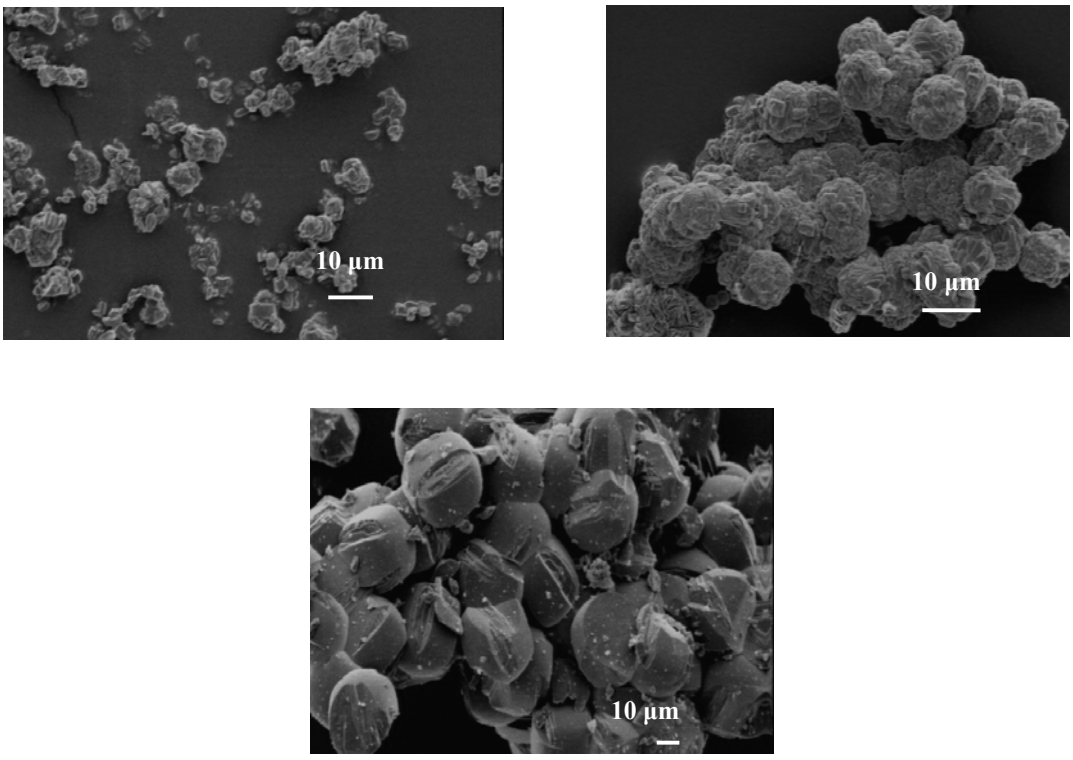

Figure 4.6. SEM images of silicalite-1 (top, left), ZSM-5 (top, right), and [B]ZSM-5 (bottom).

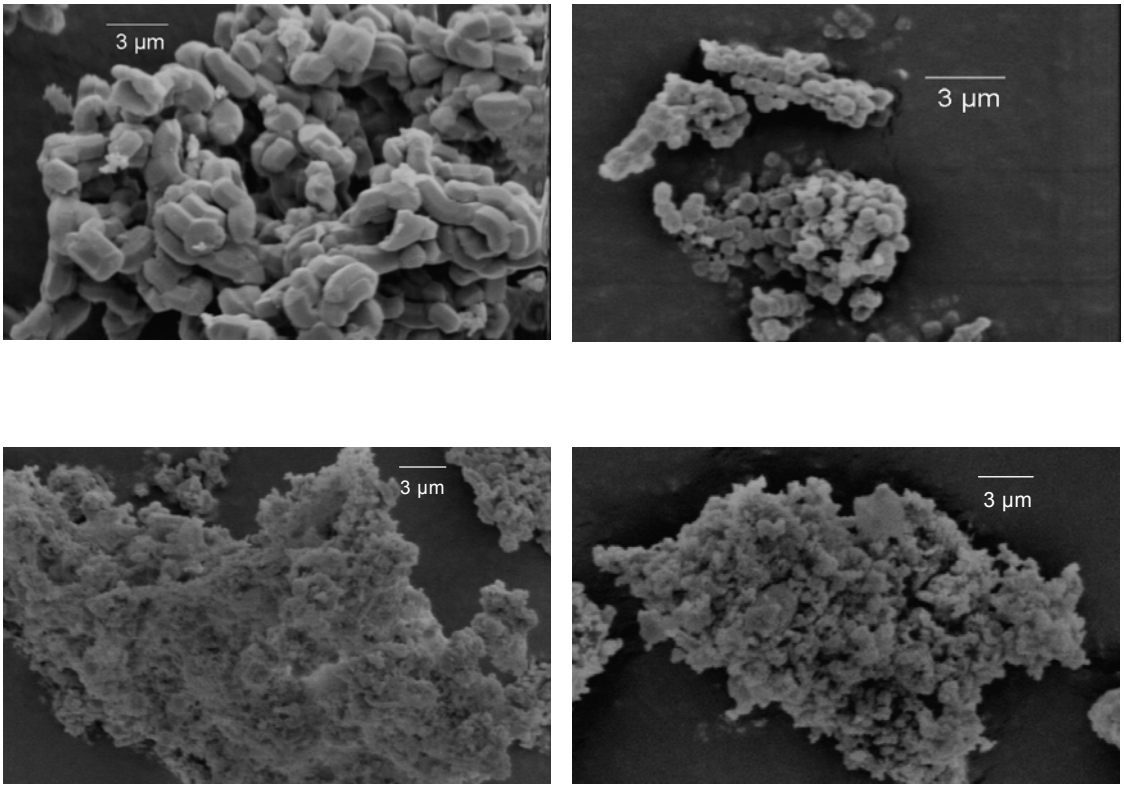

Figure 4.7. SEM images of mesoporous SBA-15 (top, left), [Al]SBA-15 (top, right), Na-[Si]MCM-41 (bottom, left), and Na-[Al]MCM-41 (bottom, right) materials.

In this thesis, the morphological studies were carried out on a CAM SCAN 44 electron microscope. Since the solid sample must be electrically conductive for the SEM measurements, gold sputtering was done prior to the analysis. Fig. 4.6 represents the SEM images of silicalite-1, ZSM-5, and [B]ZSM-5. All the three zeolite samples show well-defined morphologies indicating highly crystalline materials. The crystal size of silicalite-1, ZSM-5 and [B]ZSM-5 are < 5, < 10, and > 10 µm, respectively. The SEM images of mesoporous materials are represented in Fig. 4.7. In comparison to zeolites, mesoporous materials display different images due to their amorphous nature. The SBA-15 and [Al]SBA-15 materials show noodle-like shapes, which are typical for SBA-15 materials [35, 36]. In contrast, mesoporous H-[Si]MCM-41 and H-[Al]MCM-41 material show no well-defined crystal structures as represented by the agglomerated morphologies in Fig. 4.7, bottom.

4.3 Introduction to solid-state NMR spectroscopy

4.3.1 Principles of solid-state NMR spectroscopy

Nuclear magnetic resonance (NMR) is a physical phenomenon, which is utilized to elucidate physical, chemical, electronic, and structural information on molecules in solution and of compounds in the solid state. For the general principles of NMR, see Refs. [145-147]. The liquid- and solid-state NMR spectroscopy are distinguished by their Hamiltonians. In liquid NMR spectroscopy, signal averaging is achieved by thermal motion of the molecules. In contrast, nuclei in solids, such as solid catalysts and adsorbate complexes, are fixed in space and experience solid-state interactions leading to a strong line-broadening of NMR signals. In addition to the Zeeman interaction, the dominating line-broadening interactions in solid-state NMR are described by the following equation [148]:

$$\hat{H} = \hat{H}_{\mathrm{II}} + \hat{H}_{\mathrm{IS}} + \hat{H}_{\mathrm{CSA}} + \hat{H}_{\mathrm{Q}} \qquad (1)$$

in which the total Hamiltonian is the sum of the Hamiltonians of the homonuclear and heteronuclear dipole-dipole interactions, the chemical shift anisotropy, and the quadrupolar interaction (for spins $I > ½$), respectively [148].

4.3.2 Dipolar interactions

Dipolar interactions result from the interaction of the nuclear spin under study with the dipole moments of neighboring nuclear spins. This is a direct through space interaction, which depends on the magnetogyric ratio γ of each nucleus as well as the distance r_{ij} between two nuclei. The homonuclear dipolar interaction is the interaction between the magnetic dipole moments of equal nuclei, while the heteronuclear interaction is the interaction between the magnetic dipole moments of different nuclei. The Hamiltonian of the homonuclear interaction describes the dipolar coupling between the nuclei i and j having the same nuclear spins I [149]:

$$\hat{H}_{\mathrm{II}} = ½\, \gamma_{\mathrm{I}}^2 h^2 r_{ij}^{-3}\, (\hat{I}_i\hat{I}_j - 3\hat{I}_{iz}\hat{I}_{jz})(3\cos^2\theta_{ij} - 1) \qquad (2)$$

where γ_I is nuclear magnetogyric ratios of the interacting nuclei *i* and *j*. Here, r_{ij} is the internuclear distance, and θ_{ij} is the angle between the vectors of r_{ij} and the external magnetic field $\boldsymbol{B_0}$.

In the case of the heteronuclear dipolar interaction between the nuclei of spins *I* and *S*, the Hamiltonian is given by [149]:

$$\hat{H}_{IS} = \frac{1}{2}\gamma_I\gamma_S h^2 r_{is}^{-3}\hat{I}_{Iz}\hat{I}_{Sz}(1 - 3\cos^2\theta_{IS}) \quad (3)$$

where γ_I, γ_S are the magnetogyric ratios of nuclei with spins *I* and *S*, r_{is} is the internuclear distance, and θ_{IS} is the angle between the vectors of r_{ij} and the external magnetic field $\boldsymbol{B_0}$.

4.3.3 Chemical shift anisotropy

The chemical shielding interaction, also described as chemical shift anisotropy (CSA), is defined as the interaction of the nuclear spins with their surrounding electrons. It depends on the shielding of the nuclear spin by its electronic environment (*e.g.* electronegativity). The analytical expression of the Hamiltonian is described by [150]:

$$\hat{H}_{CSA} = \gamma h I \sigma B_0 \quad (4)$$

where σ is the shielding tensor. The isotropic shielding value (σ_{iso}) is obtained by [148]:

$$\sigma_{iso} = (\sigma_{11} + \sigma_{22} + \sigma_{33})/3 \quad (5)$$

The isotropic value of the chemical shift is

$$\delta_{iso} = (\delta_{11} + \delta_{22} + \delta_{33})/3 \quad (6)$$

where δ_{11}, δ_{22}, δ_{33} are the principle values of the chemical shift tensor. By the assumption of the inequality of the principle values ($\delta_{11} > \delta_{22} > \delta_{33}$), the chemical shift anisotropy, δ_{CSA}, and the asymmetry parameter, η_{CSA}, are defined in the case of $|\delta_{11} - \delta_{iso}| \geq |\delta_{33} - \delta_{iso}|$, by [150]:

$$\delta_{CSA} = 3(\delta_{11} - \delta_{iso})/2 \quad (7)$$

and

$$\eta_{CSA} = (\delta_{22} - \delta_{33})/(\delta_{11} - \delta_{iso}) \quad (8)$$

while in the case of $|\delta_{11} - \delta_{iso}| \leq |\delta_{33} - \delta_{iso}|$, by

$$\delta_{CSA} = 3(\delta_{33} - \delta_{iso})/2, \quad (9)$$

and

$$\eta_{CSA} = (\delta_{22} - \delta_{11})/(\delta_{11} - \delta_{iso}). \quad (10)$$

4.3.4 Quadrupolar interaction

In addition to the above-mentioned interactions, the quadrupolar interaction further causes a line-broadening of the NMR signals of nuclei having spins $I > 1/2$ (*e.g.* ^{2}H, ^{11}B, and ^{27}Al nuclei). It is defined as the interaction of the electric quadrupole moment eQ of the nucleus with the electric field gradient (EFG) at the site of the nucleus. The EFG is a traceless tensor and it can be expressed by [149]:

$$V_{ij} = \partial^2 V / \partial x_i \partial x_j \qquad (11)$$

where V is the electric potential and x_i, x_j are Cartesian coordinates. In the principle axis system of V_{ij}, the Hamiltonian of the quadrupolar interaction of nuclei with spin $I > ½$ is

$$\hat{H}_Q = \{e^2qQ / 4I(2I - 1)\}[3I_z^2 - I^2 + \eta (I_x^2 - I_y^2)] \qquad (12)$$

with $Vzz \geq Vyy \geq Vxx$ and the z-component $Vzz = eq$ of the EFG. The characteristic parameters of quadrupole nuclei, such as the asymmetry parameter, η, and qudrupole coupling constant, C_{QCC}, are defined by [148-150]:

$$\eta = (Vxx - Vyy) / Vzz \qquad (13)$$

and

$$C_{QCC} = e^2qQ / h \qquad (14)$$

Generally, the quadrupolar interaction is weaker than the Zeeman interaction ($\hat{H}_Q << \hat{H}_0$) and can be considered as a perturbation. In this case, the frequency function of the $m - 1 \rightarrow m$ transition is described by a first- and second-order frequency function [149]:

$$\nu_m = \nu_0 + \nu_m^{(1)} + \nu_m^{(2)} \qquad (15)$$

In the case of central transition (m = -1/2 to +1/2), the second-order frequency function is given by [149]:

$$\nu_{1/2} = -(\nu_Q^2 / 16\,\nu_L)(I(I + 1) - 3/4)(1 - \cos^2\theta)(9\cos^2\theta - 1) \qquad (16)$$

where θ is the angle between z-axis in the principle system and the external magnetic field $\boldsymbol{B_0}$. The quadrupole frequency is given by [149]:

$$\nu_Q = 3e^2qQ / 2hI(2I - 1) \qquad (17)$$

4.4 High-resolution solid-state NMR techniques

Due to the interactions described in Sections 4.3.2 to 4.3.4, solid-state NMR signals are often affected by line-broadening mechanisms. As a result, the important structural information can be lost or hidden in the broad signals. In the past decades,

several sophisticated experimental techniques have been developed in order to improve the spectral resolution. These techniques allow an averaging of interactions. The most frequent techniques are described in the following Sections.

4.4.1 Magic Angle Spinning

Magic angle spinning (MAS) is a high-resolution solid-state NMR technique, which involves the rotation of solid samples at spinning rates of several kHz around a fixed axis at an angle of 54.74° to the direction of the external magnetic field [151]. Fig. 4.8 indicates the schematic representation of MAS. The angle θ_m = 54.74° is obtained from the geometric term ($3\cos^2\theta_m$ - 1), which becomes zero leading to a maximum averaging of solid-state interactions. By applying this technique, most of the anisotropic interactions in solid samples can be averaged and the MAS NMR signal consists of a narrow central line at the centre of gravity ν_{cg}, and spinning sidebands at [148]:

$$\nu_k = \nu_{cg} + k\nu_{rot} \qquad (18)$$

where $k = \pm 1, \pm 2, \ldots$ denotes the order of spinning sidebands and ν_{rot} is the sample spinning rate [148, 151]. In the case of MAS at low spinning rates, the NMR spectrum consists of many spinning sidebands. The number of spinning sidebands can be reduced by using high spinning rates.

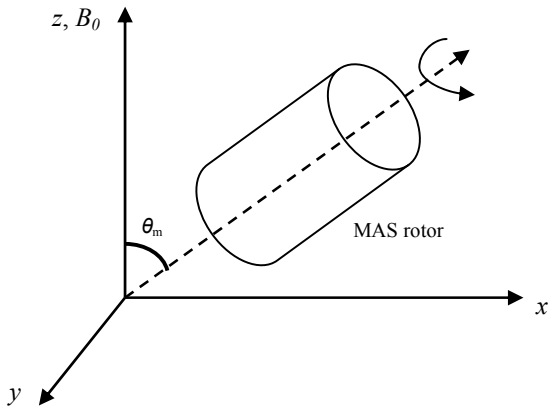

Figure 4.8. Schematic representation of MAS [151].

4.4.2 Cross polarization (CP)

The NMR spectra of nuclei with small magnetogyric ratios and low natural abundance (*e.g.* ^{15}N nuclei) are often affected by low signal to noise ratios. It is, therefore, necessary to apply double resonance techniques, such as cross polarization (CP). It improves the signal to noise ratio significantly, if applied together with magic angle spinning (MAS). This technique is most frequently applied to nuclei having low natural abundance (*e.g.* ^{15}N) interacting with nuclei having high natural abundance (*e.g.* ^{1}H). The pulse sequence used for CP experiments is shown in Fig. 4.9.

The experiment consists of the application of a $\pi/2$ pulse to the high abundant spins *I* and the polarization transfer from the spins *I* to the rare spins *S* during the contact pulse (τ_{CP}) applied simultaneously to spins *I* and *S*. After the contact period, the free induction decay of the spins *S* is observed, while a decoupling pulse is applied to the spins *I* in order to average the dipolar interactions. The maximum polarization transfer is achieved if the Hartmann-Hahn condition is fulfilled [152]:

$$\alpha_I \gamma_I B_{1I} = \alpha_S \gamma_S B_{1S} \qquad (19)$$

where $\boldsymbol{B_{1I}}$ and $\boldsymbol{B_{1S}}$ denote the amplitude of the radio frequency fields applied to the spins *I* and *S*, respectively. The parameter α_I is equal to $(I(I + 1) - m(m - 1))^{1/2}$, provided that the radio frequency pulse applied to spins *I* selectively induces transitions between the levels with the magnetic spin quantum numbers m - 1 and m. The same expression can be used for α_S.

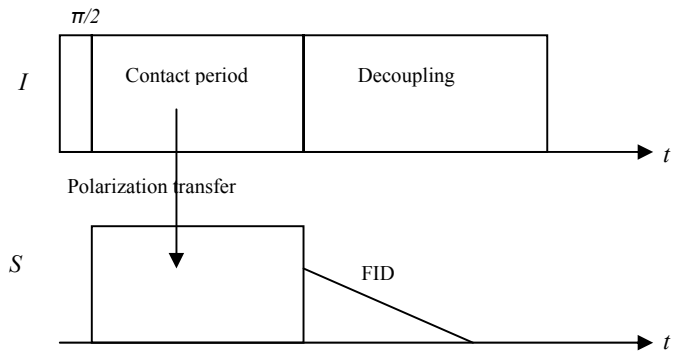

Figure 4.9. Experimental scheme of the CP pulse sequence [14].

4.5 Characterization by solid-state MAS NMR spectroscopy

4.5.1 ^{1}H MAS NMR measurements

^{1}H MAS NMR measurements were performed on a Bruker MSL 400 spectrometer at the resonance frequency of 400.1 MHz using a 4 mm probe with sample spinning rates of 8.0 to 9.0 kHz. The spectra were recorded by applying a $\pi/2$ pulse with a length of 2.1 μs and a recycle delay of 10 s. For the quantitative evaluation of ^{1}H MAS NMR signals, dehydrated zeolite H,Na-Y (n_H = 1.776 mmol g^{-1}) with a cation exchange degree of 35% was used as an external intensity standard.

4.5.2 ^{2}H MAS NMR measurements

^{2}H MAS NMR measurements were acquired on a Bruker MSL 400 spectrometer at the resonance frequency of 61.4 MHz using a 2.5 mm MAS NMR probe with the sample spinning rate of *ca.* 25 kHz. The spectra were recorded by applying a $\pi/2$ pulse with a length of 4.0 μs and a recycle delay of 2 s.

4.5.3 *In situ* and *ex situ* solid-state ^{11}B MAS NMR measurements

To study the nature of active sites and the coordination change of framework boron atoms in H-[B]ZSM-5 zeolite (see Chapter 5), probe molecules, such as pyridine, ammonia, and acetone, were adsorbed on H-[B]ZSM-5 zeolite using the *in situ* injection equipment described in Fig. 4.10 [153, 154]. The main components of the equipment are a double-bearing 4 mm MAS NMR probe, a saturator, an injection tube inserted into the MAS NMR rotor, and a mass flow controller. The saturator is used to load the carrier gas with probe molecules, which are adsorbed on zeolite sample under study. The saturator is connected to a cryostat, which is used to maintain the temperature at *ca.* 285 K. The amounts of adsorbed molecules were controlled by the flow of the carrier gas (dry nitrogen) *via* the mass flow controller and the duration of the flow.

Before the *in situ* MAS NMR investigations under flow conditions, the dehydrated H-[B]ZSM-5 zeolite was filled into a 4 mm MAS rotor under dry nitrogen flow in a glove box. The catalyst in the rotor was carefully shaped to a cylindrical catalyst bed using a special tool. The rotor was closed by a cap with a hole, which is blocked by a plug. Subsequently, this rotor with the cap was transferred into the turbine.

The plug on the cap was removed and the injection tube was quickly inserted into the rotor. During the transportation and insertion of injection tube, nitrogen gas was purged to avoid the rehydration of the dehydrated sample.

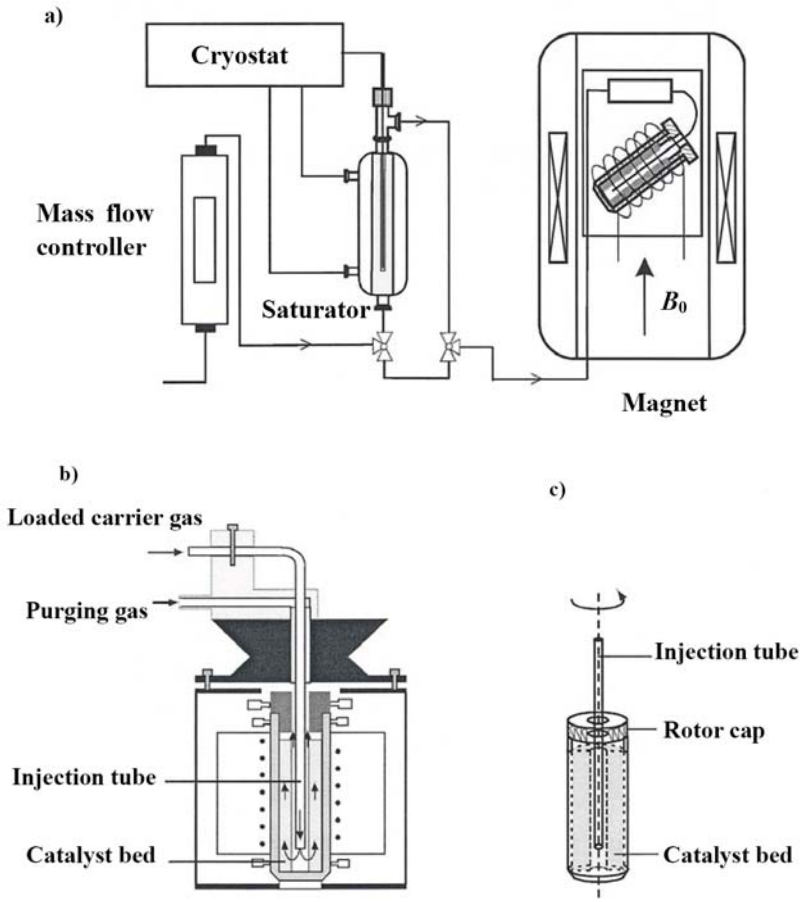

Figure 4.10. *In situ* MAS NMR injection for studies under flow conditions (a), individual components (b and c) [153,154].

Probe molecules with low vapor pressures, such as dimethyl sulfoxide (DMSO), tetrahydrothiophene and acetamide, were *ex situ* loaded. In this case, the dehydrated zeolite H-[B]ZSM-5 and the probe molecule were quantitatively mixed in a glass bottle and then transferred into a glass tube and sealed. To reach a proper distribution of the probe molecules over the H-[B]ZSM-5 particles, the mixtures in the sealed glass tubes were heated at 323 K (dimethyl sulfoxide, tetrahydrothiophene) or 352 K (acetamide) for

1 h. To describe the coverage of hydroxyl groups with probe molecules, the equivalent number *equiv.* was used. This is the ratio of the number of adsorbed molecules n_{ad} and the number of SiOH groups n_H, both determined by ^{1}H MAS NMR spectroscopy. For the quantitative evaluation of ^{1}H MAS NMR signals, dehydrated zeolite H,Na-Y Y (n_H = 1.776 mmol g^{-1}) with a cation exchange degree of 35% was used as an external intensity standard (see Section 4.5.1).

^{11}B MAS NMR spectra were acquired on a Bruker MSL 400 spectrometer at the resonance frequency of 128.3 MHz using a 4 mm MAS NMR probe with sample spinning rates of 8.0 to 9.0 kHz. The spectra were recorded by applying a single pulse excitation with a pulse length of 1 μs (π/8) and a recycle delay of 2 s.

4.5.4 *In situ* solid-state ^{15}N NMR measurements

The ^{15}N CP and HPDEC MAS NMR spectra were recorded at ambient temperature on a Bruker MSL 400 spectrometer at the resonance frequency of 40.53 MHz and using a 7 mm MAS NMR probe with sample spinning rates of 3.5 to 4.7 kHz. The ^{15}N CP/MAS NMR spectra were obtained with the contact period of 5 ms and the recycle delay of 2 s. To record ^{15}N HPDEC MAS NMR spectra, a pulse length of 8 μs and the recycle delay of 5 s were applied. Between 1600 (H-ZSM-5) and 40000 (silicalite-1) decays were accumulated for each spectrum. All ^{15}N MAS NMR spectra were referenced to nitromethane (0.0 ppm) by calibrating to ^{15}N-enriched pyridine (-62.0 ppm) [155].

4.5.5 *In situ* ^{13}C CP/MAS NMR measurements

The ^{13}C CP/MAS NMR spectra were recorded at ambient temperature on a Bruker MSL 400 spectrometer at the resonance frequency of 100.58 MHz and using a 7 mm MAS NMR probe with the sample spinning rate of *ca.* 3.5 kHz. The ^{15}N CP/MAS NMR spectra were obtained with the contact period of 5 ms and the recycle delay of 2 s. All ^{13}C CP/MAS NMR spectra were referenced to tertramethylsilane (0.0 ppm) by calibrating to adamantane (38.55 ppm).

4.5.6 ^{29}Si HPDEC MAS NMR measurements

^{29}Si HPDEC MAS NMR spectra were acquired on a Bruker MSL 400 spectrometer at the resonance frequency of 79.5 MHZ using a 7 mm probe with sample spinning rates of 3.0 kHz to 4.0 kHz. The spectra were recorded by applying the dipolar decoupling technique (HPDEC). A pulse length of 5 μs (*ca.* π/4) and the recycle delay of 60 s were applied. Prior to the ^{29}Si MAS NMR measurements, the samples were fully rehydrated in a desiccator.

5 Characterization of zeolite H-[B]ZSM-5 upon the adsorption of probe molecules studied by ^{11}B and ^{1}H MAS NMR spectroscopy

5.1 Introduction

In comparison to aluminum-containing zeolites, boron-containing zeolites can only generate moderate acidity in the vicinity of framework boron atoms. This medium acidity is sometimes very interesting and an advantage for several heterogeneous catalytic processes, such as the vapor-phase Beckmann rearrangement [86, 89], aldehyde-ketone rearrangement [156], double bond isomerization [157], and dehydration reactions [158]. Therefore, much attention has been focused on these materials in the past two decades. To date, several boron-containing zeolites were synthesized and characterized. In particular, the H-[B]ZSM-5 zeolite has widely been applied and studied as a potential catalyst in the vapor-phase Beckmann rearrangement of cyclohexanone oxime [86, 89]. Röseler *et al*. [86] studied the vapor-phase Beckmann rearrangement using B-MFI zeolites and observed up to 95% selectivity towards ε-caprolactam on this catalyst by optimizing the reaction conditions.

In aluminum-containing zeolites, the framework aluminum is tetrahedrally coordinated, while in boron-containing zeolites the framework boron exists in both trigonal and tetrahedral coordination depending on the dehydrated and hydrated states, respectively. According to the bond-order conservation principle and quantum-chemical calculations [139, 159-162], the weaker Brønsted acid sites in boron-substituted zeolites are attributed to the longer bond distance between the framework boron atom and the framework oxygen atom bound to the hydroxyl proton. The bond between framework boron and oxygen atoms in boron-substituted zeolites can effectively be formed and broken upon the hydration and dehydration, respectively [163-166]. Therefore, boron exists in a tetrahedral ($B^{[4]}$) coordination in the hydrated state and in a trigonal ($B^{[3]}$) coordination in the dehydrated state of boron-substituted zeolites [139, 163-167]. In addition, both kinds of boron species can occur in these materials depending on the hydration state and the presence of counter ions, such as template molecules [139, 163,167].

In 1985, Scholle and Veeman [164] applied solid-state ^{11}B MAS NMR spectroscopy to study the coordination change of boron atoms in H-boralite upon dehydration and rehydration. The coordination change of boron species was found to be accompanied by a variation of the ^{11}B quadrupole coupling constant C_{QCC} of framework boron atoms from C_{QCC} = 2.55±0.02 MHz for $B^{[3]}$ species to a very small C_{QCC} value for $B^{[4]}$ species. Generally, the quadrupole coupling constant C_{QCC} is a measure of the strength of the quadrupolar interaction between the electric quadrupole moment of nuclei with spin $I > 1/2$ (^{11}B: spin $I = 3/2$) and the electric field gradient at their sites (see Section 4.3.4).

Axon and Klinowski [165] reported the coordination change of boron upon the adsorption and desorption of polar organic molecules, such as anhydrous methanol and ethanol, on zeolite [Si,B]ZSM-5. In addition, it was found that non-polar solvents like anhydrous benzene could not induce a coordination change of boron [165]. Recently, Hwang *et al*. [166] investigated the boron coordination in zeolites [B]Beta, [B]SSZ-33, and [B]SSZ-42 and revealed an intermediate stage referred as defective trigonal boron species ($B^{[3]}$-I) upon the hydration of dehydrated samples characterized by a ^{11}B quadrupole coupling constant of C_{QCC} = 2.55 ± 0.1 MHz. Koller *et al*. [167] studied the boron coordination in dehydrated zeolites H-[B]Beta and H,Na-[B]Beta. While the ^{11}B MAS NMR spectra of dehydrated zeolite H-[B]Beta consist only of signals of trigonal boron species, both trigonal and tetragonal boron species were observed for dehydrated zeolite H,Na-[B]Beta with alkaline counter ions [167].

The literature concerning the nature of active centers in H-[B]ZSM-5 zeolite for the reactant molecules, and the effect of acidity or basicity of reactant molecule on the change of framework boron coordination in H-[B]ZSM-5 zeolite is scarce. The present work is a systematic investigation of the effect of probe molecules with proton affinities in the range of PA = 812 to 930 kJ mol^{-1} on the local structure of boron atoms in dehydrated zeolite H-[B]ZSM-5. Since the coordination change of $B^{[3]}$ into $B^{[4]}$ species can be accompanied by a proton transfer from the zeolite framework to the probe molecules, simultaneous ^{11}B and ^{1}H MAS NMR studies have been performed. Furthermore, the reactant in the vapor-phase Beckmann rearrangement, *i.e.* cyclohexanone oxime, has two different PA values at N-site and O-site, respectively. The

proton affinity values for certain oximes were given elsewhere [127-129]. The *PA* values for many oximes at N-site are in the range of 800 to 900 kJ mol^{-1}, while at O-site are < 800 kJ mol^{-1}. Therefore, the results obtained in this work by the adsorption of different probe molecules help to understand the role of framework boron atoms in zeolites H-[B]ZSM-5 for their application as solid acid catalysts in reactions like the vapor-phase Beckmann rearrangement of cyclohexanone oxime.

5.2 *In situ* MAS NMR investigations of dehydrated zeolite H-[B]ZSM-5 upon adsorption of pyridine

Fig. 5.1, left, shows the ^{1}H MAS NMR spectra of unloaded zeolite H-[B]ZSM-5 and zeolite H-[B]ZSM-5 loaded with pyridine (*PA* = 930 kJ mol^{-1}). The ^{1}H MAS NMR spectrum of unloaded zeolite H-[B]ZSM-5 consists of signals at 1.9, 2.5, and 3.2 ppm due to silanol groups at defect sites and SiOH[B] groups in the vicinity of framework boron species [139, 163]. The quantitative evaluation of the ^{1}H MAS NMR signals at 1.9, 2.5, and 3.2 ppm gave concentrations of 0.062 ± 0.01, 0.402 ± 0.02, and 0.155 ± 0.01 mmol g^{-1}, respectively. Upon adsorption of pyridine, three new signals occurred at *ca*. 7.4, 7.9, and 8.7 ppm (Figs. 5.1b to 5.1e, left), which are explained by hydrogen atoms bound to the rings of pyridine molecules [168]. A weak signal at *ca*. 16 ppm (inserts in Figs. 5.1b and 5.1c) indicates that proton transfer occurs from the acid sites of zeolite H-[B]ZSM-5 to the probe molecules and lead to the formation of pyridinium ions ($PyrH^{+}$) [169]. Interestingly, the pyridine loading affects mainly the ^{1}H MAS NMR signal at 2.5 ppm (see Section 5.5 and Fig. 5.8). This finding indicates that this signal has to be assigned to the Brønsted acidic SiOH[B] groups in the vicinity of framework boron species, which is supported by the number of 0.409 ± 0.02 mmol g^{-1} boron atoms introduced into the framework of zeolite H-[B]ZSM-5.

The ^{11}B MAS NMR spectra of unloaded zeolite H-[B]ZSM-5 and zeolite H-[B]ZSM-5 loaded with pyridine are shown at the right-hand side of Fig. 5.1. The quadrupole pattern occurring in the ^{11}B MAS NMR spectrum of the unloaded material has singularities at *ca*. -5 and 6 ppm and corresponds to that of trigonal boron species $B^{[3]}$ described in former publications [139, 165]. Upon starting the adsorption of pyridine on zeolite H-[B]ZSM-5, the appearance of a signal of tetragonal boron species $B^{[4]}$ was

observed at -3.6 ppm (Figs. 5.1b to 5.1e). Upon higher loadings of pyridine, a coordination change of $B^{[3]}$ into $B^{[4]}$ species occurs as indicated by the decrease of the quadruple pattern of $B^{[3]}$ species. This coordination change is completed after a loading of zeolite H-[B]ZSM-5 with *ca*. 2.3 *equiv.* pyridine (Fig. 5.1e).

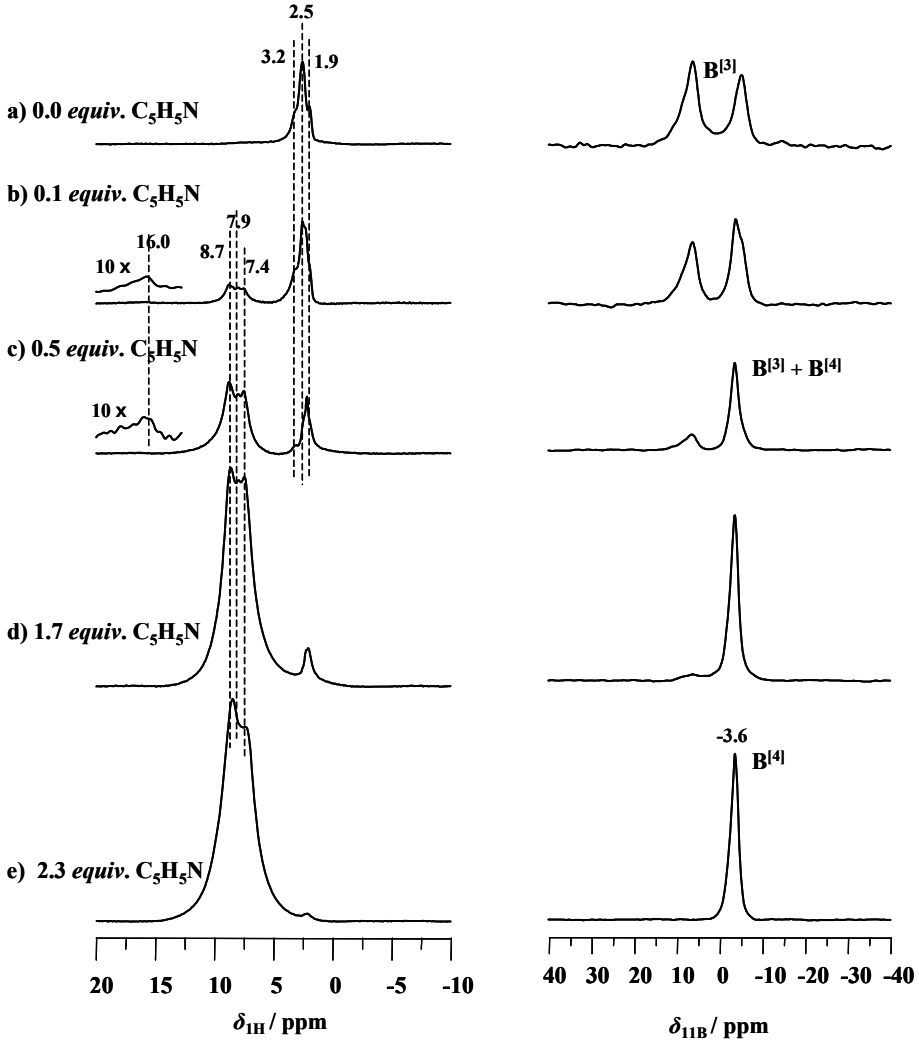

Figure 5.1. ^{1}H (left) and ^{11}B MAS NMR spectra (right) of dehydrated zeolite H-[B]ZSM-5 recorded upon *in situ* adsorption of pyridine (*PA* = 930 kJ mol^{-1}).

For the quantitative evaluation of the signals of $B^{[3]}$ and $B^{[4]}$ species in the spectra of dehydrated zeolite H-[B]ZSM-5 with different pyridine loadings, the ^{11}B MAS NMR spectra were simulated as shown in Fig. 5.2. In this case, the ^{11}B MAS NMR spectrum

was separated into two components due to $B^{[3]}$ and $B^{[4]}$ species. The parameters obtained by simulation, such as the quadrupole coupling constants C_{QCC} and the asymmetry parameters η, are summarized in Table 5.1. The quadrupole coupling constant of 0.85 MHz for $B^{[4]}$ species is the maximum C_{QCC} value, which explains the experimentally observed broadening of the corresponding ^{11}B MAS NMR signal. In Fig. 5.3, the contents of $B^{[3]}$ and $B^{[4]}$ species at different stages of the pyridine loading are plotted.

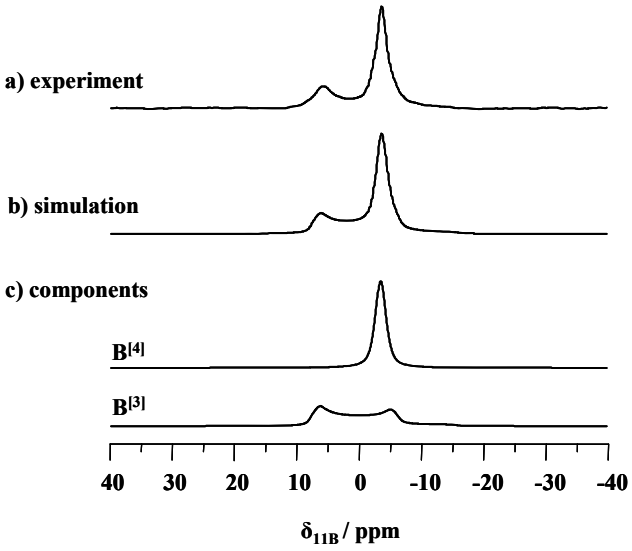

Figure 5.2. ^{11}B MAS NMR spectra of dehydrated zeolite H-[B]ZSM-5 recorded upon adsorption of 0.5 *equiv.* pyridine.

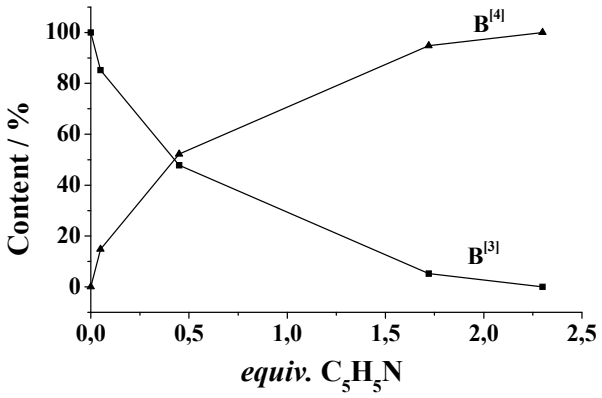

Figure 5.3. Contents of $B^{[3]}$ and $B^{[4]}$ species in dehydrated zeolite H-[B]ZSM-5 plotted as a function of the pyridine loading as obtained by an evaluation of the ^{11}B MAS NMR spectra in Fig. 5.1.

Table 5.1. Proton affinities *PA* [170] of the probe molecules used in this study, quadrupole coupling constants C_{QCC}, and asymmetry parameters η of $B^{[3]}$ and $B^{[4]}$ species in dehydrated zeolite H-[B]ZSM-5 upon adsorption of *ca*. 1 *equiv.* probe molecules.

Probe molecule	Proton affinity / kJ mol^{-1}	$B^{[3]}$		$B^{[4]}$	
		C_{QCC} / MHz	η	C_{QCC} / MHz	η
pyridine	930	2.65	0.10	0.85	0.00
dimethyl sulfoxide	884	2.75	0.10	0.85	0.00
acetamide	864	2.65	0.10	0.85	0.00
ammonia	854	2.70	0.10	0.85	0.00
tetrahydrothiophene	849	2.70	0.10	–	–
acetone	812	2.65	0.10	–	–
Nitrogen	494	2.65	0.10	–	–

5.3 *In situ* MAS NMR investigations of dehydrated zeolite H-[B]ZSM-5 upon adsorption of ammonia

The ^{1}H and ^{11}B MAS NMR studies of dehydrated zeolite H-[B]ZSM-5 loaded with different amounts of ammonia (*PA* = 854 kJ mol^{-1}) were performed using the same procedure like in Section 5.2. Upon injection of 0.1 *equiv*. ammonia into the sample volume filled with the dehydrated sample, a signal appeared at 5.0 ppm, which is shifted to 3.6 ppm after a loading of 1.7 *equiv.* ammonia (Fig. 5.4, left). In a previous work, it was found that the loading of dehydrated aluminosilicate-type zeolites with up to *ca*. 1 *equiv.* ammonia results in an ^{1}H MAS NMR signal at *ca*. 7 ppm due to chemisorption of the probe molecules, *i.e.* formation of ammonium ions [169]. The signal at 5 ppm observed for the loading of 0.1 *equiv.* ammonia on dehydrated zeolite H-[B]ZSM-5 (Fig. 5.4b, left), therefore, indicates a partial proton transfer from the zeolite framework to the probe molecules. With increasing ammonia coverage, a rapid exchange between adsorbed

(δ_{1H} = 5.0 ppm) and mobile ammonia molecules (gaseous ammonia: δ_{1H} = -0.3 ppm [51]) occurs and the low-field ^{1}H MAS NMR signal shifts to the resonance position 3.6 ppm. Again, the signal of SiOH[B] groups at 2.5 ppm is preferentially decreased upon adsorption of the probe molecules, which supports the role of these hydroxyl groups as Brønsted acid sites.

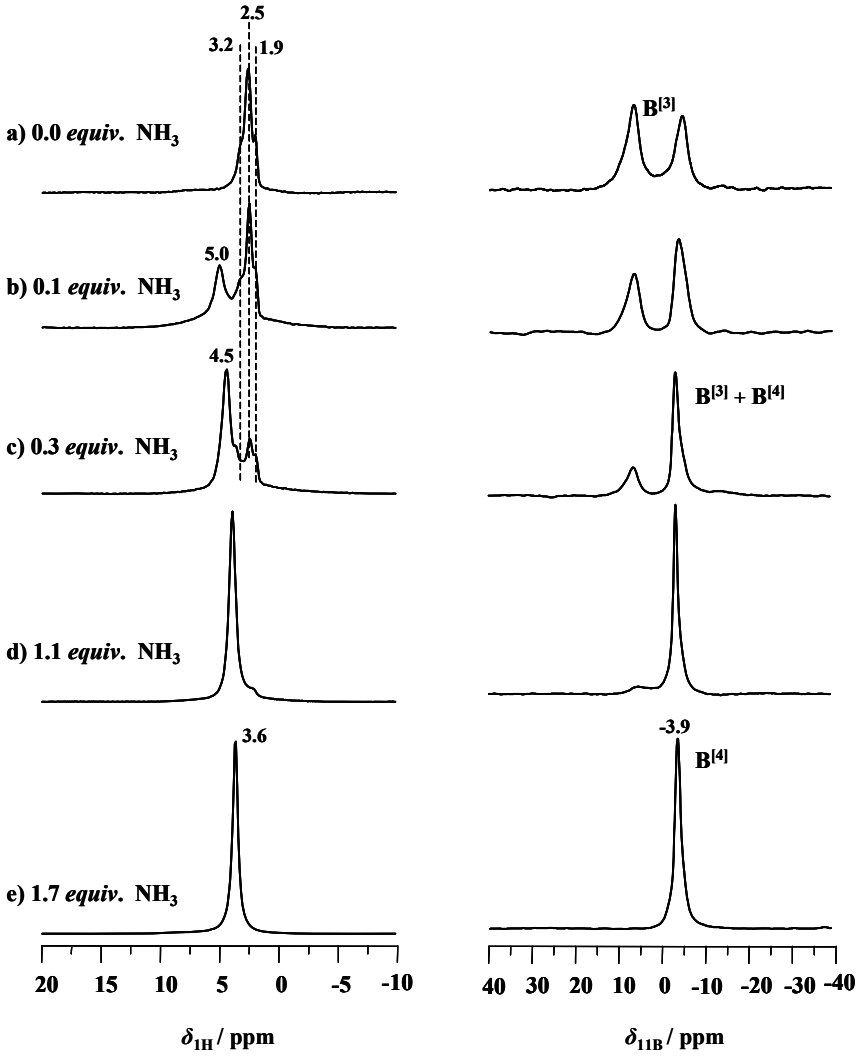

Figure 5.4. ^{1}H (left) and ^{11}B MAS NMR spectra (right) of non-hydrated zeolite H-[B]ZSM-5 recorded upon *in situ* adsorption of ammonia (*PA* = 854 kJ mol^{-1}).

The simultaneously recorded ^{11}B MAS NMR spectra of dehydrated zeolite H-[B]ZSM-5 loaded with different amounts of ammonia are shown in Fig. 5.4, right. An increasing coverage of zeolite H-[B]ZSM-5 with the probe molecules leads to a transformation of the $B^{[3]}$ into $B^{[4]}$ species resulting in an ^{11}B MAS NMR signal at -3.9 ppm (Figs. 5.4b to 5.4e). As carried out in Section 5.2, the contents of $B^{[3]}$ and $B^{[4]}$ species were evaluated and plotted as a function of the adsorbed probe molecules, which is shown in Fig. 5.5. Approximately, 1.7 *equiv.* ammonia are necessary for a complete transformation of $B^{[3]}$ into $B^{[4]}$ species. This coverage of zeolite H-[B]ZSM-5 by ammonia is slightly lower than the pyridine loading necessary for a complete transformation of $B^{[3]}$ species (2.3 *equiv.* pyridine). This may be due to the smaller size of the ammonia molecules leading to a better access of SiOH[B] groups in the vicinity of framework boron atoms.

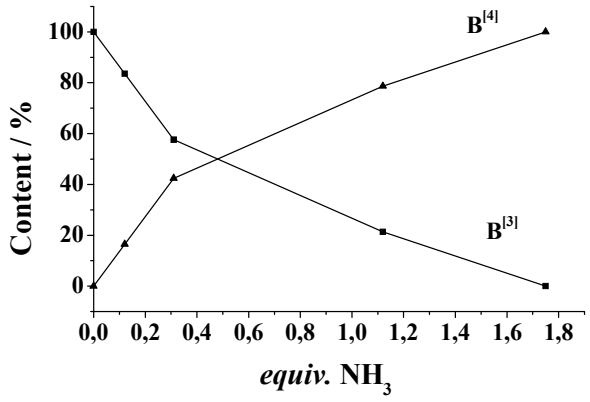

Figure 5.5. Contents of $B^{[3]}$ and $B^{[4]}$ species in dehydrated zeolite H-[B]ZSM-5 plotted as a function of the ammonia loading as obtained by an evaluation of the ^{11}B MAS NMR spectra in Fig. 5.4.

5.4 MAS NMR investigations of dehydrated zeolite H-[B]ZSM-5 upon adsorption of dimethyl sulfoxide (DMSO), acetamide, tetrahydrothiophene, and acetone

The ^{1}H and ^{11}B MAS NMR spectra obtained for dehydrated zeolite H-[B]ZSM-5 loaded with dimethyl sulfoxide, acetamide, tetrahydrothiophene, and acetone are

summarized in Fig. 5.6. In all these cases, ^{1}H MAS NMR signals of the probe molecules in the range of 2.1 to 2.7 ppm overlap the signals of hydroxyl groups at 1.9 to 3.2 ppm [168]. The application of probe molecules in natural abundance of H-isotopes (*i.e.* non-deuterated probe molecules) allowed the direct quantitative evaluation of the number of adsorbed molecules by ^{1}H MAS NMR spectroscopy.

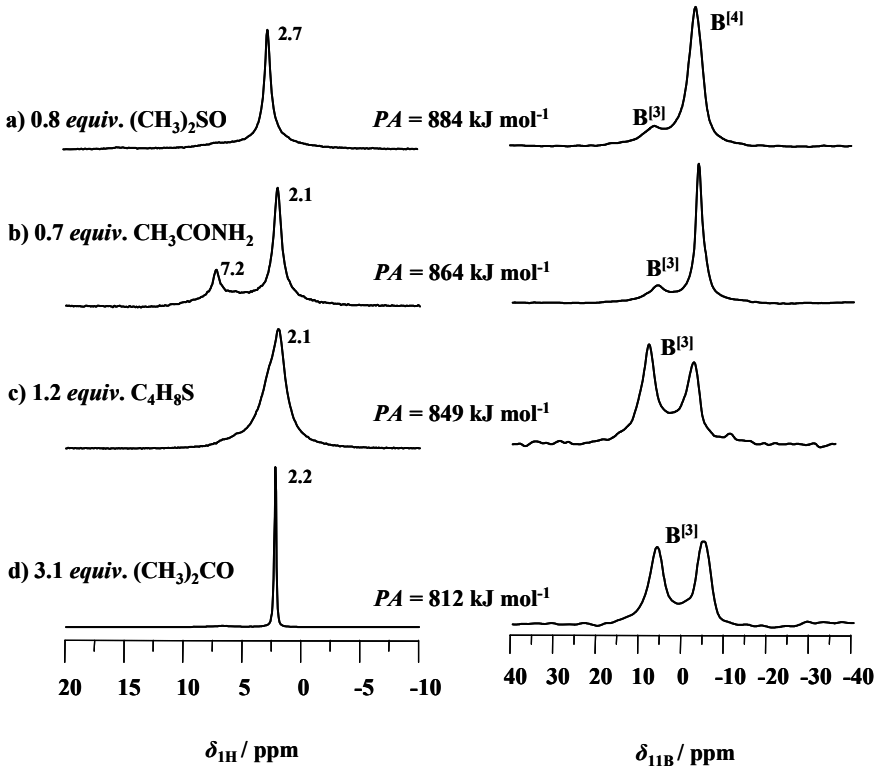

Figure 5.6. ^{1}H (left) and ^{11}B MAS NMR spectra (right) of dehydrated zeolite H-[B]ZSM-5 recorded upon adsorption of dimethyl sulfoxide (a), acetamide (b), tetrahydrothiphene (c), and acetone (d).

The ^{11}B MAS NMR spectra of zeolite H-[B]ZSM-5 loaded with the above-mentioned probe molecules show clearly two different behaviors of framework boron atoms (Fig. 5.6, right). Already the adsorption of 0.7 to 0.8 *equiv.* dimethyl sulfoxide (*PA* = 884 kJ mol^{-1}) and acetamide (*PA* = 864 kJ mol^{-1}) lead to a nearly complete transformation of B$^{[3]}$ into B$^{[4]}$ species (Figs. 5.6a and 5.6b, right). On the other hand, upon adsorption of tetrahydrothiophene (*PA* = 849 kJ mol^{-1}) and acetone (*PA* = 812 kJ

mol^{-1}), even for loadings significantly higher than 1 *equiv.*, no coordination change of $B^{[3]}$ species occurred (Figs. 5.6c and 5.6d, right).

5.5 Effect of probe molecules with different proton affinities on the acid sites and framework boron atoms in dehydrated zeolite H-[B]ZSM-5

The application of boron-substituted zeolites, such as zeolite H-[B]ZSM-5, as solid catalysts is based on the specific catalytic behavior of SiOH[B] groups in the vicinity of framework boron atoms (Scheme 5.1, left). Therefore, the relation between the interaction of these SiOH[B] groups with reactants and the local structure of framework boron atoms is an important prerequisite to understand the catalytic behavior of these zeolites. To simulate the interaction of SiOH[B] groups in dehydrated zeolite H-[B]ZSM-5 with reactants characterized by different basicities, this material was loaded with probe molecules having proton affinities of *PA* = 812 to 930 kJ mol^{-1}. In Fig. 5.7, the ^{11}B quadrupole coupling constants C_{QCC} of boron atoms in dehydrated zeolite H-[B]ZSM-5 are plotted as a function of the *PA* values of these probe molecules.

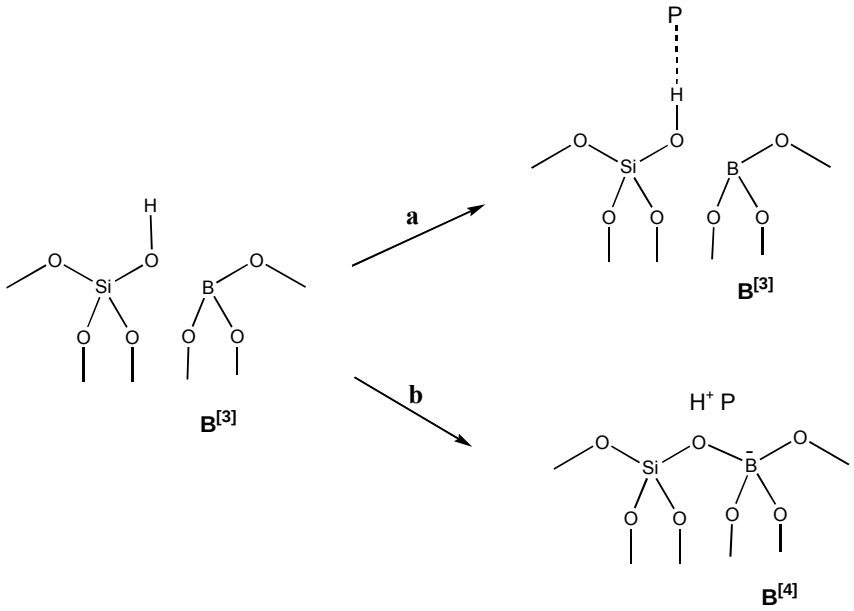

Scheme 5.1. Local structure of framework boron atoms in zeolite H-[B]ZSM-5 upon adsorption of probe molecules (P) with proton affinities of *PA* ≤ 849 kJ mol^{-1} (a) and *PA* ≥ 854 kJ mol^{-1} (b).

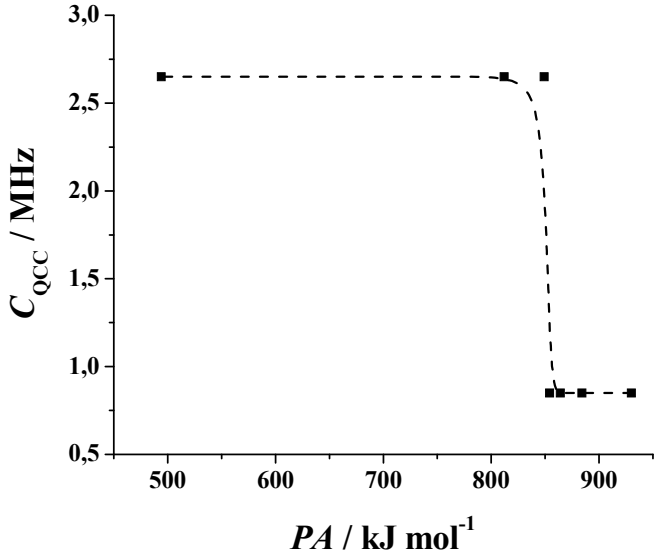

Figure 5.7. Quadrupole coupling constants C_{QCC} of boron atoms in dehydrated zeolite H-[B]ZSM-5 plotted as a function of the *PA* values of the adsorbed probe molecules.

According to the curve in Fig. 5.7, adsorption of probe molecules with *PA* values of up to 849 kJ mol^{-1} has no effect on the coordination of boron atoms in zeolite H-[B]ZSM-5. The ^{11}B MAS NMR spectra of these samples in Fig. 5.6c and 5.6d, right, are dominated by the characteristic pattern of trigonal B$^{[3]}$ species with a quadrupole coupling constant of C_{QCC} = 2.7 ± 0.1 MHz in agreement with that of the unloaded material covered by nitrogen (Table 5.1). Since the reactant (cyclohexanone oxime) in the vapor-phase Beckmann rearrangement has *PA* values at the N-site in the range of 800 to 900 kJ mol^{-1}, while at the O-site the *PA* value is < 800 kJ mol^{-1}, it can be predictable that there could be a coordination transformation of B$^{[3]}$ species into B$^{[4]}$ species due to a proton transfer upon adsorption of cyclohexanone oxime on H-[B]ZSM-5 (see Chapter 7).

Although the probe molecules with *PA* values up to 849 kJ mol^{-1} could not induce the coordination transformation of B$^{[3]}$ into B$^{[4]}$ species, the corresponding probe molecules, however, interact with the Brønsted acidic SiOH[B] of zeolite H-[B]ZSM-5 *via* hydrogen bondings (Scheme 5.1a), which is evidenced by ^{1}H MAS NMR

spectroscopy upon adsorption of deuterated probe molecules. Fig. 5.8 shows the ^{1}H MAS NMR spectra recorded upon adsorption of deuterated probe molecules, such as acetone-D_6 (Fig. 5.8b) on unloaded, dehydrated H-[B]ZSM-5 zeolite (Fig. 5.8a). The weak ^{1}H NMR signal at *ca*. 6.9 ppm in Fig. 5.8b is due to the interaction of acetone-D_6 molecule (PA = 812 kJ mol^{-1}) with SiOH[B] of zeolite H-[B]ZSM-5 *via* weak hydrogen bonding (Scheme 5.1a).

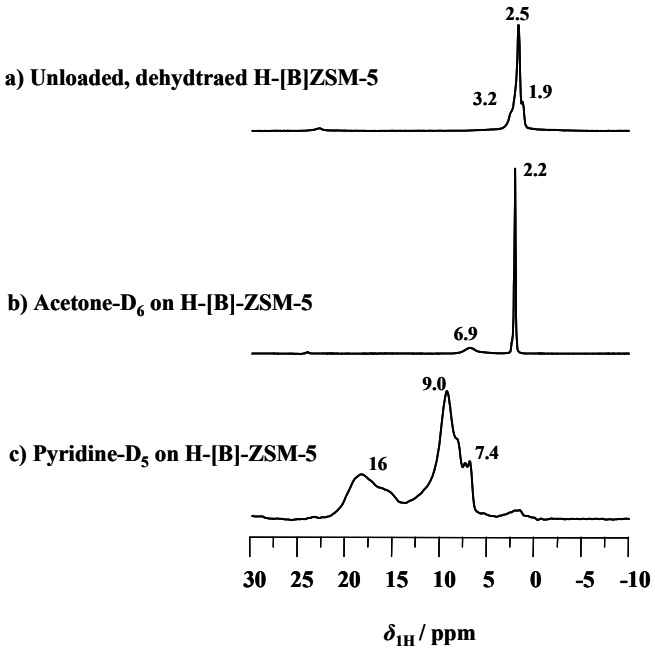

Figure 5.8. ^{1}H MAS NMR spectra of dehydrated H-[B]-ZSM-5 zeolite (a), acetone-D_6 loaded (b), and pyridine-D_5 loaded H-[B]ZSM-5 (c).

On the other hand, a further increase of the proton affinity of the adsorbed probe molecules to PA = 854 kJ mol^{-1}, such as in the case of ammonia adsorption, leads to a decrease of the quadrupole coupling constant of boron atoms in zeolite H-[B]ZSM-5 to $C_{QCC} \leq 0.85$ MHz, which indicates a transformation of $B^{[3]}$ into $B^{[4]}$ species. Simultaneously, a protonation of the adsorbed ammonia was observed in the ^{1}H MAS NMR spectrum of ammonia-loaded zeolite H-[B]ZSM-5 (Fig. 5.4b, left, and Scheme 5.1b). The proton affinity of PA = 854 kJ mol^{-1} is slightly higher in comparison with the proton affinity of PA = 821 kJ mol^{-1} required for the protonation of probe molecules adsorbed on Brønsted acidic aluminosilicate-type zeolites [171, 172]. This indicates that

the Brønsted acidity of H-[B]ZSM-5 zeolite is weaker than that of aluminum-containing zeolites.

The protonation of probe molecules is further evidenced by the ^{1}H MAS NMR spectrum, such as upon adsorption of pyridine-D_5 (PA = 930 kJ mol^{-1}) on H-[B]ZSM-5 zeolite (Fig. 5.8c). The broad signal at *ca*. 16 ppm in Fig. 5.8c is due to the formation of pyridinium ions ($PyrH^+$) caused by protonation (Scheme 5.1b).

5.6 Conclusions

To clarify the chemical behaviors of acid sites in boron-substituted zeolite ZSM-5 (zeolite H-[B]ZSM-5 with n_{Si} / n_B = 38) and their relation to the coordination of boron atoms, the adsorption of probe molecules with different proton affinities has been studied by ^{1}H and ^{11}B MAS NMR spectroscopy. In the ^{1}H MAS NMR spectrum of the dehydrated and unloaded zeolite H-[B]ZSM-5, three signals of silanol groups were observed at 1.9, 2.5, and 3.2 ppm. Upon adsorption of ammonia and pyridine, the signal at 2.5 ppm could be assigned to acidic hydroxyl groups in the vicinity of framework boron atoms, *i.e.* SiOH[B] groups.

By ^{11}B MAS NMR spectroscopy of zeolite H-[B]ZSM-5, a transformation of trigonal boron species ($B^{[3]}$) into tetragonal boron species ($B^{[4]}$) was found in the case of adsorption of probe molecules with proton affinities of $PA \geq 854$ kJ mol^{-1}. This coordination change was identified by the decrease of the ^{11}B quadrupole coupling constant from C_{QCC} = 2.7 ± 0.1 MHz ($B^{[3]}$) to $C_{QCC} \leq 0.85$ MHz ($B^{[4]}$). Adsorption of probe molecules with proton affinities of $PA \geq 854$ kJ mol^{-1} at the SiOH[B] groups of zeolite H-[B]ZSM-5 was accompanied by a protonation of these molecules. The above-mentioned PA value is *ca*. 30 kJ mol^{-1} higher than the proton affinity of PA = 821 kJ mol^{-1} required for the protonation of probe molecules adsorbed on Brønsted acidic aluminosilicate-type zeolites [171, 172]. This finding can be explained by the lower acid strength of SiOH[B] groups in zeolite H-[B]ZSM-5 in comparison with bridging OH groups (SiOHAl) in aluminum-containing zeolites.

6 Study of surface sites and their interactions with reactant molecules by solid-state ^{2}H and ^{1}H NMR spectroscopy

6.1 Introduction

As mentioned in Chapter 3, some authors [62, 173-175] claim that the vapor-phase Beckmann rearrangement must occur on the external surface or near the pore mouth of the MFI crystals due to the pore diffusion limitations for ε-caprolactam through micropores of MFI-type zeolites. In contrast, by adsorption [92], solid-state NMR [125], and FT IR spectroscopic studies [124], others concluded that cyclohexanone oxime is able to penetrate into the pores of MFI-type zeolites, and that at least a part of reaction must occur in the interior pores of the MFI-type zeolites. Therefore, the interaction of oximes with the active sites and the location of active sites of catalysts were studied by ^{1}H and ^{2}H MAS NMR spectroscopy in the present work.

In zeolites and mesoporous materials, different kinds of surface hydroxyl groups exist. These hydroxyl groups are active sites or proton donors and, therefore, very important in catalyzing the reaction. To date, the surface hydroxyl protons and bridging hydroxyl groups are extensively studied by ^{1}H MAS NMR spectroscopy [169, 176]. In addition, deuterium solid-state NMR (^{2}H NMR) spectroscopy is utilized to clarify the local structure of surface hydroxyl protons, and especially of Brønsted acid sites [177-180]. ^{2}H nuclei have a spin $I = 1$ and their electric quadrupole moment interacts with electric field gradient (EFG) at the site of the ^{2}H nucleus. The EFG is described by a second-order tensor containing the electric potential V (see Chapter 4, Eq. (11)). In general, the interaction of quadrupolar nuclei is described by two important parameters: The qudrupole coupling constant (C_{QCC}) and the asymmetry parameter (η). The ^{2}H nucleus has a relatively small electric quadrupole moment of $Q = 2.8 \times 10^{-31}$ m^2, which gives rise to C_{QCC} values in the range of 140 to 320 kHz and η has values between 0 and 1.

Several difficulties are associated in measuring the ^{2}H nucleus by solid-state NMR spectroscopy. Due to the presence of quadrupolar interactions, ^{2}H NMR signals often are very broad and require special techniques, such as quadrupole-echo or solid-echo pulse sequences [177-181]. Application of these techniques needs special attention

to adjust the equipment, *e.g.* finding the echo maximum (point of maximum amplitude of refocused FID). On the other hand, single pulse experiments can be utilized by applying the magic-angle spinning (MAS) technique, rather than echo sequences. At low sample spinning rates, the one-dimensional ^{2}H MAS NMR spectra yield a series of sideband patterns, and makes it very difficult to distinguish the peaks. The alternative method of one-dimensional ^{2}H MAS NMR spectroscopy is the strong increase of the spinning rate. For this purpose, special MAS NMR probes are necessary to spin the samples at rates of up to *ca.* 40 kHz. In this work, a Bruker 2.5 mm MAS NMR probe with the spinning rate of *ca.* 25 kHz was used. Since the natural abundance of deuterium is only 0.015%, the catalysts were deuterated for the ^{2}H MAS NMR studies.

6.2 Characterization of catalysts by ^{1}H MAS NMR spectroscopy

The ^{1}H MAS NMR spectra of the dehydrated catalysts under study are represented in Fig. 6.1. The ^{1}H MAS NMR spectrum of dehydrated H-ZSM-5 show two signals at 1.8 ppm and 4.0 ppm and a broad shoulder at *ca.* 7.0 ppm. The signals at 1.8 ppm and 4.0 ppm are due to silanol groups and bridging OH groups in the vicinity of framework aluminum atoms, respectively [169, 176]. The broad shoulder at *ca.* 7.0 ppm is caused by disturbed bridging OH groups in H-ZSM-5, which are influenced by additional electrostatic interactions with the zeolite framework [169, 176]. The quantitative evaluation of the signals at 1.8 and 4.0 ppm and the shoulder at 7.0 ppm yielded concentrations of 0.08 ± 0.02 mmol g^{-1}, 0.86 ± 0.04 mmol g^{-1}, and 0.28 ± 0.04 mmol g^{-1}, respectively. The assignment of the signals at 4.0 ppm and 7.0 ppm is supported by the number of *ca.* 1.12 mmol g^{-1} aluminum atoms introduced into the framework of zeolite H-ZSM-5.

The ^{1}H MAS NMR spectra of silicalite-1, aluminum-containing SBA-15 ([Al]SBA-15), and siliceous SBA-15 consist of a single signal at *ca.* 1.8 ppm, which is due to silanol groups at the external surface or at lattice defects. The quantitative evaluation of the ^{1}H MAS NMR signals of OH groups in silicalite-1, [Al]SBA-15, and SBA-15 gives concentrations of 0.31 ± 0.02 mmol g^{-1}, 1.29 ± 0.06 mmol g^{-1}, and 2.89 ± 0.10 mmol g^{-1}, respectively. In contrast to the ^{1}H MAS NMR spectrum of H-ZSM-5, the ^{1}H MAS NMR spectrum of [Al]SBA-15 (Fig. 6.1c) does not contain a signal of Brønsted

acid sites (*ca.* 4.0 ppm), though it is a Brønsted acidic catalyst. Since the Brønsted acid sites in [Al]SBA-15 catalyst are caused by silanol groups in the vicinity of framework aluminum atoms (no bridging hydroxyl groups), the observation of these acid sites is very difficult by ^{1}H MAS or ^{1}H/^{27}Al TRAPDOR NMR spectroscopy [48]. Nevertheless, Hu *et al.* [48] concluded on the basis of ^{31}P MAS and ^{13}C CP/MAS NMR spectroscopic studies of the [Al]SBA-15 material loaded with base molecules, such as trimethylphosphine oxide (TMPO), trimethylphosphine (TMP), and acetone, that Brønsted acid sites exist.

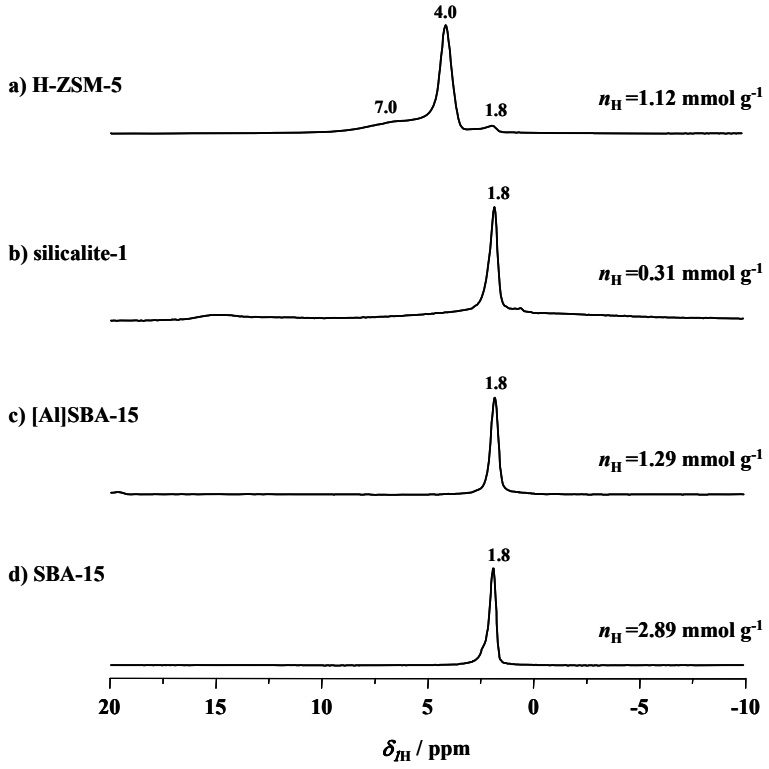

Figure 6.1. ^{1}H MAS NMR spectra of dehydrated H-ZSM-5 (n_{Si} / n_{Al} = 14) (a), silicalite-1 (n_{Si} / n_{Al} = 1700) (b), [Al]SBA-15 (n_{Si} / n_{Al} = 9) (c), and siliceous SBA-15 (n_{Si} / n_{Al} = 1800) (d).

6.3 Location of acid sites on H/D-ZSM-5, H/D-[Al]SBA-15, and H/D-SBA-15 catalysts studied by ^{2}H MAS NMR spectroscopy

In general, the interaction of reactant molecules with the surface OH groups of solid catalysts can be studied by ^{1}H MAS NMR spectroscopy, provided the reactant

molecules are *ca.* 100% deuterated. However, commercially, it was not possible to obtain the highly deuterated reactant molecules, such as cyclohexanone and cyclododecanone oximes. Moreover, only *ca.* 83% of deuteration degree was obtained for the prepared cyclohexanone oxime-D_{11} (see Section 6.4). Therefore, the alternative technique to study the interaction of the reactant molecules with surface OH groups is by ^{2}H MAS NMR spectroscopy. Since the natural abundance of deuterium nuclei is only 0.015%, deuterated catalysts are necessary to study the interaction with non-deuterated reactant molecules. In the present work, the solid catalysts, such as H-ZSM-5, [Al]SBA-15, and siliceous SBA-15 catalysts, were deuterated as described in Chapter 4, Section 4.1.9. The H/D exchange degrees of deuterated catalysts as evaluated by ^{1}H MAS NMR spectroscopy were *ca.* 50%, 65%, and 90% for H/D-ZSM-5, H/D-[Al]SBA-15, and H/D-SBA-15 catalysts, respectively. Non-deuterated oxime molecules, such as cyclohexanone and cyclododecanone oximes, were adsorbed on the above-mentioned catalysts as described in Section 4.1.10. These reactant molecules have molecular diameters of *ca.* 0.65 nm [175] and *ca.* 0.9 nm [102], respectively.

To date, ^{2}H MAS NMR measurements were performed on deuterated zeolites by applying quadrupole-echo, solid-echo, and two-dimensional ^{2}H MAS NMR spectroscopy at low spinning rates [177-181]. But poor resolution was obtained by the application of these techniques. In Table 6.1, the C_{QCC} values of different deuterated zeolites and their OD species are given. In the case of MAS NMR spectroscopy of spin $I = 1$ nuclei, the quadrupolar interaction affects the distribution of the spinning sideband intensities. In the case of a strong quadrupolar interaction, such as C_{QCC} *ca.* 240 kHz, the sideband pattern is distributed over a spectral range of *ca.* 360 kHz. MAS NMR spectroscopy with low sample spinning rate leads to a large number of spinning sidebands with low intensity, also for the central line. Therefore, a high sample spinning rate is required to reach suitable signal intensity for the central line. On the other hand, the quadrupolar interaction does not influence the line width of the individual signals if the magic angle is adjusted in a correct manner. Since the experimentally observed central line is due to satellite transitions (spin $I = 1$), the quadrupolar interaction is not the dominating line-broadening mechanism. The most important reasons for the residual line-broadening are the distribution of chemical shifts and dipolar interactions, especially the homonuclear

dipolar interaction. The dipolar interactions, however, are averaged by the application of MAS with high sample spinning rates.

Table 6.1. Quadrupole coupling constants of various OD species in zeolites obtained by ^{2}H MAS NMR spectroscopy [177-180].

Catalyst/active sites	C_{QCC} / kHz	η	Ref.
H-X (n_{Si} / n_{Al} = 1.4)	236 ± 10	0.10 ± 0.05	[177]
H-Y(n_{Si} / n_{Al} = 2.4)	236 ± 10	0.06 ± 0.05	[177]
bridging hydroxyls	224	0.10 ± 0.05	[178]
H-ZSM-5 (n_{Si} / n_{Al} = 22)	208 ± 10	0.15 ± 0.05	[177]
AlOH groups	67	0.2	[178]
SiOH groups	75	0.6	[178]

The current study is the first high-speed ^{2}H MAS NMR spectroscopy at the sample spinning rates of 25 kHz with a suitable spectral resolution. Figs. 6.2 to 6.4 show the ^{2}H MAS NMR spectra of the deuterated (H/D-exchanged) catalysts before and after adsorption of reactant molecules, *i.e.* of cyclohexanone and cyclododecanone oxime. As shown in Fig. 6.2a, the ^{2}H MAS NMR spectrum of deuterated ZSM-5 (H/D-ZSM-5) consists of two signals at 1.8 ppm and *ca.* 5.7 ppm. These signals are due to silanol groups and bridging OH groups in the vicinity of framework aluminum atoms, respectively. In contrast to the ^{1}H MAS NMR spectrum (Fig. 6.1a), the ^{2}H MAS NMR spectrum of H/D-ZSM-5 consists of broad signals and the chemical shifts were slightly displaced. Nevertheless, acceptable resolution between the signals of silanols and bridging hydroxyls was achieved. In comparison with the spectra obtained by static (no spinning) echo techniques [177-181], such as quadrupole-echo sequence, the spectrum obtained in the present study consists of narrow signals.

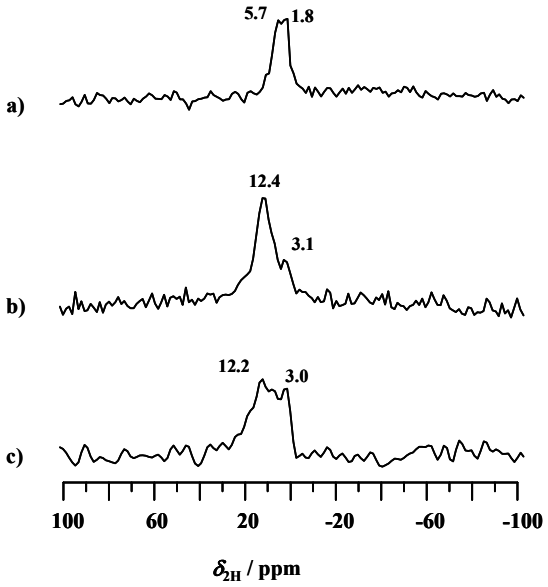

Figure 6.2. ^{2}H MAS NMR spectra of dehydrated H/D-ZSM-5 before (a), and after loading with non-deuterated cyclohexanone oxime (b), and cyclododecanone oxime (c).

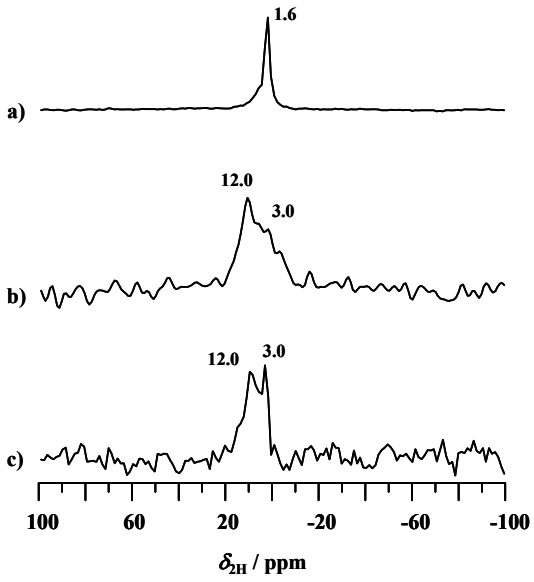

Figure 6.3. ^{2}H MAS NMR spectra of dehydrated H/D-[Al]SBA-15 before (a), and after loading with non-deuterated cyclohexanone oxime (b), and cyclododecanone oxime (c).

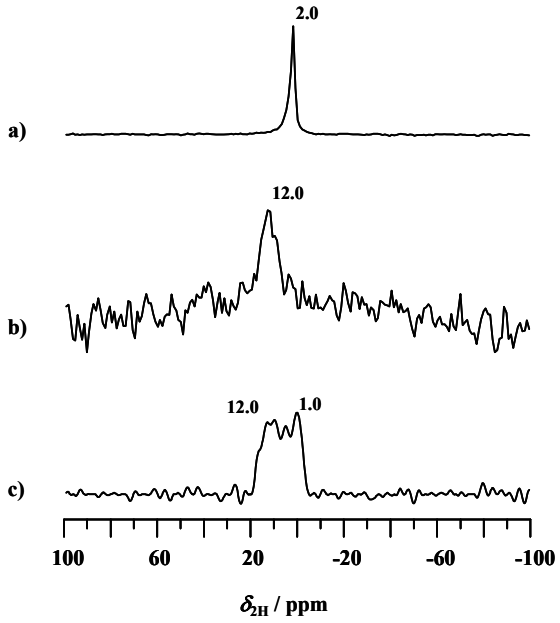

Figure 6.4. ^{2}H MAS NMR spectra of dehydrated, siliceous H/D-SBA-15 before (a), and after loading with non-deuterated cyclohexanone oxime (b), and cyclododecanone oxime (c).

The ^{2}H MAS NMR spectra (Figs. 6.3a and 6.4a) of deuterated [Al]SBA-15 (H/D-[Al]SBA-15) and deuterated siliceous SBA-15 (H/D-SBA-15) show similar narrow signals, like in the ^{1}H MAS NMR spectra of Fig. 6.1c and 6.1d at *ca.* 1.6 ppm and 2.0 ppm, respectively. These signals are due to the silanol groups at the external surface or at lattice defects. The ^{2}H MAS NMR signals of SiOD groups in the H/D-[Al]SBA-15 and H/D-SBA-15 catalysts (Figs. 6.3a and 6.4a) are narrow and strong in comparison with the signals of bridging hydroxyl groups of H/D-ZSM-5 catalyst (see, Fig. 6.2a, Table 6.1). As shown in the Table 6.1, the C_{QCC} values are much higher for bridging hydroxyl groups (*ca.* 224 kHz) than for AlOH groups (*ca.* 67 kHz) and SiOH groups (*ca.* 75 kHz). Since the static quadrupolar pattern is much broader for ^{2}H nuclei with larger C_{QCC} values, the number of acquisitions required for recording the ^{2}H MAS NMR spectra of H/D-SBA-15 and H/D-[Al]SBA-15 catalysts with reasonable signal to noise ratios is much smaller in comparison with the ^{2}H MAS NMR spectra of the H/D-ZSM-5 catalyst. The number of

accumulations required for the ^{2}H MAS NMR spectra of the H/D-SBA-15, H/D-[Al]SBA-15, and H/D-ZSM-5 catalysts were 5200, 30400, and 34800, respectively.

Upon the adsorption of non-deuterated cyclohexanone oxime on H/D-exchanged catalysts, the ^{2}H MAS NMR spectra of the H/D-ZSM-5 (Fig. 6.2b), H/D-[Al]SBA-15 (Fig. 6.3b), and H/D-SBA-15 (Fig. 6.4b) catalysts show a dominating ^{2}H MAS NMR signal at *ca.* 12 ppm. This ^{2}H MAS NMR signal indicates the interaction of cyclohexanone oxime with SiOH groups and Brønsted acid sites or bridging hydroxyl groups in the above-mentioned catalysts. Since the H/D-SBA-15 and H/D-[Al]SBA-15 catalysts have pore diameters of *ca.* 5.6 and 9.0 nm, respectively, the cyclohexanone oxime molecule with smaller molecular diameter (*ca.* 0.65 nm [175]) can easily enter the interior parts of these materials. In contrast, the pore diameter of H-ZSM-5 catalyst is only *ca.* 0.55 nm. Hence, it is very difficult for cyclohexanone oxime molecule to enter into the interior parts of this material. Nevertheless, Kath *et al.* [92] confirmed by adsorption studies, and Fernández *et al.* [124, 125] by FT IR and MAS NMR studies, the diffusion of cyclohexanone oxime into the interior pores of MFI-type zeolites under vapor-phase conditions. From these aforementioned studies and from the current results obtained by ^{2}H MAS NMR spectroscopy, the ^{2}H NMR signal at *ca.* 12 ppm supports the interaction of cyclohexanone oxime with SiOH groups and Brønsted acid sites or bridging hydroxyl groups of the above-mentioned catalysts.

However, the above ^{2}H MAS NMR results upon the adsorption of cyclohexanone oxime do not contradict the interaction of cyclohexanone oxime with the active sites located on the external surface. To confirm this, a larger oxime molecule, such as cyclododecanone oxime (*ca.* 0.9 nm), was adsorbed on the aforementioned H/D-exchanged catalysts, and the results are depicted in Figs. 6.2c, 6.3c, and 6.4c. The corresponding ^{2}H MAS NMR spectra also show a signal at *ca.* 12.0 ppm. But upon adsorption of cyclododecanone oxime, the intensity content of the signal at *ca.* 12 ppm is much smaller than upon adsorption of cyclohexanone oxime. Therefore, the ^{2}H MAS NMR spectra of the catalysts loaded with cyclododecanone oxime indicate an interaction of the large oxime with external SiOH groups or with Brønsted acid sites located near the pore mouth. The current results were further supported by the recent solid-state ^{15}N NMR spectroscopic studies reported by Fernández *et al*. [125]. The authors studied the location

of active sites upon the adsorption and conversion of ^{15}N-cyclohexanone and ^{15}N-cyclododecanone oximes on silicalite-1 and H-ZSM-5 catalysts. From their studies, they concluded that cyclododecanone oxime can not enter into the interior parts of MFI-type zeolites, and can only interact with the active sites, such as SiOH groups on the external surface or small concentration of Brønsted acid sites near the pore mouth *via* hydrogen bonding [125]. In contrast, cyclohexanone oxime can enter also into the interior parts of MFI-type zeolites and the reaction occurs inside the pores of MFI-type zeolites.

6.4 Vapor-phase Beckmann rearrangement of cyclohexanone oxime-D_{11} on silicalite-1 and H-ZSM-5 studied by *in situ* ^{1}H MAS NMR spectroscopy

In this Chapter, an attempt is made to study the Beckmann rearrangement of cyclohexanone oxime-D_{11} by *in situ* ^{1}H MAS NMR spectroscopy. To study the reaction, deuterium-enriched cyclohexanone oxime (*i.e.* cyclohexanone oxime-D_{11}) was synthesized according to the procedure described in Chapter 4, Section 4.1.11. The deuterium-enrichment as evaluated by ^{1}H MAS NMR spectroscopy was *ca.* 83% for cyclohexanone oxime-D_{11}. Remaining non-enrichment (17%) of cyclohexanone oxime results in the occurrence of ^{1}H MAS NMR signals of the reactant molecules. In addition, with increasing reaction temperatures of the oxime-D_{11}/catalyst mixtures, the H/D exchange occurs between the OH groups of zeolites and the non-enriched part (17%) of the cyclohexanone oxime-D_{11} with the O-D (N-OD group) or C-D groups (in the ring) of the enriched-cyclohexanone oxime-D_{11}.

Fig. 6.5 shows the ^{1}H MAS NMR spectra of dehydrated silicalite-1 and cyclohexanone oxime-D_{11}/silicalite-1 mixtures heated at reaction temperatures between 393 K and 523 K for 20 minutes. All the ^{1}H MAS NMR spectra were recorded at room temperature. The signal at 1.8 ppm in dehydrated sample (Fig. 6.5a) is due to SiOH groups. After the adsorption of cyclohexanone oxime-D_{11} on silicalite-1 and heating at 393 K, different new ^{1}H MAS NMR signals occurred as shown in Fig. 6.5b. These signals are caused by the incomplete deuterated cyclohexanone oxime-D_{11} molecules and the H/D exchange between the surface OH groups of silicalite-1 with the reactant, products and by-products of the Beckmann rearrangement. The assignments of the signals observed in this study were accomplished by the support of the HNMR predictor

software [182]. In Table 6.2, the chemical shift values observed in the experimental spectra are compared with the values obtained by the ACD labs software [182].

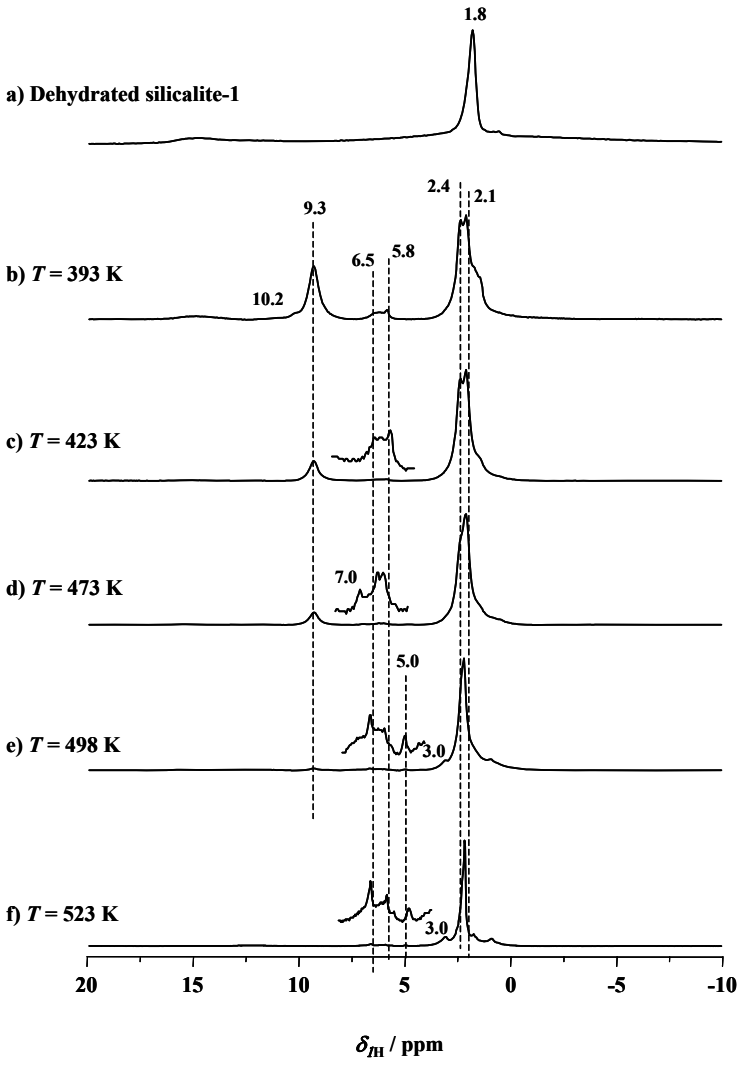

Figure 6.5. ^{1}H MAS NMR spectra of dehydrated silicalite-1 before (a) and after loading with cyclohexanone oxime-D_{11} (b-f). Reaction temperatures are indicated in the Figure.

Table 6.2. Assignments of ^{1}H NMR signals of the species observed during the vapor-phase Beckmann rearrangement of cyclohexanone oxime-D_{11} on silicalite-1 and H-ZSM-5.

δ_{1H} / (ppm)[a]	δ_{1H} / (ppm)[b]	Assignments
1.8-2.5	1.8-2.5	ring-protons in cyclohexanone oxime
1.8-3.5	1.0-3.5	ring-protons in ε-caprolactam
1.8-3.5	1.1-2.8	chain-protons in non- or N-protonated ε-aminocapric acid
5.0	5.1	hydroxylamine formed on SiOH groups of silicalite-1
5.8	5.1-5.8	5-cyano-1-pentene formed on SiOH groups of silicalite-1
6.5-7.0	7.6	ε-caprolactam formed on SiOH groups of silicalite-1
6.5-7.9	6.6	N-protonated ε-caprolactam, exclusively observed on Brønsted acid sites of H-ZSM-5
6.5-7.9	6.0	non-protonated ε-aminocapric acid, exclusively observed on Brønsted acid sites of H-ZSM-5
6.5-7.9	7.9	N-protonated ε-aminocapric acid, exclusively observed on Brønsted acid sites of H-ZSM-5
9.3-10.2	9.6	N-OH groups in unconverted cyclohexanone oxime
10.2-11.2	-	hydrogen-bonded cyclohexanone oxime on SiOH groups
13.0	12.2	N-protonated cyclohexanone oxime, exclusively observed on Brønsted acid sites of H-ZSM-5
14.2	14.9	O-protonated ε-caprolactam, exclusively observed on Brønsted acid sites of H-ZSM-5

[a]) experimental values obtained in this work, [b]) values obtained by the HNMR predictor software [182].

In the ^{1}H MAS NMR spectra of silicalite-1 loaded with H/D-exchanged cyclohexanone oxime-D_{11} (Fig. 6.5), the signal at 9.3 is due to the unconverted cyclohexanone oxime-D_{11} caused by the non-enriched (17%) N-OH groups in the

reactant molecules. The signals in the range of 1.8 ppm to 2.5 ppm are caused by the non-enriched ring-protons of cyclohexanone oxime-D_{11}. The latter signals are overlapped by the signals of SiOH groups (1.8 ppm). In addition, a weak shoulder at *ca.* 10.2 ppm indicates the interaction of cyclohexanone oxime-D_{11} with the SiOH groups *via* hydrogen bonding (see Chapter 7). The signals at *ca.* 5.0 ppm and *ca.* 5.8 ppm are caused by the formation of by-products due to the hydration and dehydration of cyclohexanone oxime, respectively (see Chapter 7, Scheme 7.2). In Chapter 7, ^{15}N MAS NMR spectroscopic studies reveal the formation of by-products, such as hydroxylamine and 5-cyano-1-pentene during the vapor-phase Beckmann rearrangement on silicalite-1. Therefore, the ^{1}H MAS NMR signals at *ca.* 5.0 ppm and *ca.* 5.8 ppm are assigned to hydroxylamine and 5-cyano-1-pentene, respectively [182].

In addition, signals in the range of 6.5 ppm to 7.0 ppm were observed, which are due to the formation of ε-caprolactam, the main product of the Beckmann rearrangement reaction. The signal corresponding to the ring-protons of ε-caprolactam appears at *ca.* 3.0 ppm (Figs. 6.5e and 6.5f). Except the signals in the range of 1.8 ppm to 2.5 ppm and at 9.3 ppm, all the remaining signals of the reactant, product and by-products have very small intensities (Fig. 6.5). This may be due to the lower H/D exchange degree between the deuterated reactant, product and by-product molecules of the Beckmann rearrangement with the SiOH groups of silicalite-1. Since silicalite-1 contains a small amount of SiOH groups (n_H = 0.31 ± 0.02 mmol g^{-1}), only a small number of hydroxyl protons can be exchanged with deuterated reactants.

Fig. 6.6 shows the ^{1}H MAS NMR spectra of dehydrated H-ZSM-5 and cyclohexanone oxime-D_{11}/H-ZSM-5 mixtures heated at reaction temperatures between 393 K and 523 K. The ^{1}H MAS NMR spectrum of the dehydrated zeolite H-ZSM-5 consists of signals at 1.8 ppm, 4.0 ppm, and 7.0 ppm, which are due to the silanol groups on the external surface and framework defects, bridging OH groups, and disturbed bridging OH groups in H-ZSM-5, respectively (Fig. 6.5a). When the cyclohexanone oxime-D_{11}/H-ZSM-5 mixture was heated at 393 K, the occurrence of new ^{1}H NMR signals indicate the conversion of cyclohexanone oxime-D_{11} (Fig. 6.5b). The signal at *ca.* 10.4 ppm is due to the unconverted cyclohexanone oxime-D_{11} caused by the non-enriched N-OH groups in the reactant molecule, while the signal *ca.* 11.2 ppm is due to

the cyclohexanone oxime-D_{11} interacting with the silanol groups of H-ZSM-5 *via* hydrogen bonding.

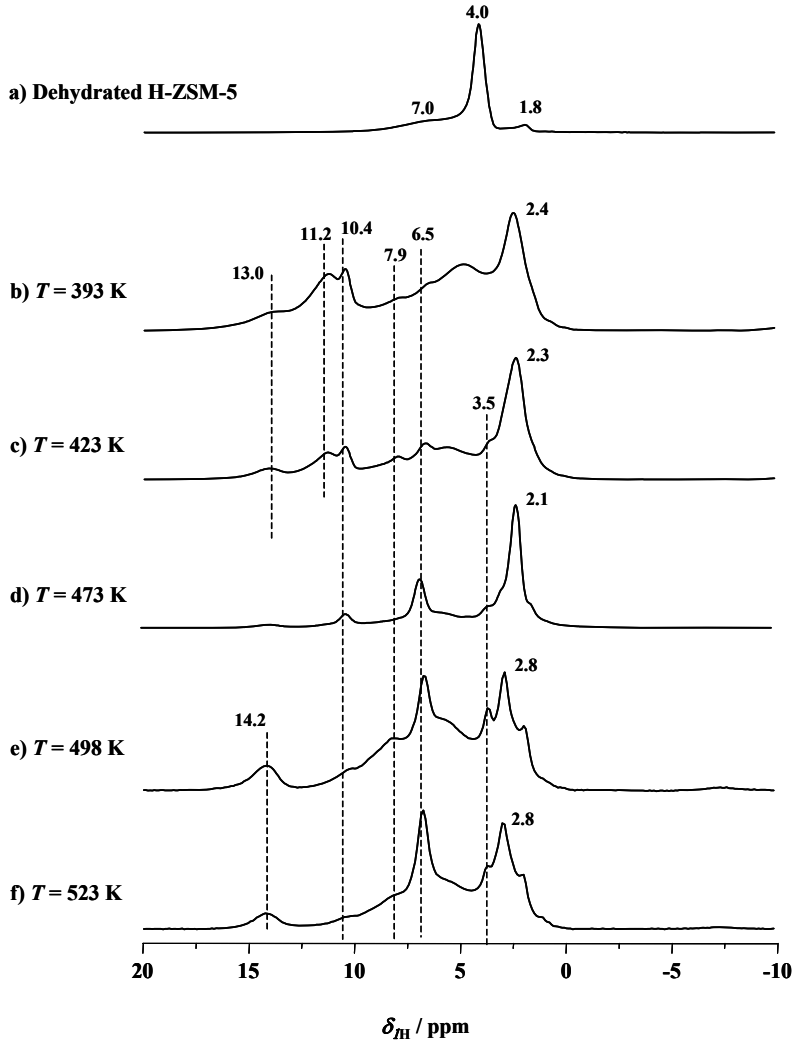

Figure 6.6. ^{1}H MAS NMR spectra of dehydrated H-ZSM-5 before (a) and after loading with cyclohexanone oxime-D_{11} (b-f). Reaction temperatures are indicated in the Figure.

As revealed by ^{15}N MAS NMR studies (see Chapter 7), the ^{1}H MAS NMR study of the Beckmann rearrangement of cyclohexanone oxime-D_{11} on zeolite H-ZSM-5 also confirms the formation of N-protonated cyclohexanone oxime-D_{11} on the bridging hydroxyl groups of H-ZSM-5. In the ^{1}H MAS NMR spectra, this is evidenced by the

signal at *ca.* 13 ppm (Figs. 6.5b and 6.5c). Since the predicted ^{1}H NMR chemical shift value for the N-protonated cyclohexanone oxime is *ca.* 12.2 ppm [182], the signal at *ca.* 13 ppm is assigned to this species (see Table 6.2). After increasing the reaction temperature (Figs. 6.6e and 6.6f), additional signals occur at *ca.* 6.5 ppm, *ca.* 7.9 ppm, and *ca.* 14.2 ppm. As concluded by the ^{15}N MAS NMR spectroscopic results (see Chapter 7, Scheme 7.4), and by the support of the HNMR predictor software [182], the signals in the range of 6.5 to 7.9 ppm and at *ca.* 14.2 ppm are due to the formation of N-protonated *ε*-caprolactam or non- or N-protonated *ε*-aminocapric acid, and O-protonated *ε*-caprolactam, respectively (Table 6.2). Furthermore, the weak signal at *ca.* 3.5 ppm is caused by the chain-protons in non- or N-protonated *ε*-aminocapric acid (see Table 6.2).

6.5. Conclusions

Deuterated catalysts, such as H/D-ZSM-5, H/D-[Al]SBA-15, and H/D-SBA-15, were successfully applied to study the interaction of cyclohexanone and cyclododecanone oximes with the surface sites of these materials. Acceptable spectral resolution of the signals of SiOH groups and bridging hydroxyl groups was achieved by recording ^{2}H MAS NMR spectra of H/D-ZSM-5 at the spinning rate of *ca.* 25 kHz. Furthermore, by adsorption of smaller and larger oxime molecules, ^{2}H MAS NMR studies reveal the accessibility of SiOH groups, Brønsted acid sites or bridging hydroxyl groups in the aforementioned H/D-exchanged catalysts. The current ^{2}H MAS NMR results support other studies and conclude that cyclohexanone oxime is able to enter the interior parts of MFI-type zeolites and mesoporous materials, while it is difficult for cyclododecanone oxime to enter into the MFI-type zeolites, such H/D-ZSM-5. Nevertheless, it can be concluded that the hydroxyl groups, such as silanols, silanol nests, or Brønsted acid sites located on the external surface, near the pore mouth, or in the interior pores of H/D-ZSM-5 zeolite, are accessible for the reaction.

On the other hand, the vapor-phase Beckmann rearrangement of cyclohexanone oxime-D_{11} on silicalite-1 and H-ZSM-5 catalysts (non-deuterated) was studied at different reaction temperatures by *in situ* ^{1}H MAS NMR spectroscopy. From the ^{1}H MAS NMR studies of oxime-D_{11}/silicalite-1 mixtures, the formation of reaction intermediates,

such as hydrogen-bonded cyclohexanone oxime-D_{11} with SiOH groups, by-products, such as hydroxylamine and 5-cyano-1-pentene, and product ε-caprolactam was observed. In contrast, on strongly acidic H-ZSM-5, the formation of reaction intermediates, such as N-protonated cyclohexanone oxime-D_{11}, reaction products, such as strongly adsorbed O-protonated ε-caprolactam, and other products, such as N-protonated ε-caprolactam, or non- or N-protonated ε-aminocapric acid on bridging hydroxyl groups was identified.

7 Vapor-phase Beckmann rearrangement of ^{15}N-cyclohexanone oxime on MFI-type zeolites and mesoporous catalysts studied by *in situ* ^{15}N MAS NMR spectroscopy

7.1 Introduction

A new synthesis method for the production of ε-caprolactam is the vapor-phase Beckmann rearrangement of cyclohexanone oxime using heterogeneous catalysts. This route has gained increasing interest as an environmentally, economically, and energetically favorable process [46, 47, 62]. In the first industrial application, the vapor-phase Beckmann rearrangement process is performed on siliceous MFI zeolite as catalyst and methanol vapor is used as additive in this reaction system [46, 62]. As discussed in Chapter 3, until now, various solid catalysts including zeolites and mesoporous materials have been investigated for the vapor-phase Beckmann rearrangement of cyclohexanone oxime. But the highest selectivity towards ε-caprolactam was achieved by using MFI-type zeolites with high silica content [78-98]. However, there have been discussions on the nature (silanol or bridging OH groups) of the active sites present in the catalysts [62, 85, 88, 183]. In earlier studies, strong Brønsted acid sites in zeolites were suggested to be crucial in catalyzing this reaction by protonating the oxime [85]. However, further investigations showed that weakly acidic silanol groups and nest silanols are responsible for the high activity and selectivity towards the ε-caprolactam [88].

To date, much effort has been devoted by researchers for this reaction to find the best catalyst or to develop the vapor-phase Beckmann rearrangement process. Nevertheless, little is known about the chemistry of the reaction, adsorption state, and reaction behavior of reactants, intermediates, products, and by-products of this reaction on different active sites of the catalyst. In addition, the major problem of the vapor-phase Beckmann rearrangement process is catalyst deactivation. In the literature, the reasons for the catalyst deactivation during the vapor-phase Beckmann rearrangement were not clearly explained. In the present work, ^{15}N CP and ^{15}N HPDEC MAS NMR spectroscopy were utilized to study the complete chemistry of the vapor-phase Beckmann rearrangement of cyclohexanone oxime on different solid catalysts.

Nitrogen has two stable isotopes, namely ^{14}N and ^{15}N. The natural abundance of ^{14}N nuclei is 99.63%, but it is a quadrupolar nucleus with a spin of $I = 1$. Due to the existence of qudrupolar interactions, ^{14}N MAS NMR measurements often give very broad ^{14}N NMR signals. As a result, most of the important information about the species can be hidden in the broad signals. The alternative way to measure nitrogen nuclei is by ^{15}N NMR spectroscopy. Since ^{15}N is a spin $I = ½$ nucleus, good signal resolution can be achieved by applying high resolution solid-state NMR techniques, such as cross-polarization (CP) or high-power decoupling (HPDEC) together with magic angle spinning (MAS). However, due to the low natural abundance of ^{15}N nuclei (0.37%), the ^{15}N NMR signals suffer from a poor signal-to-noise ratio (S/N). In order to improve the S/N ratio of the signals, ^{15}N-enriched materials are necessary for the ^{15}N NMR spectroscopic measurements. Therefore, ^{15}N-labeled cyclohexanone oxime was synthesized as described in Section 4.1.13.

7.2 Characterization of ^{15}N-cyclohexanone oxime by MAS NMR spectroscopy

The purity of the *ε*-caprolactam, *i.e.* the main product of the vapor-phase Beckmann rearrangement reaction, primarily depends on the purity of the reactant, *i.e.* cyclohexanone oxime. Hence, it is important to know the purity of the prepared reactant molecule. The possible impurities that may be present in the cyclohexanone oxime were mentioned in Ref. [91]. In this work, the chemical purity of the ^{15}N-labeled cyclohexanone oxime was studied by solid-state ^{15}N and ^{13}C MAS NMR spectroscopy.

As shown in Figs. 7.1a and 7.1b, the ^{15}N MAS NMR spectra consist of a single signal at -55 ppm corresponding to the ^{15}N-label in cyclohexanone oxime [134, 184]. The ^{13}C MAS NMR spectra of ^{15}N-cyclohexanone oxime shown in Figs. 7.1c and 7.1d contain the signals in the range of *ca*. 27 to 31 ppm and at 160 ppm. The signals at *ca*. 27 to 31 ppm are due to the non-enriched aliphatic methylene ($-CH_2$) groups in the ring of cyclohexanone oxime molecule, while the signal at *ca*. 160 ppm is due to the $C=^{15}N$ group of cyclohexanone oxime. These results indicate that the prepared ^{15}N-cyclohexanone oxime is free of impurities.

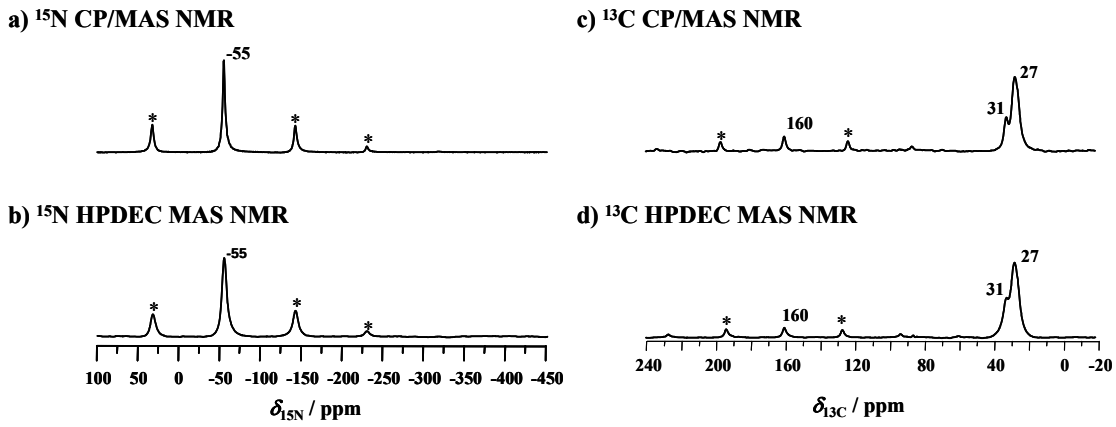

Figure 7.1. ^{15}N CP (a), ^{15}N HPDEC (b), ^{13}C CP (c), and ^{13}C HPDEC (d) MAS NMR spectra of ^{15}N-cyclohexanone oxime. Asterisks in the NMR spectra denote spinning sidebands.

7.3 Vapor-phase Beckmann rearrangement of cyclohexanone oxime on weakly acidic silicalite-1

Silicalite-1 (n_{Si} / n_{Al} = 1700) is an MFI-type zeolite containing silanol groups only, but no bridging OH groups acting as strong Brønsted acid sites. This catalyst is known to be a weakly acidic zeolite. The step-wise transformation of ^{15}N-cyclohexanone oxime into ε-caprolactam *via* the vapor-phase Beckmann rearrangement on silicalite-1 was studied by *in situ* solid-state ^{15}N NMR spectroscopy and the results are shown in the spectra of Fig. 7.2. Since it is sometimes difficult to observe mobile compounds by cross-polarization technique, both ^{15}N CP and ^{15}N HPDEC MAS NMR spectra were recorded in order to obtain the complete information about the species. According to Fig. 7.2a, the ^{15}N MAS NMR spectra recorded after preparing the ^{15}N-cyclohexanone oxime/silicalite-1 mixture and heating at 393 K show the signals at -55 ppm and -46 ppm. The signal at -55 ppm is due to unconverted ^{15}N-cyclohexanone oxime [134, 184], while the low-field signal appearing at -46 ppm is caused by ^{15}N-cyclohexanone oxime interacting with the SiOH groups of silicalite-1 *via* hydrogen bonding (an overview on the assignments of ^{15}N MAS NMR signals is given in Table 7.1). A similar low-field

shift of *ca*. 10 ppm was observed by Fernández *et al.* [125, 133] for the hydrogen bonding of ^{15}N-acetophenone oxime and ^{15}N-cyclohexanone oxime with the SiOH groups of siliceous zeolite Beta and silicalite-1, respectively. Upon heating the mixture at 423 K and 473 K, all the ^{15}N-oxime molecules interact with SiOH groups *via* hydrogen bonding as indicated by a single signal at -46 ppm in Figs. 7.2b and 7.2c.

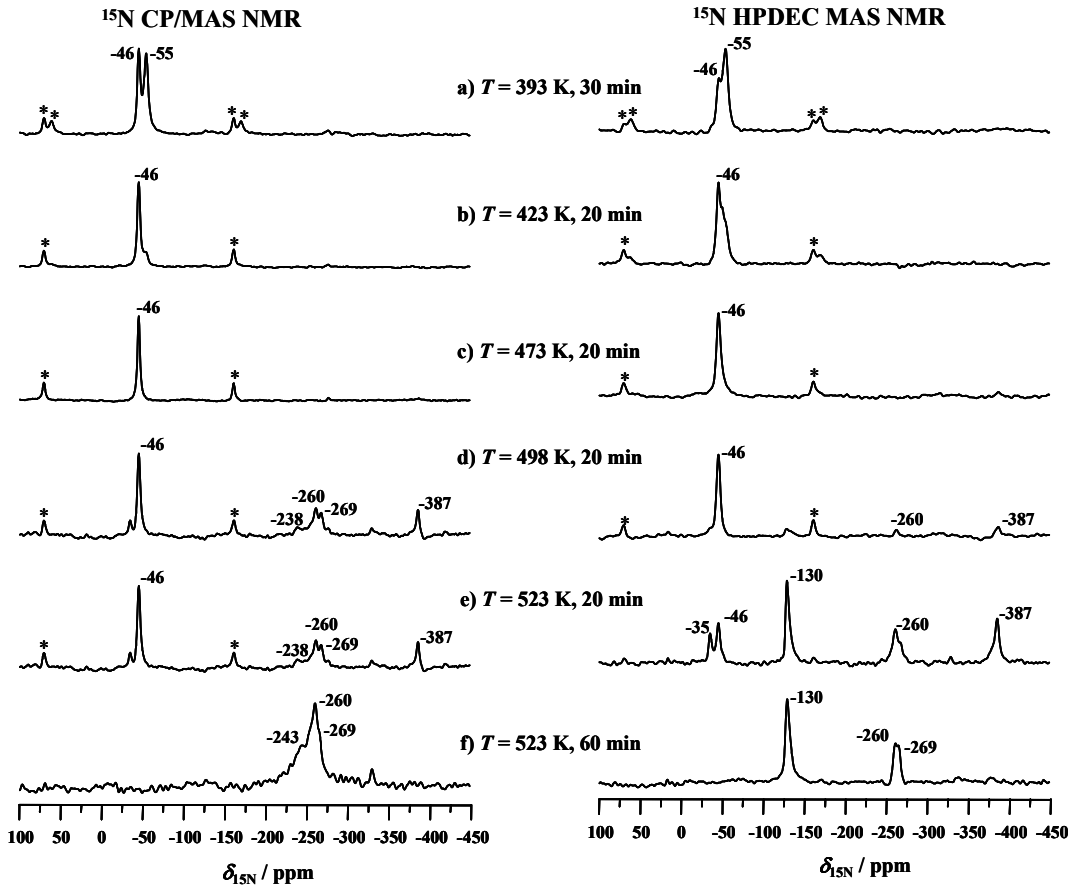

Figure 7.2. ^{15}N CP (left) and ^{15}N HPDEC (right) MAS NMR spectra recorded upon conversion of ^{15}N-cyclohexanone oxime on silicalite-1 (n_{Si} / n_{Al} = 1700). The reaction temperature and heating times are given in the Figure. Asterisks in the NMR spectra denote spinning sidebands.

Further heating of the ^{15}N-oxime/silicalite-1 mixture at *ca*. 498 K leads to the partial conversion of ^{15}N-oxime into the products and by-products as evidenced by new

signals at -260, -269, and -387 ppm (Fig. 7.2d). The signal at -260 ppm is caused by the formation of ε-caprolactam, the final product of the Beckmann rearrangement, while the signals at -269 ppm and -387 ppm are hints for the formation of by-products, such as hydroxylamine and amine, respectively [133, 134, 184]. Hydroxylamine is formed as a result of the hydration of ^{15}N-cyclohexanone oxime into cyclohexanone and hydroxylamine (see Section 7.8, Scheme 7.2), which is a frequent side-reaction during the vapor-phase Beckmann rearrangement of cyclohexanone oxime [75, 98, 109].

In addition, a weak signal in the range of *ca.* -237 to -243 ppm was observed. Tentatively, this signal has been attributed to nitrilium ions [134], an intermediate in the Beckmann rearrangement reaction or to O-protonated ε-caprolactam [125]. The former assignment was supported by the NNMR predictor software [184]. According to this software, the ^{15}N NMR shift of -224 ppm was predicted for the intermediate nitrilium ions. This led to the assumption that these species may be responsible for the signal at -237 ppm [134]. The latter assignment, *i.e.* O-protonated ε-caprolactam has been supported by theoretical calculations [125]. In agreement with previous studies, and considering the fact that the carbonyl group is more basic than the amide group, the formation of O-protonated ε-caprolactam is more favorable than the formation of N-protonated ε-caprolactam [183, 185]. Therefore, it is reasonable to assign the peak at -237 ppm to O-protonated ε-caprolactam. However, it has been reported that these species are formed exclusively on materials with strong Brønsted acid sites, such as H-ZSM-5 and mordenite [125, 183]. In contrast, in the present study, it will be shown that these species are observed on weakly, mediumly and strongly acidic catalysts. Nevertheless, the intensity of the signal at -237 ppm is weaker for silicalite-1 than for H-ZSM-5 and other catalysts (see Figs. 7.4 to 7.8). The reason for the different signal intensities are explained in Section 7.4.

When the ^{15}N-oxime/silicalite-1 mixture was heated at 523 K for 20 min, slight differences in the ^{15}N CP (Fig. 7.2e, left) and ^{15}N HPDEC (Fig. 7.2e, right) spectra were noticed. New signals at -35 ppm and -130 ppm exclusively appeared in the ^{15}N HPDEC MAS NMR spectrum (Fig. 7.2e, right). The absence of these signals in the ^{15}N CP/MAS NMR spectrum indicates that these species are mobile compounds. According to Shouro *et al.* [109] and Forni *et al.* [98], dehydration of cyclohexanone oxime leads to the

formation of 5-cyano-1-pentene, a by-product of the Beckmann rearrangement. Since 5-cyano-1-pentene has a predicted ^{15}N NMR shift of -136 ppm [184], this species is probably the reason for the signal at -130 ppm observed in the ^{15}N HPDEC MAS NMR spectra of silicalite-1. This is further supported by Fernández *et al.* [125], who observed the signal at -130 ppm on silicalite-1 and assigned it to nitriles. The signal at -35 ppm may be due to the reactant ^{15}N-cyclohexanone oxime in different adsorbed state. To achieve the complete conversion of hydrogen-bonded ^{15}N-oxime (-46 ppm), heating at 523 K for 60 min is required as shown in Fig. 7.2f.

7.4 Vapor-phase Beckmann rearrangement of ^{15}N-cyclohexanone oxime on mesoporous siliceous SBA-15 and MCM-41 materials

The mesoporous siliceous SBA-15 (n_{Si} / n_{Al} = 1800) and H-[Si]MCM-41 (n_{Si} / n_{Al} = 1080) materials under study are characterized by large pore diameters of *ca.* 6 and 3 nm, respectively. Therefore, no pore diffusion limitations are associated with respect to both the reactant ^{15}N-cyclohexanone oxime and the reaction product ε-caprolactam. On the other hand, the concentration of silanol groups is significantly higher in SBA-15 (n_H = 2.81 mmol g^{-1}) and H-[Si]MCM-41 (n_H = 2.69 mmol g^{-1}) in comparison with silicalite-1 (n_H = 0.31 mmol g^{-1}). Furthermore, different kinds of silicon environments, such as Q^4 ($Si(OSi)_4$), Q^3 ($Si(OSi)_3OH$), and Q^2 ($Si(OSi)_2(OH)_2$) species exist in mesoporous materials, while there are exclusively Q^4 and Q^3 species in silicalite-1 (Fig. 7.3). According to Rosenholm *et al.* [186], the silanol groups of Q^3 species (pK_a values are in the range of 2 to 4.5 [186]) are more acidic than those of Q^2 species (pK_a value of *ca.* 8.5 [186]). As shown in Fig. 7.3, the relative intensity of Q^3 silanol groups ($Si(OSi)_3OH$) in SBA-15 (30%) and H-[Si]MCM-41 (22%) is much higher than the relative intensity of these OH groups in silicalite-1 (1%). Therefore, it is interesting to perform mechanistic investigations on SBA-15 and H-[Si]MCM-41 materials .

Figs. 7.4 and 7.5 illustrate the progress of the Beckmann rearrangement upon conversion of ^{15}N-cyclohexanone oxime into ε-caprolactam on mesoporous siliceous SBA-15 and H-[Si]MCM-41 catalysts, respectively. According to Figs. 7.4 and 7.5, the ^{15}N CP and ^{15}N HPDEC MAS NMR spectra of ^{15}N-oxime/SBA-15 and ^{15}N-oxime/H-[Si]MCM-41 mixtures heated at 298 K to 423 K show two signals in the range of -55 to

-62 ppm and at -45 ppm. As assigned for the spectra of silicalite-1, the signal in the range of -55 to -62 ppm is due to the unconverted ^{15}N-cyclohexanone oxime, while the signal at -45 ppm is caused by the interaction of ^{15}N-cyclohexanone oxime with silanol groups *via* hydrogen bonding [125, 134, 184]. When ^{15}N-oxime/SBA-15 (Figs. 7.4d to 7.4f) and ^{15}N-oxime/H-[Si]MCM-41 (Figs. 7.5d to 7.5g) mixtures were heated at 473 K to 523 K, different new signals could be observed in the ^{15}N MAS NMR spectra indicating the conversion of ^{15}N-cyclohexanone oxime into products and by-products. The assignments of these signals are similar like for silicalite-1 (see Section 7.8, Table 7.1).

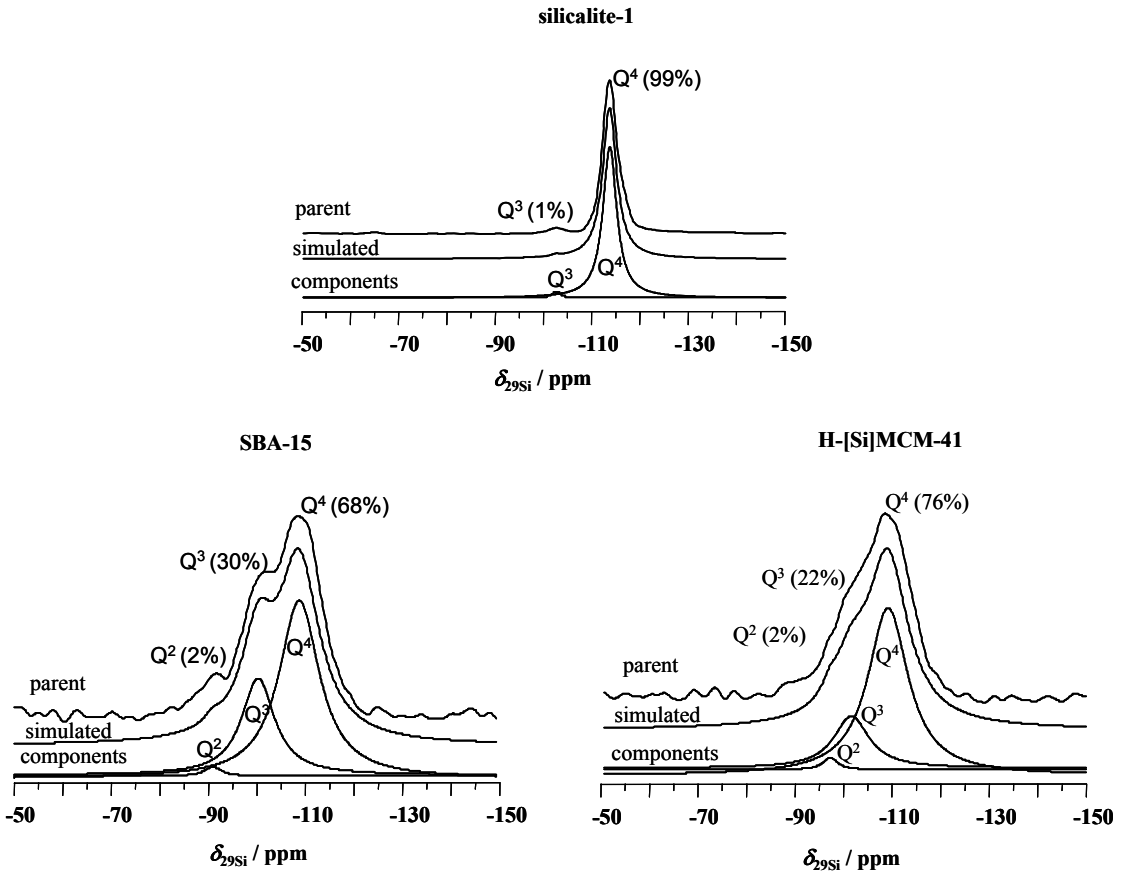

Figure 7.3. ^{29}Si HPDEC MAS NMR spectra of silicalite-1 (top), siliceous SBA-15 (left, bottom), and H-[Si]MCM-41 (right, bottom), and their simulation.

Moreover, it can be noticed that the signal of O-protonated ε-caprolactam species at *ca.* -237 ppm is more pronounced and resolved in the spectra of SBA-15 (Figs. 7.4e and 7.4f, left) and H-[Si]MCM-41 (Figs. 7.5e to 7.5g, left) than in the spectra of silicalite-1 (Figs. 7.2d and 7.2e, left). This could be due to the larger number of Q^3 silanol groups in mesoporous SBA-15 and H-[Si]MCM-41 materials than in silicalite-1. This high concentration of Q^3 silanol groups with pK_a values of 2 to 4.5 [186] in mesoporous materials is responsible for the O-protonation of ε-caprolactam. In contrast, silicalite-1 contains a much lower number of Q^3 silanol groups and the formation of O-protonated ε-caprolactam is very weak (Figs. 7.2d and 7.2e, left).

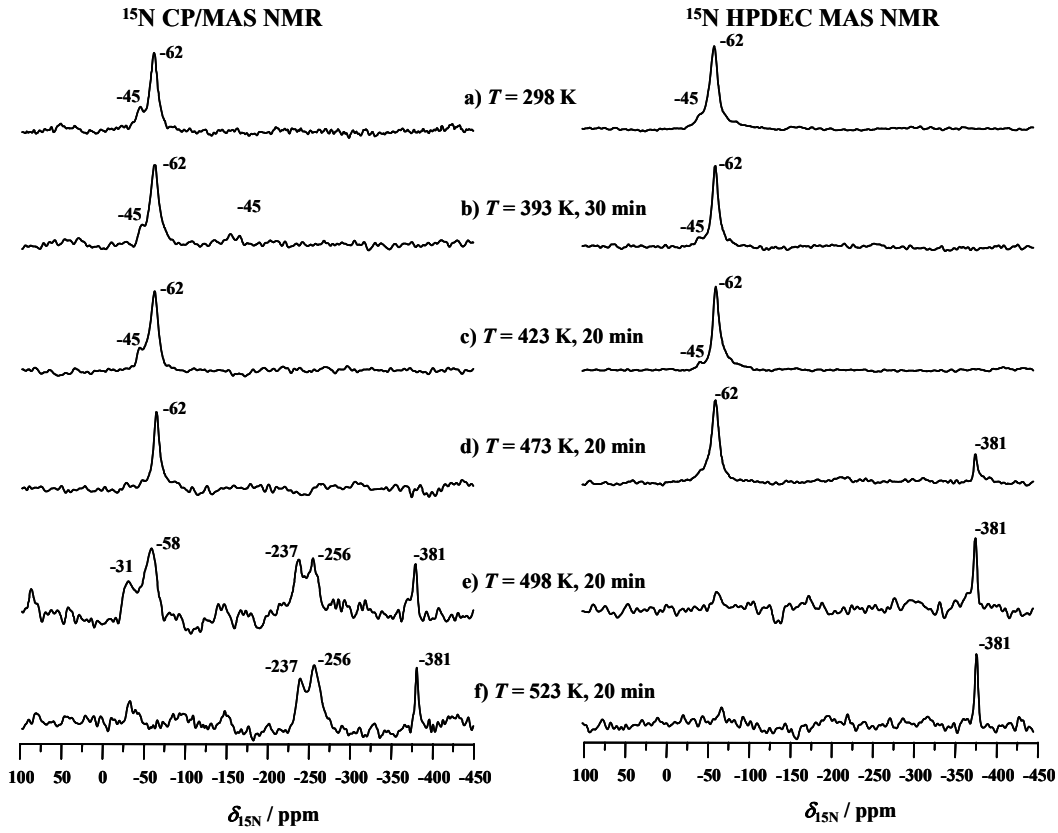

Figure 7.4. ^{15}N CP (left) and ^{15}N HPDEC (right) MAS NMR spectra recorded upon conversion of ^{15}N-cyclohexanone oxime on siliceous SBA-15 (n_{Si} / n_{Al} = 1800). The reaction temperatures and heating times are given in the Figure.

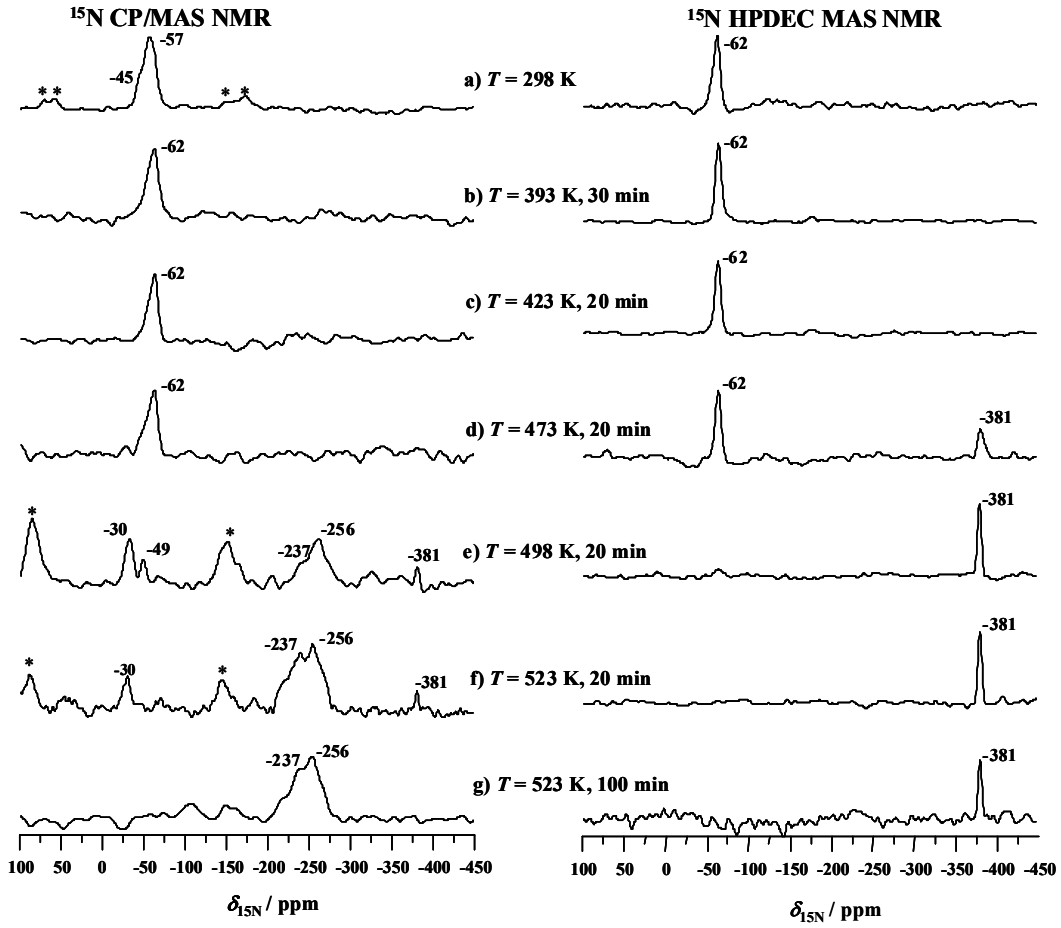

Figure 7.5. ^{15}N CP (left) and ^{15}N HPDEC (right) MAS NMR spectra recorded upon conversion of ^{15}N-cyclohexanone oxime on H-[Si]MCM-41 (n_{Si} / n_{Al} = 1080). The reaction temperatures and heating times are given in the Figure. Asterisks in the NMR spectra denote spinning sidebands.

7.5 Vapor-phase Beckmann rearrangement of ^{15}N-cyclohexanone oxime on strongly acidic H-ZSM-5 zeolite

H-ZSM-5 (n_{Si} / n_{Al} = 14) is an MFI-type zeolite contains silanol groups as well as bridging OH groups acting as strong Brønsted acid sites. Fig. 7.6 represents the ^{15}N CP and ^{15}N HPDEC MAS NMR spectra recorded upon the conversion of ^{15}N-oxime on H-ZSM-5 zeolite.

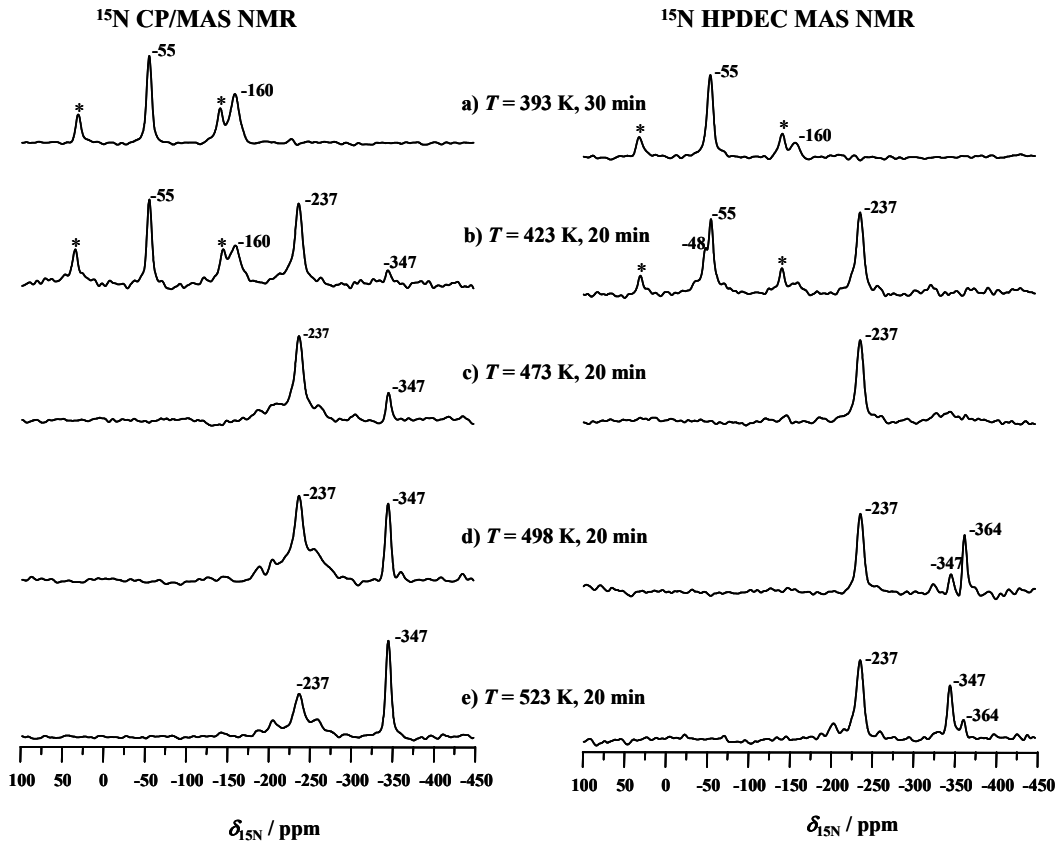

Figure 7.6. ^{15}N CP (left) and ^{15}N HPDEC (right) MAS NMR spectra recorded upon conversion of ^{15}N-cyclohexanone oxime on H-ZSM-5 (n_{Si} / n_{Al} = 14). The reaction temperature and heating times are given in the Figure. Asterisks in the NMR spectra denote spinning sidebands.

Studying the interaction of ^{15}N-cyclohexanone oxime with the Brønsted acid sites of zeolite H-ZSM-5 at 393 K for 30 min, the ^{15}N MAS NMR spectra of the ^{15}N-oxime/H-ZSM-5 mixture show a new high-field signal at -160 ppm in addition to the unconverted ^{15}N-oxime at -55 ppm (Fig. 7.6a). This signal at *ca.* -160 ppm, which did not appear in case of weakly acidic siliceous catalysts, such as silicalite-1, SBA-15, and H-[Si]MCM-41, was assigned to ^{15}N-cyclohexanone oxime, which was N-protonated by the acidic bridging OH groups (SiOHAl) in the vicinity of framework aluminum atoms in zeolite H-ZSM-5 [125, 134, 184]. A similar high-field shift of *ca*. 110 ppm was observed by

Fernández *et al.* [125, 133] for the N-protonated ^{15}N-acetophenone oxime, and ^{15}N-cyclohexanone oxime adsorbed on the bridging hydroxyl groups of Al-containing zeolites H-Beta and H-ZSM-5, respectively. It is noteworthy to mention that the N-protonation occurring exclusively on Brønsted acid sites always leads to a high-field shift (lower chemical shift values) of the resonance position [184].

The vapor-phase Beckmann rearrangement of ^{15}N-cyclohexanone oxime on zeolite H-ZSM-5 starts at *ca.* 423 K as indicated by the new signals in the ^{15}N MAS NMR spectra (Fig. 7.6b). In addition to the signal of protonated and non-interacting ^{15}N-cyclohexanone oxime at -160 ppm and -55 ppm, respectively, a dominating signal at -237 ppm corresponding to O-protonated ε-caprolactam occurs. The intensity of this signal (-237 ppm) is much higher than in the case of siliceous catalysts, such as SBA-15 and H-[Si]MCM-41, which is due to the strongly acidic nature of bridging hydroxyl groups of H-ZSM-5 (n_{Si} / n_{Al} = 14). In addition, new signals in the range of -347 to -364 ppm appear when the ^{15}N-oxime/H-ZSM-5 mixture was heated at 423 to 523 K for 20 min. These signals, which did not appear in case of siliceous catalysts, were exclusively observed on Brønsted acidic catalysts. The signals in the range of -347 to -364 ppm may be due to the further conversion of ε-caprolactam into N-protonated ε-caprolactam or ε-aminocapric acid or protonated ε-caprolactam species. The conversion of ε-caprolactam was further supported by the decrease of the signal intensity at -237 ppm, while the increase of the signal intensity at -347 ppm.

7.6 Vapor-phase Beckmann rearrangement of ^{15}N-cyclohexanone oxime on aluminum-containing mesoporous SBA-15 and MCM-41 materials

The existence of strong Brønsted acid sites in aluminum-containing zeolites, such as H-ZSM-5, is due to the presence of bridging hydroxyl groups in the vicinity of framework aluminum atoms. In contrast, the Brønsted acid sites of aluminum-containing mesoporous SBA-15 ([Al]SBA-15) and MCM-41 (H-[Al]MCM-41) materials are caused by terminal silanol groups in the vicinity of framework aluminum atoms [48]. In the vapor-phase Beckmann rearrangement of cyclohexanone oxime, [Al]SBA-15 is more selective towards ε-caprolactam than siliceous SBA-15 [114], while H-ZSM-5 is less selective than silicalite-1 [85, 93]. Furthermore, the Brønsted acid sites of [Al]SBA-15

have the lower acid strength in comparison with those of H-ZSM-5 [48]. Therefore, it is interesting to study the behavior of the different species formed on these materials *via* the Beckmann rearrangement of ^{15}N-cyclohexanone oxime. The ^{15}N CP and ^{15}N HPDEC MAS NMR spectra recorded upon the Beckmann rearrangement of ^{15}N-cyclohexanone oxime on both [Al]SBA-15 (n_{Si} / n_{Al} = 9) and H-[Al]MCM-41 (n_{Si} / n_{Al} = 11) are depicted in Figs. 7.7 and 7.8, respectively.

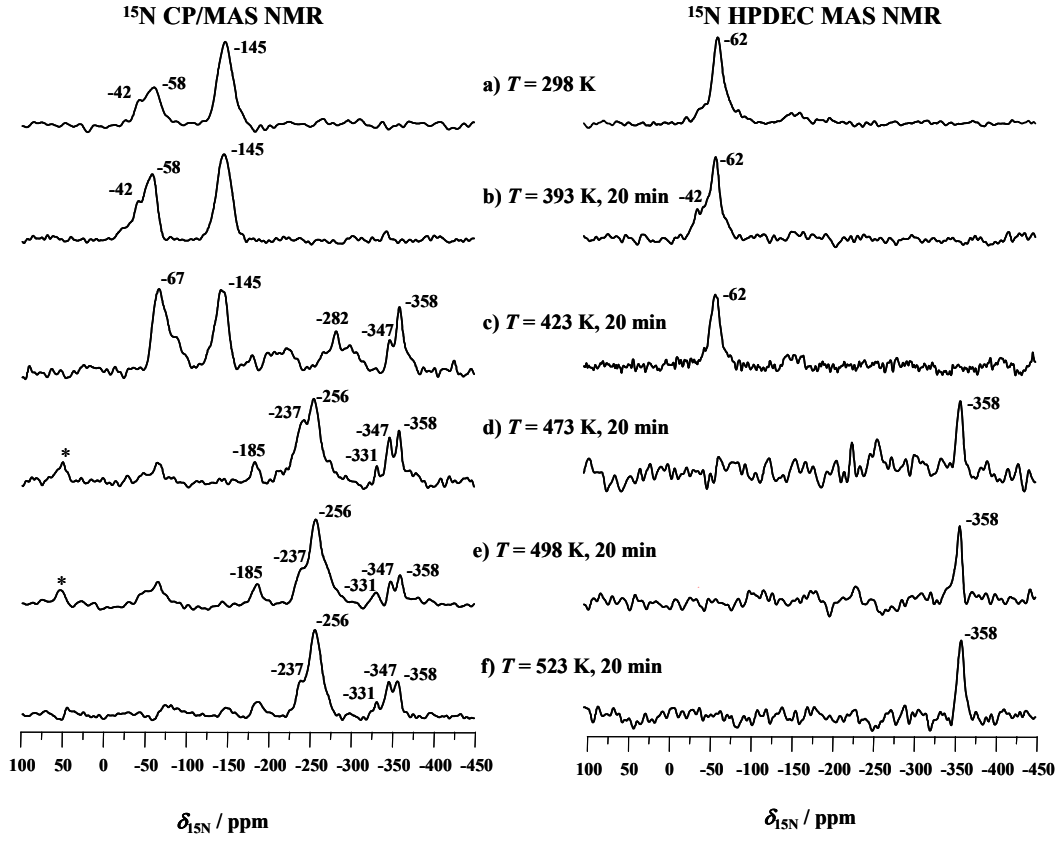

Figure 7.7. ^{15}N CP (left) and ^{15}N HPDEC (right) MAS NMR spectra recorded upon conversion of ^{15}N-cyclohexanone oxime on [Al]SBA-15 (n_{Si} / n_{Al} = 9). The reaction temperatures and heating times are given in the Figure. Asterisks in the NMR spectra denote spinning sidebands.

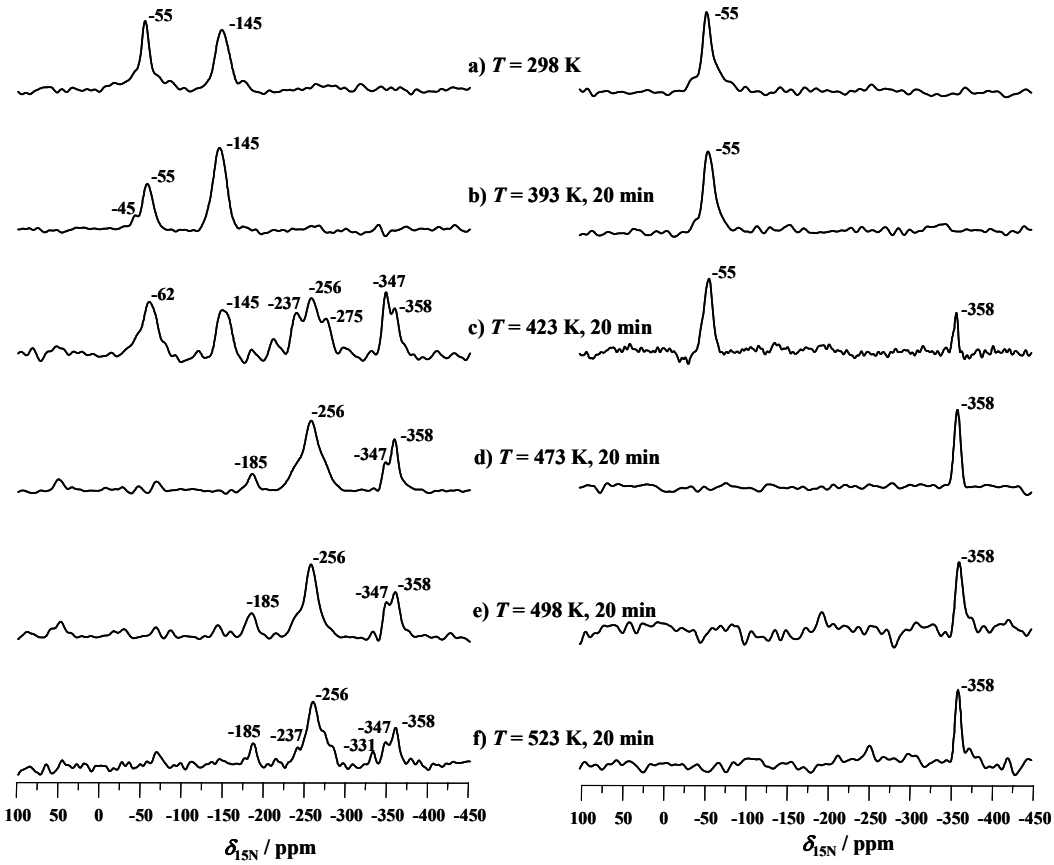

Figure 7.8. ^{15}N CP (left) and ^{15}N HPDEC (right) MAS NMR spectra recorded upon conversion of ^{15}N-cyclohexanone oxime on H-[Al]MCM-41 (n_{Si} / n_{Al} = 11). The reaction temperatures and heating times are given in the Figure.

The ^{15}N CP and ^{15}N HPDEC MAS NMR spectra of the ^{15}N-oxime/[Al]SBA-15 (Figs.7.7a and 7.7b) and ^{15}N-oxime/H-[Al]MCM-41 (Figs. 7.8a and 7.8b) mixtures heated at 298 K and 393 K show signals in the range of -55 to -62 ppm, -42 to -45 ppm, and at -145 ppm. These signals are assigned to unconverted oxime, oxime hydrogen-bonded to SiOH groups, and N-protonated oxime adsorbed on Brønsted acidic OH groups, respectively [125, 133, 134, 184]. The vapor-phase Beckmann rearrangement reaction on mesoporous Brønsted acidic catalysts, such as [Al]SBA-15 and H-[Al]MCM-41, occurs upon heating the mixtures at 423 K as shown in Figs. 7.7c and 7.8c. In addition to the signals corresponding to the unconverted oxime (*ca.* -62 ppm) and N-protonated oxime (*ca.* -145 ppm), new signals in the range of -275 to -282 ppm, and

-347 to -358 ppm were observed. As in the case of ^{15}N-oxime/H-ZSM-5 mixtures, the signals in the range of -347 to -358 ppm are due to the further conversion of ε-caprolactam into N-protonated ε-caprolactam or non- or N-protonated ε- aminocapric acid species. The signal in the range of -275 to -282 ppm, which also appeared in the case of silicalite-1 (-269 ppm) catalyst (Fig. 7.2), is due to the formation of hydroxylamine as result of the hydration reaction of cyclohexanone oxime into cyclohexanone and hydroxylamine (see Section 7.8, Scheme 7.3).

At higher reaction temperatures (473 K to 523 K), complete conversion of ^{15}N-cyclohexanone oxime occurs as indicated by the disappearance of the signal corresponding to ^{15}N-cyclohexanone oxime, and the appearance of the signals of products and by-products of the Beckmann rearrangement (Figs. 7.7d to 7.7f, and 7.8d to 7.8f). The signals of O-protonated and non-protonated ε-caprolactam were observed at -237 and -256 ppm, respectively. In addition to the signals discussed above, small peaks at -185 and -331 ppm were noticed. The signals at -185 and -331 ppm are due to the formation of partially protonated 5-cyano-1-pentene and aniline, respectively [184]. Dehydration of cyclohexanone oxime causes the formation of 5-cyano-1-pentene [98, 109]. Assuming a partial protonation of this compound, a predicted mean resonance position of -194 ppm is obtained. Therefore, the ^{15}N CP/MAS NMR signal at -185 ppm is assigned to partially protonated 5-cyano-1-pentene, a by-product in the vapor-phase Beckmann rearrangement.

7.7 Vapor-phase Beckmann rearrangement of ^{15}N-cyclohexanone oxime on mediumly acidic H-[B]ZSM-5 zeolite

H-[B]ZSM-5 (n_{Si} / n_B = 38) zeolite is an MFI-type zeolite with a specific Brønsted acidic behavior. This zeolite contains both silanol groups as well as weak Brønsted acid sites in the vicinity of framework boron atoms. The acidic nature and the coordination change of boron in H-[B]ZSM-5 zeolite was extensively studied by adsorption of probe molecules, and has already been discussed in Chapter 5. This zeolite was reported to be a selective catalyst in the vapor-phase Beckmann rearrangement reaction [86, 89]. Since the Brønsted acid sites in H-[B]ZSM-5 are caused by terminal silanol groups in the vicinity of framework boron atoms (SiOH[B]), the acidic and catalytic behavior of

H-[B]ZSM-5 is expected to be similar to that of mesoporous [Al]SBA-15 and H-[Al]MCM-4 materials. In order to understand the catalytic behavior, the vapor-phase Beckmann rearrangement of ^{15}N-cyclohexanone oxime on H-[B]ZSM-5 was studied by ^{15}N CP and ^{15}N HPDEC MAS NMR spectroscopy. The ^{15}N MAS NMR spectra of ^{15}N-oxime/H-[B]ZSM-5 mixture were presented in Fig. 7.9.

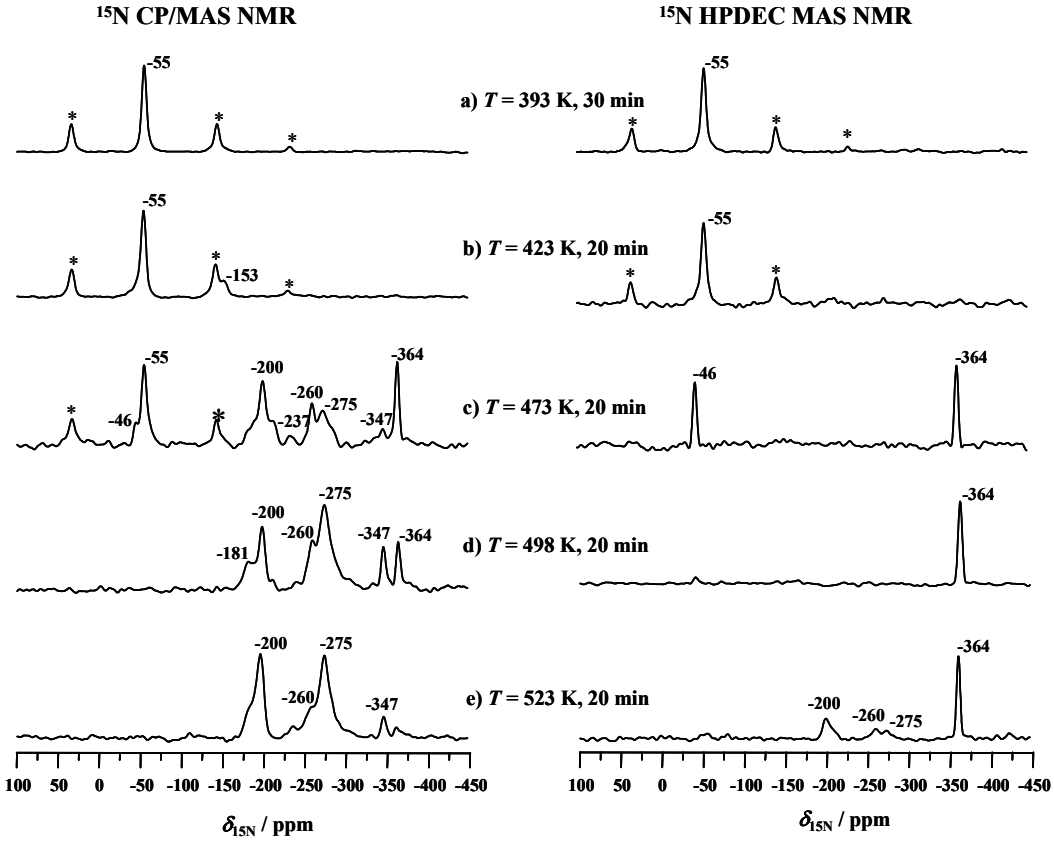

Figure 7.9. ^{15}N CP (left) and ^{15}N HPDEC (right) MAS NMR spectra recorded upon conversion of ^{15}N-cyclohexanone oxime on H-[B]ZSM-5 (n_{Si} / n_B = 38). The reaction temperatures and heating times are given in the Figure. Asterisks in the NMR spectra denote spinning sidebands.

As shown in Figs. 7.9a and 7.9b, upon heating the ^{15}N-oxime/H-[B]ZSM-5 mixture at 393 K and 423 K, the ^{15}N MAS NMR spectra show signals at -55 and -153

ppm due to the unconverted ^{15}N-cyclohexanone oxime and N-protonated cyclohexanone oxime formed on Brønsted acid sites, respectively [125, 133, 134, 184]. The vapor-phase Beckmann rearrangement on H-[B]ZSM-5 starts at 473 K as indicated by new signals (Fig. 7.9c), while complete conversion occurs at 498 K and 523 K (Figs. 7.9d and 7.9e). In addition to the signals of unconverted oxime (*ca.* -55 ppm) and ^{15}N-oxime interacting with SiOH groups *via* hydrogen bonding (-46 ppm), other new signals were observed. The assignment of the signals at -181 to -200 ppm, -237 ppm, -260 ppm, -275 ppm, and -347 to -364 ppm is similar to that of H-ZSM-5, [Al]SBA-15, and H-[Al]MCM-41 catalysts (see Section 7.8, Table 7.1). The signals at -237 and -260 ppm correspond to O-protonated and non-protonated *ε*-caprolactam, respectively [125, 133, 134, 184]. The signals in the range of -347 to -364 ppm, which are exclusively observed on Brønsted acidic catalysts, such as H-ZSM-5, [Al]SBA-15 and H-[Al]MCM-41, are due to the further conversion of *ε*-caprolactam into N-protonated *ε*-caprolactam or non- or N-protonated *ε*-aminocapric acid species. As observed in the spectra of ^{15}N-oxime/[Al]SBA-15 and ^{15}N-oxime/ H-[Al]MCM-41 mixtures, the signals in the range of -181 to -200 ppm were assigned to partially protonated 5-cyano-1-penetene. The signal at -275 ppm is due the side-reaction leading to the formation of hydroxyl ammine [98, 134, 184].

Furthermore, the nature and coordination transformation of framework boron atom in H-[B]ZSM-5 zeolite during the vapor-phase Beckmann rearrangement at different reaction temperatures was studied by ^{11}B MAS NMR spectroscopy. As observed by ^{15}N MAS NMR spectroscopy, ^{15}N-cyclohexanone oxime interacts with Brønsted acid sites of H-[B]ZSM-5 zeolite and leading to the N-protonation of cyclohexanone oxime due to the proton transfer from Brønsted acid sites. This is further supported by ^{11}B MAS NMR spectroscopy as shown in Fig. 7.10. The ^{11}B MAS NMR spectrum of dehydrated H-[B]ZSM-5 zeolite show a qudrupolar pattern (C_{QCC} = 2.7 ± 0.1 MHz) of trigonally coordinated framework boron ($B^{[3]}$). However, upon heating the ^{15}N-oxime/H-[B]ZSM-5 mixture at 423 K, a slight change in the ^{11}B MAS NMR spectrum was observed. This change indicates that there is a coordination change of framework boron from $B^{[3]}$ into $B^{[4]}$ species due to the proton transfer. From Fig. 7.9, it is evident that the vapor-phase Beckmann rearrangement occurs at 473 K to 523 K. During the vapor-phase Beckmann

rearrangement, water is released (see Section 7.8, Scheme 7.1). At higher reaction temperatures (473 K to 523 K) and in the presence of water, almost complete transformation of $B^{[3]}$ species into $B^{[4]}$ species was observed (Figs. 7.10c to 7.10e).

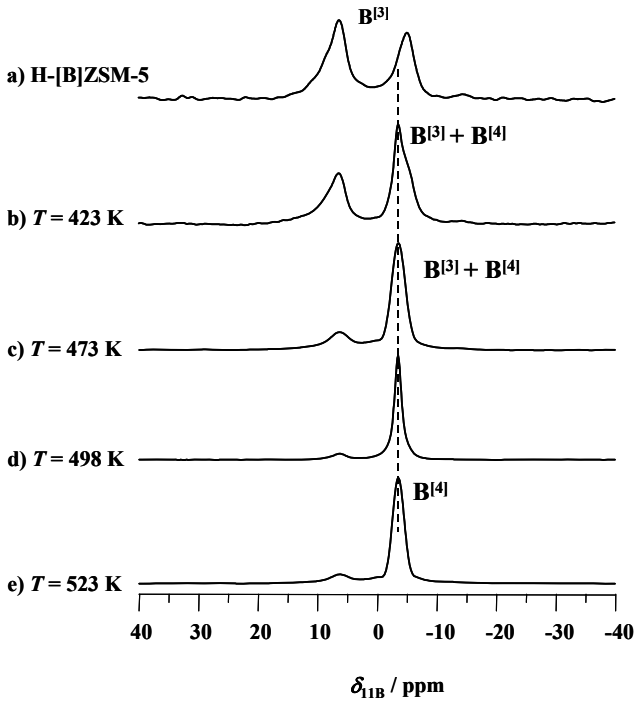

Figure 7.10. ^{11}B MAS NMR spectra of dehydrated H-[B]ZSM-5 zeolite (a) and mixtures of ^{15}N-cyclohexanone oxime and H-[B]ZSM-5 zeolite heated at different reaction temperatures as indicated in the Figure (b-e).

7.8 Establishing the reaction mechanism of Vapor-phase Beckmann rearrangement on solid catalysts

The assignments of the ^{15}N NMR signals observed experimentally on different solid catalysts are summarized in Table 7.1. The ^{15}N MAS NMR results obtained in this work led to the reaction mechanism of the vapor-phase Beckmann rearrangement of cyclohexanone oxime represented in Scheme 7.1.

Table 7.1. Assignments of ^{15}N NMR signals of the species observed during the vapor-phase Beckmann rearrangement of ^{15}N-cyclohexanone oxime.

δ_{15N} / (ppm)	Assignments	Ref.
-30 to -46	^{15}N-cyclohexanone oxime interacting with SiOH groups of zeolites and mesoporous materials *via* hydrogen bonding	[133, 134, 184]
-51 to -62	unconverted ^{15}N-cyclohexanone oxime on zeolites and mesoporous materials	[125, 134, 184]
-145 to -160	N-protonated cyclohexanone oxime, exclusively formed on Brønsted acid sites of zeolites and mesoporous materials	[125, 133, 134, 184]
-237 to -243	O-protonated ε-caprolactam on Q^3 silanol groups ($Si(OSi)_3OH$) and Brønsted acid sites	[125]
-255 to -262	physically adsorbed ε-caprolactam on SiOH groups and Brønsted acid sites	[125, 133, 134, 184]
-269 to -280	hydroxylamine	[133, 184]
-331	aniline	[184]
-347 to -364	N-protonated ε-caprolactam, or non- or N-protonated ε-aminocapric acid, exclusively formed on Brønsted acid sites	[134, 184, 187]
-375 to -387	amines formed on SiOH groups of siliceous zeolites and mesoporous materials	[125, 134, 184]

The first steps of the Beckmann rearrangement of cyclohexanone oxime on the solid catalysts under study are the adsorption of the reactant molecules *via* hydrogen bonding at SiOH groups (**A**) in siliceous and Brønsted acidic catalysts, or the N-protonation of the reactant by Brønsted acid sites (**B**), which occurs exclusively on Brønsted acidic catalysts. Quantum chemical studies of Bucko *et al.* [183] indicate that the 1,2-H shift leading to O-protonated cyclohexanone oxime (**C**) is followed by the formation of carbenium ions (**D**) and nitrilium ions (**E**) as intermediates. Since the ^{15}N

MAS NMR signals corresponding to the species **C**, **D**, and **E** were not observed by ^{15}N MAS NMR spectroscopy, it indicates that these species were unstable intermediates in the Beckmann rearrangement reaction. The final step of this reaction is the formation of ε-caprolactam (**F**), the main product of the vapor-phase Beckmann rearrangement. However, in the presence of more acidic Q^3 silanol groups ($Si(OSi)_3OH$) or Brønsted acid sites, the product is strongly adsorbed leading to the formation of O-protonated ε-caprolactam (**G**).

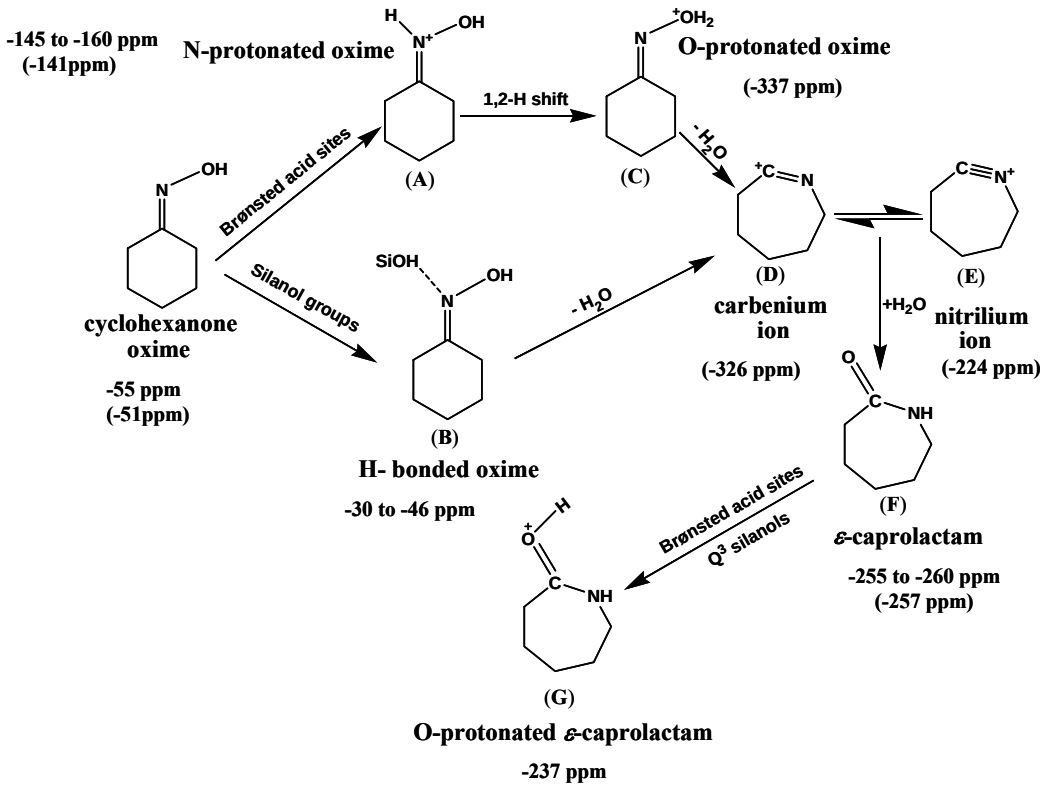

Scheme 7.1. Reaction mechanism of the vapor-phase Beckmann rearrangement on siliceous and Brønsted acidic catalysts. The ^{15}N NMR shifts observed experimentally in the present study were mentioned without parentheses, while the chemical shift values given in parentheses were obtained from the NNMR predictor software [184].

In addition, the ^{15}N MAS NMR results obtained in this work provide the information about the reasons of the catalyst deactivation in the vapor-phase Beckmann rearrangement reaction. In the case of weakly acidic catalyst, such as silicalite-1, two side-reactions, such as dehydration and hydration reactions of cyclohexanone oxime occur during the vapor-phase Beckmann rearrangement (Scheme 7.2). The product of the dehydration reaction is 5-cyano-1-pentene, while the products of the hydration reaction of cyclohexanone oxime are cyclohexanone and hydroxyl amine. In the case of mediumly acidic catalysts, such as [Al]SBA-15, H-[Al]MCM-41, and H-[B]ZSM-5, similar side-reactions like those on silicalite-1 occur (Scheme 7.3). However, due to the existence of Brønsted acid sites, the by-product 5-cyano-1-pentene is partially protonated and the signal for this mobile compound occurs in the range of *ca.* -185 to -200 ppm. The ^{15}N NMR results obtained in this work can be qualitatively compared with catalytic results [85, 86, 114]. The aforementioned side-reactions leading to the formation of by-products are the main reasons for the loss of selectivity towards ε-caprolactam.

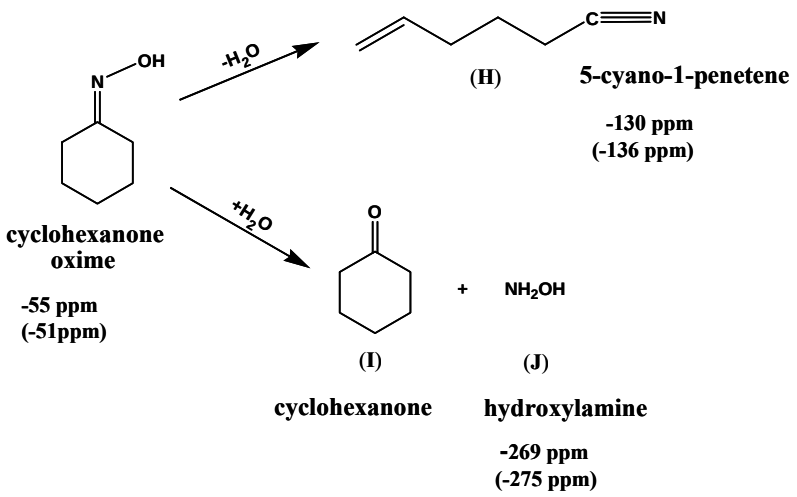

Scheme 7.2. Side-reactions occurring during the vapor-phase Beckmann rearrangement on silicalite-1 catalyst. The ^{15}N NMR shifts observed experimentally in the present study were mentioned without parentheses, while the chemical shift values given in parentheses were obtained from the NNMR predictor software [184].

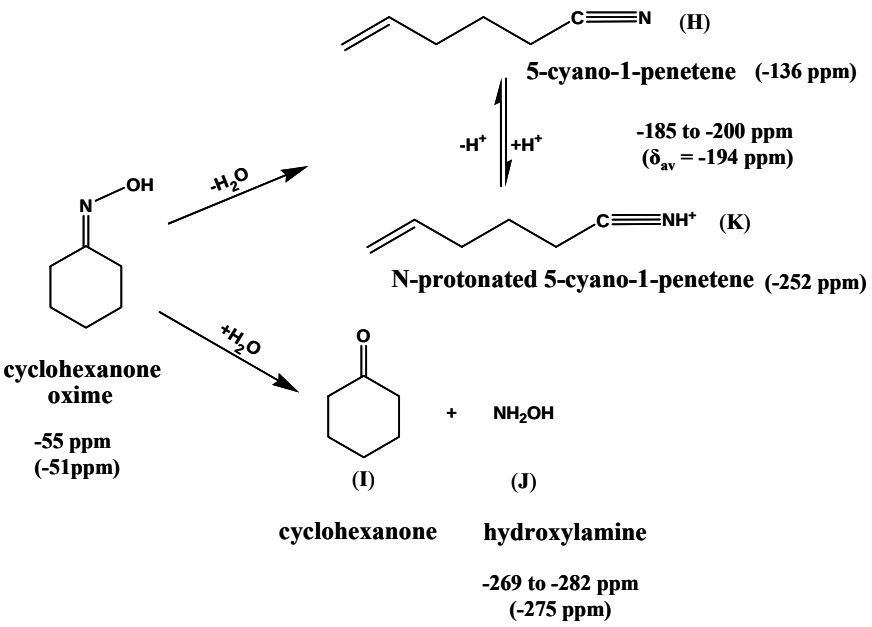

Scheme 7.3. Side-reactions occurring during the vapor-phase Beckmann rearrangement of ^{15}N-cyclohexanone oxime on [Al]SBA-15, H-[Al]MCM-41 and H-[B]ZSM-5 catalysts. The ^{15}N NMR shifts observed experimentally in the present study were mentioned without parentheses, while the chemical shift values given in parentheses were obtained from the NNMR predictor software [184].

Further conversion of O-protonated *ε*-caprolactam into N-protonated *ε*-caprolactam or non- or N-protonated *ε*-aminocapric acid was observed exclusively on Brønsted acidic catalysts, such as H-ZSM-5, [Al]SBA-15, H-[Al]MCM-41, and H-[B]ZSM-5 (Scheme 7.4). Qualitative comparison of catalytic data available in the literature [85, 86, 114] with the results of the present ^{15}N CP/MAS NMR study of the vapor-phase Beckmann rearrangement on Brønsted acidic catalysts, indicate the following reasons for the decrease of the *ε*-caprolactam selectivity: (i) The formation of O-protonated and N-protonated *ε*-caprolactam on the catalyst surface, *i.e.* of strongly adsorbed reaction products, and (ii) the formation of by-products, such as non- or N-protonated *ε*-aminocapric acid (Scheme 7.4).

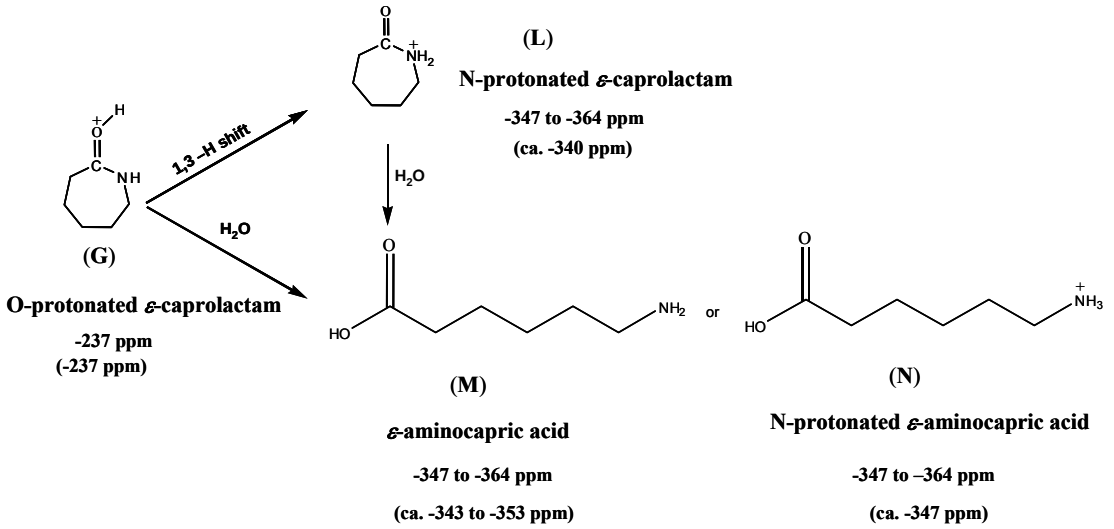

Scheme 7.4. Further conversion of O-protonated ε-caprolactam on Brønsted acidic catalysts, such as H-ZSM-5, [Al]SBA-15, H-[Al]MCM-41, and H-[B]ZSM-5. The ^{15}N NMR shifts observed experimentally in the present study were mentioned without parentheses, while the chemical shift values given in parentheses were obtained from the NNMR predictor software [184].

7.9 Conclusions

In the present work, the step-wise conversion of ^{15}N-cyclohexanone oxime into ε-caprolactam *via* the vapor-phase Beckmann rearrangement on different siliceous catalysts (silicalite-1, SBA-15 and H-[Si]MCM-41) and Brønsted acidic catalysts (H-ZSM-5, [Al]SBA-15, H-[Al]MCM-41, and H-[B]ZSM-5) was studied by *in situ* ^{15}N CP and ^{15}N HPDEC MAS NMR spectroscopy. The catalysts, such as MFI-type zeolites and mesoporous SBA-15 and MCM-41 materials were characterized by different acid strengths and pore diameters. The surface OH concentrations in silicalite-1, SBA-15, H-[Si]MCM-41, H-ZSM-5, [Al]SBA-15, H-[Al]MCM-41, and H-[B]ZSM-5 materials were determined to 0.31, 2.81, 2.69, 1.12, 1.29, 2.00, and 0.65 mmol g^{-1}, respectively.

This study demonstrates that *in situ* solid-state ^{15}N NMR spectroscopy is a very useful technique to investigate the reaction mechanism of organic reactions, such as the Beckmann rearrangement on solid catalysts. It gives information about the formation of reaction intermediates, products, and by-products in the vapor-phase Beckmann

rearrangement reaction on solid catalysts at different reaction temperatures. In addition, details on the adsorption state, and reaction behavior of reactant, reaction intermediates, products and by-products of the Beckmann rearrangement were obtained.

This work concludes that both silanol groups and Brønsted acid sites of solid catalysts are accessible and active in the vapor-phase Beckmann rearrangement reaction. On silanol groups, the reactant, product, and by-products of the Beckmann rearrangement reaction are weakly adsorbed *via* hydrogen bonding. In contrast, on Brønsted acid sites, the reactant cyclohexanone oxime and the product ε-caprolactam were strongly adsorbed leading to an N- and O-protonation, respectively. The investigations also revealed that O-protonated ε-caprolactam is formed on both siliceous and Brønsted acidic catalysts. However, the formation of O-protonated ε-caprolactam on siliceous catalysts depend on the number of acidic Q^3 silanol groups ($Si(OSi)_3OH$). Further conversion of O-protonated ε-caprolactam was observed exclusively on Brønsted acidic catalysts. The reasons for the loss of selectivity on solid catalysts were found by observing the by-products caused by the side-reactions.

8 Influence of ^{13}C-methanol as an additive in the vapor-phase Beckmann rearrangement of ^{15}N-cyclohexanone oxime on MFI-type zeolites and mesoporous SBA-15 materials studied by *in situ* ^{15}N and ^{13}C MAS NMR spectroscopy

8.1 Introduction

In the vapor-phase Beckmann rearrangement reaction of cyclohexanone oxime into ε-caprolactam, significant improvement in the selectivity towards ε-caprolactam can be achieved by the addition of solvents or additives [46, 62]. From the literature, the detailed description on the use of different solvents and their influence in the vapor-phase Beckmann rearrangement has already been presented in Chapter 3. Among different additives used in the Beckmann rearrangement of cyclohexanone oxime, the application of polar additives, like methanol, led to lower deactivation rates of the catalysts and higher selectivities towards the desired product than non-polar additives, such as benzene [46, 62, 93]. There have been some explanations of the role of additives. In the literature, it was reported that the improved selectivities could be due to the blockage of silanols at the outer surface of silicalite-1 particles [46, 62, 93]. This is further supported by FT IR studies, which showed the reaction of terminal silanols with methanol to methoxy species [93]. Another explanation for the improved selectivities is the effect of the polarity of methanol molecules and of their OH groups [86, 136]. Since polar additives increase desorption rate of ε-caprolactam by decreasing the contact time on the catalyst surface, the additives also minimize the deactivation of the catalyst [86].

However, the literature on the influence of additives on the species (reactants, products, and by-products) formed during the Beckmann rearrangement, the adsorption and desorption behavior of these species in the absence and presence of methanol, and the conversion of additives at different reaction temperatures is very scarce. By *in situ* ^{15}N MAS NMR spectroscopy, the conversion of cyclohexanone oxime into ε-caprolactam *via* the vapor-phase Beckmann rearrangement in the absence of additives on different solid-catalysts was studied and discussed in Chapter 7. In this Chapter, the influence of additives, by adding ^{13}C-methanol in the reaction system during the vapor-phase

Beckmann rearrangement of cyclohexanone oxime on MFI-type zeolites and mesoporous SBA-15 catalysts was studied by ^{15}N and ^{13}C MAS NMR spectroscopy.

8.2 Influence of ^{13}C-methanol as an additive in the vapor-phase Beckmann rearrangement of ^{15}N-cyclohexanone oxime on silicalite-1

The ^{15}N CP/MAS NMR spectra in Fig. 8.1 (left and middle) were recorded after the conversion of ^{15}N-cyclohexanone oxime into ε-caprolactam on silicalite-1 catalyst in the absence and presence of ^{13}C-methanol as an additive, respectively. In order to obtain the complete information, ^{15}N and ^{13}C HPDEC MAS NMR spectra were also recorded, and the results were represented in Fig. 8.2. The assignments of the ^{15}N MAS NMR signals observed in this work were summarized in Table 7.1 of Chapter 7. The ^{15}N MAS NMR signal at -55 ppm in Figs. 8.1 and 8.2 is due to unconverted ^{15}N-cyclohexanone oxime [134, 184]. The additional signal at -46 ppm is a result of the interaction of ^{15}N-oxime with silicalite-1 *via* hydrogen bonding [125, 133, 134]. When the ^{15}N-oxime/silicalite-1 mixture containing no methanol was heated to 523 K for 20 and 60 min (Figs. 8.1 and 8.2, left), the appearance of new signals indicate the conversion of ^{15}N-oxime. The corresponding signals at -260 ppm, -269 ppm, and -387 ppm are caused by the formation of ε-caprolactam, hydroxylamine, and amines, respectively [134, 184]. Due to the residual line width of solid-state NMR spectroscopy, the signal of hydroxyl amine (-269 ppm) could not be resolved in Fig. 8.1c, but it occurs as a broad shoulder. In addition, a small peak in the range of -237 to -243 ppm appears in Figs. 8.1b and 8.1c, which is due to the formation of O-protonated ε-caprolactam on Q^3 silanol groups of silicalite-1 (see Chapter 7, Sections 7.3 and 7.4). Furthermore, exclusively in the ^{15}N HPDEC MAS NMR spectra (Figs. 8.2b and 8.2c), a signal at -130 ppm was observed, which is due to the formation of 5-cyano-1-pentene, a mobile compound and by-product in the vapor-phase Beckmann rearrangement (see Chapter 7, Section 7.3).

When the ^{15}N-oxime/silicalite-1 mixture containing ^{13}C-methanol was heated to 523 K for 20 and 60 min (Figs. 8.1 and 8.2, middle), slightly different spectra occur in comparison with the experiments performed without ^{13}C-methanol (Figs. 8.1 and 8.2, left). Under the presence of methanol as an additive, the signal corresponding to O-protonated ε-caprolactam (-237 to -243 ppm) was not observed, while the signal

corresponding to the amines (-387 ppm) was suppressed (Figs. 8.1 and 8.2, middle). This indicates that the enhanced selectivity to ε-caprolactam in the gas phase could be caused by a decrease of the energy barrier for the product desorption, and no side reactions leading to the formation of amines occur when methanol was added as an additive.

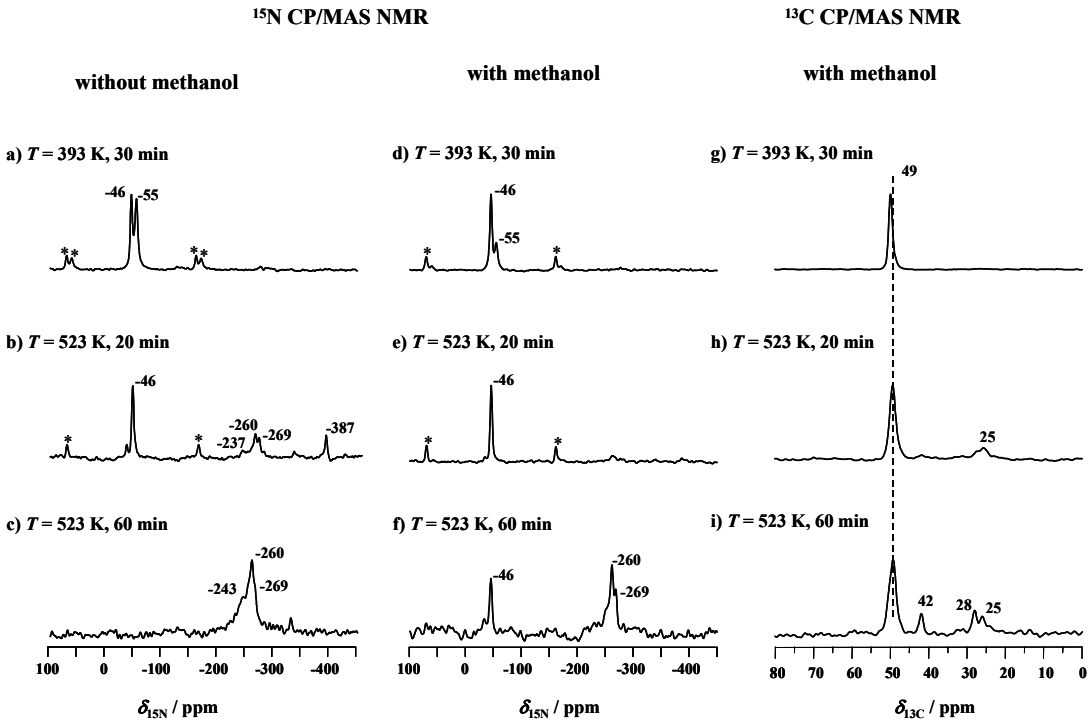

Figure 8.1. ^{15}N CP/MAS NMR spectra recorded upon conversion of ^{15}N-cyclohexanone oxime on silicalite-1 (n_{Si} / n_{Al} = 1700) in the absence (left) and presence (middle) of ^{13}C-methanol. ^{13}C CP/MAS NMR spectra (right) show the conversion of ^{13}C-methanol. The reaction temperatures and heating times are given in the Figure. Asterisks in the NMR spectra denote spinning sidebands.

The above-mentioned finding is supported by catalytic studies of Ichihashi and Kitamura [93]. These authors reported that the selectivity to ε-caprolactam increases with increasing n_{Si} / n_{Al} ratio, *i.e.* for silicalite-1 in comparison with H-ZSM-5 [93]. For silicalite-1, the selectivity towards ε-caprolactam increases from *ca.* 75% to 95% upon

addition of methanol to the reaction system [93]. Another difference is the observation of a signal at -130 ppm due to the formation of 5-cyano-1-pentene (Figs. 8.2e and 8.2f), even after addition of methanol. Surprisingly, this result shows that methanol could not influence the desorption or the formation of this by-product during the vapor-phase Beckmann rearrangement.

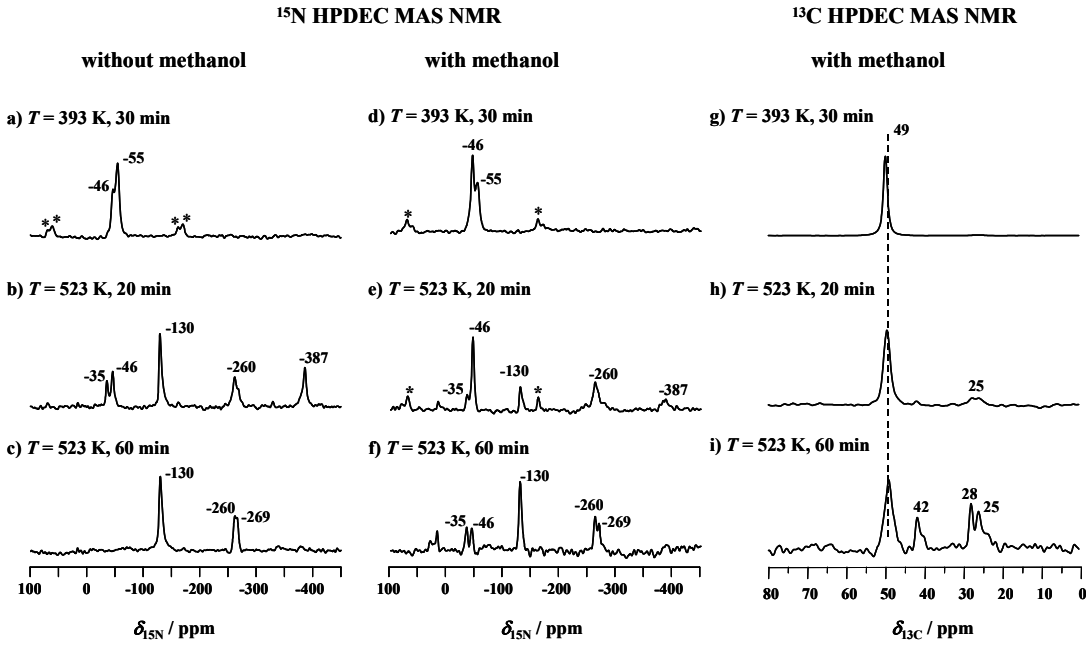

Figure 8.2. ^{15}N HPDEC MAS NMR spectra recorded upon conversion of ^{15}N-cyclohexanone oxime on silicalite-1 (n_{Si} / n_{Al} = 1700) in the absence (left) and presence (middle) of ^{13}C-methanol. ^{13}C HPDEC MAS NMR spectra (right) show the conversion of ^{13}C-methanol. The reaction temperatures and heating times are given in the Figure. Asterisks in the NMR spectra denote spinning sidebands.

The ^{13}C CP and HPDEC MAS NMR spectra show similar results as shown in Figs. 8.1 and 8.2 (right), respectively. The ^{13}C MAS NMR spectra of the ^{15}N-oxime/silicalite-1 mixture containing ^{13}C-methanol (Figs. 8.1 and 8.2, right) consist of a signal at *ca.* 49 ppm, which is attributed to ^{13}C-methanol. Due to the residual line width

of MAS NMR spectroscopy, the signal due to methoxy groups (48 to 50 ppm), if they are formed at all, could be covered by the signal of methanol (49 ppm) [188, 189]. In addition, the spectra recorded at 523 K (Figs. 8.1, and 8.2, right) show peaks at 25 ppm, 28 ppm, and 42 ppm indicating the conversion of methanol into hydrocarbons, such as isobutane, and alkylamines, such as isopropylamine [190-193]. Isopropylamine (42 ppm) may be formed *via* the reaction of isobutane with hydroxyl amine, which is formed as a by-product of the Beckmann rearrangement. Generally, the conversion of methanol is an acid catalyzed reaction. However, as observed in this work, the conversion of methanol can also occur on weakly acidic silicalite-1, which may be due to: (i) High methanol coverage (0.7 mmol g^{-1}) with respect to the small amount of silanol groups (n_H = 0.31 mmol g^{-1}) in silicalite-1, (ii) the presence of electronic confinement effects [194] for methanol clusters in the micropore system of silicalite-1, and (iii) the effect of residual framework aluminum atoms (n_{Si} / n_{Al} = 1700).

8.3 Influence of ^{13}C-methanol as an additive in the vapor-phase Beckmann rearrangement of ^{15}N-cyclohexanone oxime on H-ZSM-5

The ^{15}N and ^{13}C MAS NMR spectra recorded by utilizing cross-polarization (CP) and high-power decoupling (HPDEC) techniques upon the conversion of ^{15}N-cyclohexanone oxime into ε-caprolactam on H-ZSM-5 catalysts in the absence and presence of ^{13}C-methanol are depicted in Figs. 8.3 and 8.4. In the absence of methanol, the ^{15}N CP and HPDEC MAS NMR spectra of ^{15}N-oxime/H-ZSM-5 catalyst mixture (Figs. 8.3 and 8.4, left) show signals at -55 ppm and -160 ppm, which are due to unconverted and N-protonated ^{15}N-cyclohexanone oxime, respectively [125, 133, 134, 184]. Upon heating the mixture of ^{15}N-cyclohexanone oxime and H-ZSM-5 at 423 K to 523 K, the spectra show different new signals indicating the conversion of ^{15}N-cyclohexanone oxime (Figs. 8.3 and 8.4, left). The strongly dominating signal at -237 ppm (Fig. 4c) is due to the formation of O-protonated ε-caprolactam on bridging hydroxyl groups of H-ZSM-5 catalyst, while the signals in the range of -347 to -364 ppm are the result of further conversion of O-protonated ε-caprolactam into N-protonated ε-caprolactam or ring-opening products of ε-caprolactam (see Chapter 7, Scheme 7.4).

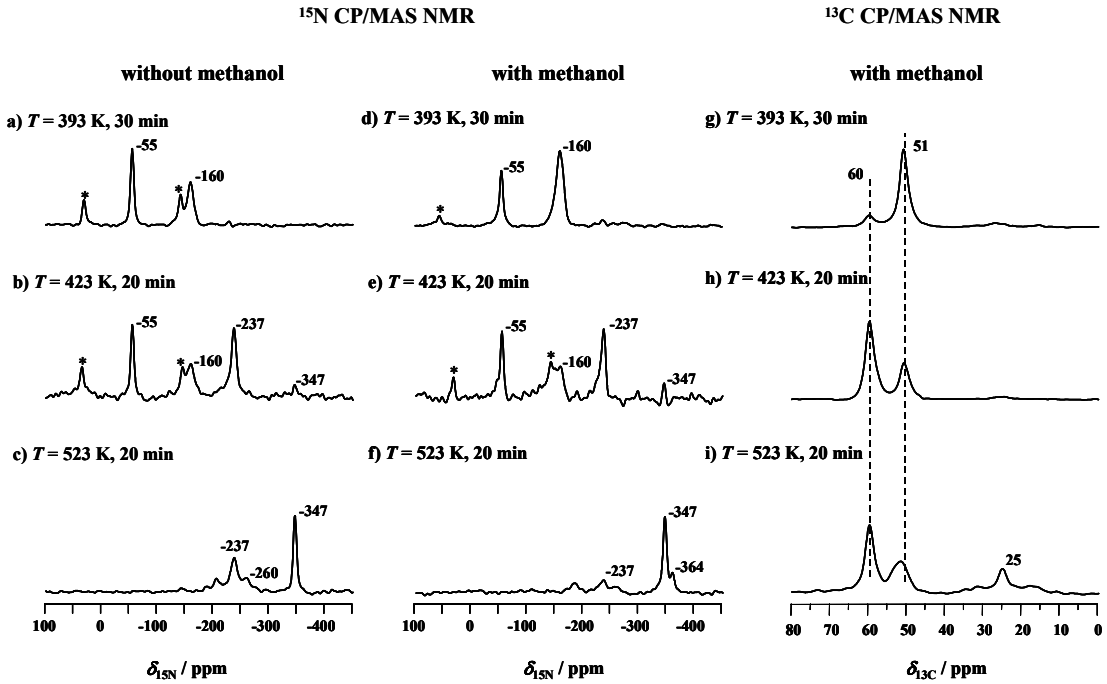

Figure 8.3. ^{15}N CP/MAS NMR spectra recorded upon conversion of ^{15}N-cyclohexanone oxime on H-ZSM-5 (n_{Si} / n_{Al} = 14) in the absence (left) and presence (middle) of ^{13}C-methanol. ^{13}C CP/MAS NMR spectra (right) show the conversion of ^{13}C-methanol. The reaction temperatures and heating times are given in the Figure. Asterisks in the NMR spectra denote spinning sidebands.

Upon addition of methanol to the ^{15}N-oxime/H-ZSM-5 mixture, significant differences were noticed in the spectra shown in Figs. 8.3 and 8.4 (middle), in comparison with the spectra of ^{15}N-oxime/H-ZSM-5 mixture without methanol (Figs. 8.3 and 8.4, left). In the absence of methanol, even after heating the ^{15}N-oxime/H-ZSM-5 mixture at 523 K, the ^{15}N MAS NMR spectra still contain a signal at -237 ppm, which is due to the formation of O-protonated ε-caprolactam on bridging hydroxyl groups of H-ZSM-5 catalyst (Fig. 8.3 and 8.4, left). When the ^{15}N-oxime/H-ZSM-5 mixture containing methanol was heated at 523 K, the ^{15}N MAS NMR spectra show only signals in the range of -347 to -364 ppm. This indicates that the further conversion of O-protonated ε-caprolactam into N-protonated ε-caprolactam or non- or N-protonated

ε-aminocapric acid is more severe when methanol is present as an additive in the reaction system. This is evidenced by the strong decrease of the signal corresponding to O-protonated ε-caprolactam (-237 ppm) and rising of the signals in the range of -347 to -364 ppm. This explanation is further supported by analyzing the ^{13}C MAS NMR spectra shown in Figs. 8.3 and 8.4, right.

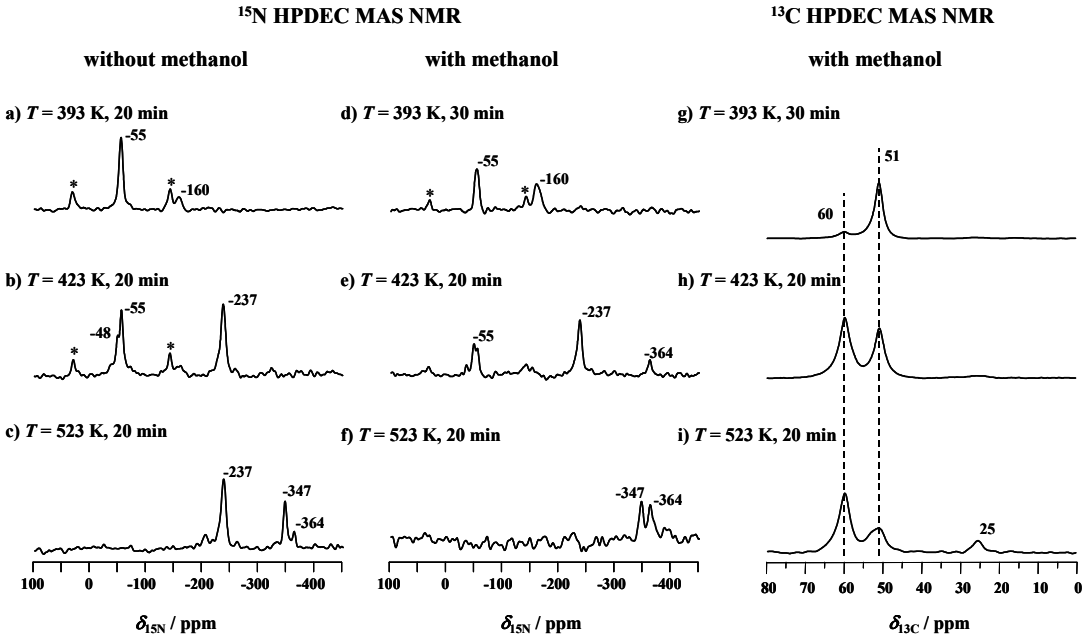

Figure 8.4. ^{15}N HPDEC MAS NMR spectra recorded upon conversion of ^{15}N-cyclohexanone oxime on H-ZSM-5 (n_{Si} / n_{Al} = 14) in the absence (left) and presence (middle) of ^{13}C-methanol. ^{13}C HPDEC MAS NMR spectra (right) show the conversion of ^{13}C-methanol. The reaction temperatures and heating times are given in the Figure. Asterisks in the NMR spectra denote spinning sidebands.

The ^{13}C MAS NMR spectra of the ^{15}N-oxime/H-ZSM-5/^{13}C-methanol mixture heated at 393 K show a strong signal at 51 ppm and a weak signal at 60 ppm. These signals are due to methanol and dimethylether (DME), respectively. The formation of dimethylether is caused by the dehydration reaction of methanol on strongly acidic H-ZSM-5 catalyst. When the heating temperature of the mixture was increased to 423 K and

523 K, the conversion of methanol into dimethylether was increased as indicated by the decrease of the signal at 51 ppm and the rise of the signal at 60 ppm. During the dehydration of methanol into dimethylether, water is formed as a by-product. This water is the reason for promoting the further conversion of O-protonated ε-caprolactam into N-protonated ε-caprolactam or ring-opening products of caprolactam (see Scheme 7.4 of Chapter 7). In addition, the formation of hydrocarbons, such as isobutane, occurs during the vapor-phase Beckmann rearrangement in the presence of methanol, which is indicated by the ^{13}C MAS NMR signal at 25 ppm (Figs. 8.3i and 8.4i).

8.4 Influence of ^{13}C-methanol as an additive in the vapor-phase Beckmann rearrangement of ^{15}N-cyclohexanone oxime on mesoporous siliceous SBA-15 and [Al]SBA-15 catalysts

The ^{15}N and ^{13}C CP/MAS NMR spectra recorded to study the influence of ^{13}C-methanol during the vapor-phase Beckmann rearrangement of ^{15}N-cyclohexanone oxime on siliceous SBA-15 and [Al]SBA-15 catalysts are represented in Figs. 8.5 and 8.6, respectively. When the ^{15}N-oxime/SBA-15 (Fig. 8.5, left) and ^{15}N-oxime/[Al]SBA-15 (Fig. 8.6, left) mixtures containing no methanol were heated at different reaction temperatures, the ^{15}N CP/MAS NMR spectra show different signals. The assignment of these signals and their explanation were described in Chapter 7, Table 7.1, and Sections 7.4 and 7.6. Briefly, the ^{15}N MAS NMR signals (Fig. 8.5, left) at -30 to -45 ppm, -58 to -62 ppm, -237 ppm, -256 ppm, and -381 ppm are due to the formation of hydrogen-bonded ^{15}N-oxime on SiOH groups, unconverted ^{15}N-oxime, O-protonated ε-caprolactam on Q^3 silanol groups, physically adsorbed ε-caprolactam, and amines, respectively. Similarly, the ^{15}N MAS NMR signals in the spectra of Fig. 8.6 (left) at -145 ppm, -237 ppm, -185 ppm, -331 ppm, -347 to -358 ppm are due to the formation of N-protonated ^{15}N-oxime, O-protonated ε-caprolactam, partially protonated 5-cyano-1-pentene, aniline, and N-protonated ε-caprolactam or ring-opening products of ε-caprolactam on Brønsted acid sites of the [Al]SBA-15 catalyst, respectively.

Surprisingly, even in the presence of methanol, the spectra of ^{15}N-oxime/SBA-15 (Fig. 8.5, middle) and ^{15}N-oxime/[Al]SBA-15 (Fig. 8.6, middle) mixtures yield similar results and consist of the same signals as observed in the spectra of mixtures containing

no methanol (Figs. 8.5 and 8.6, left). This indicates that methanol has no effect in improving the selectivity towards ε-caprolactam during the vapor-phase Beckmann rearrangement of cyclohexanone oxime on mesoporous SBA-15 catalysts. Furthermore, also the ^{15}N HPDEC MAS NMR spectra recorded for the ^{15}N-oxime/SBA-15/^{13}C-methanol and ^{15}N-oxime/[Al]SBA-15/^{13}C-methanol mixtures (not shown) show the same results like those of mixtures without ^{13}C-methanol (see Figs. 7.4 and 7.7, right, in Chapter 7).

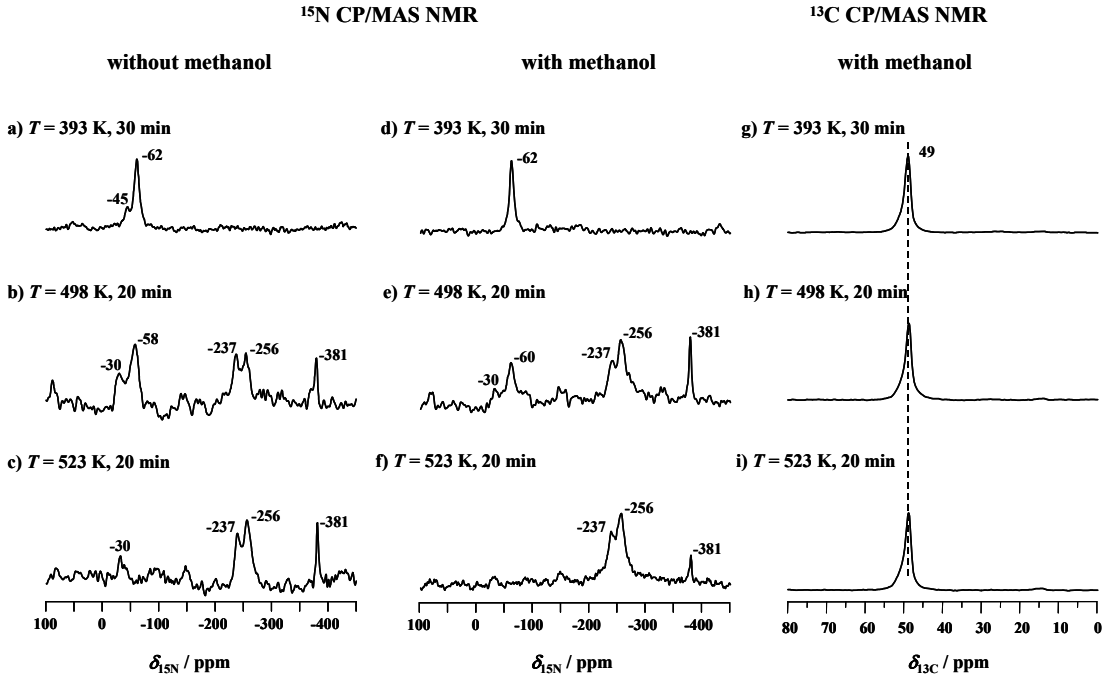

Figure 8.5. ^{15}N CP/MAS NMR spectra recorded upon conversion of ^{15}N-cyclohexanone oxime on siliceous SBA-15 (n_{Si} / n_{Al} = 1800) in the absence (left) and presence (middle) of ^{13}C-methanol. ^{13}C CP/MAS NMR spectra (right) show the presence of ^{13}C-methanol. The reaction temperatures and heating times are given in the Figure.

On the other hand, the ^{13}C CP/MAS NMR spectra of the ^{15}N-oxime/SBA-15/^{13}C-methanol and ^{15}N-xome/[Al]SBA-15/^{13}C-methanol mixtures recorded upon heating at different reaction temperatures (Figs. 8.5 and 8.6, right) consist of a single signal at *ca.*

49 ppm due to ^{13}C-methanol. This finding indicates that no conversion of methanol occurs on weakly acidic siliceous SBA-15 and Brønsted acidic [Al]SBA-15 catalysts in contrast to the conversion of methanol on silicalite-1. This may be due to the (i) low methanol coverage (1.4 mmol g^{-1}) with respect to the large number of OH groups in SBA-15 (n_H = 2.81 mmol g^{-1}) and [Al]SBA-15 (n_H = 1.29 mmol g^{-1}) catalysts and the (ii) lack of electronic confinement effects for the methanol molecules in the mesopores of these catalysts, which leads to a weaker interaction of methanol molecules with the OH groups of siliceous SBA-15 and [Al]SBA-15 catalysts.

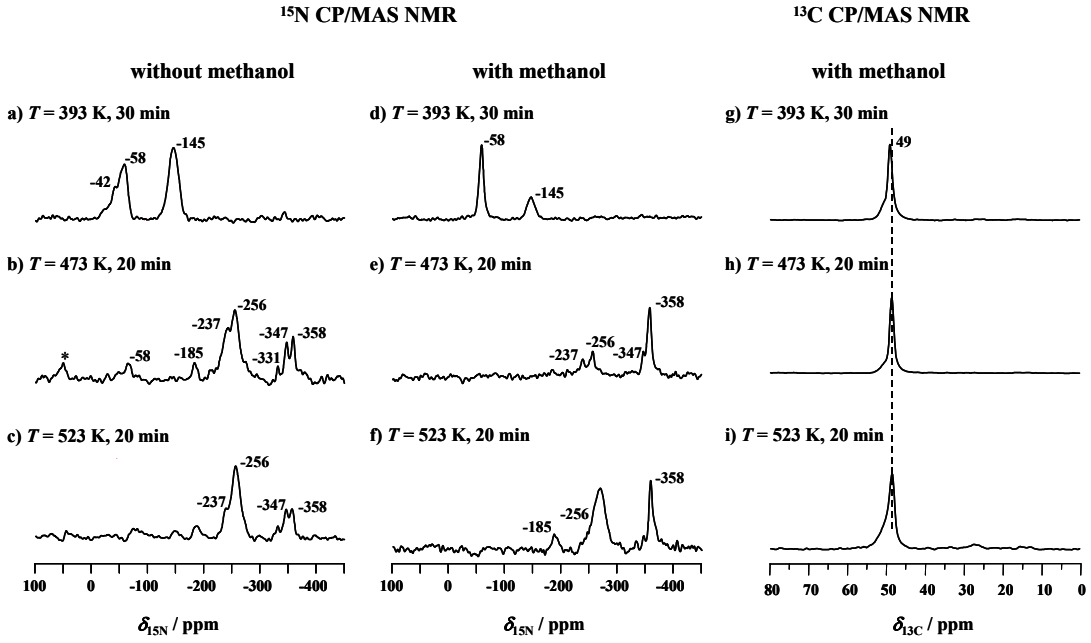

Figure 8.6. ^{15}N CP/MAS NMR spectra recorded upon conversion of ^{15}N-cyclohexanone oxime on [Al]SBA-15 (n_{Si} / n_{Al} = 8.7) in the absence (left) and presence (middle) of ^{13}C-methanol. ^{13}C CP/MAS NMR spectra (right) show the presence of ^{13}C-methanol. The reaction temperatures and heating times are given in the Figure. Asterisk in the NMR spectra denote spinning sidebands.

From the *in situ* MAS NMR spectroscopic results, the reasons for the catalyst deactivation leading to the lower selectivity towards ε-caprolactam on mesoporous SBA-15 type catalysts can be explained by the following statements: (i) On both SBA-15 and

[Al]SBA-15 catalysts, the product is adsorbed in the O-protonated state (signal at -237 ppm), *i.e.* much stronger adsorption of the reaction product on these catalysts, (ii) formation of by-products, such as of amines (signals at -380 ppm) in the case of SBA-15, and the formation of partially-protonated 5-cyano-1-penetene, aniline, and N-protonated ε-caprolactam or ring-opening products of ε-caprolactam on [Al]SBA-15, and (iii) no effect of methanol addition on the above-mentioned species in these catalysts.

8.5 Conclusions

The vapor-phase Beckmann rearrangement of ^{15}N-cyclohexanone oxime on MFI-type zeolites and mesoporous SBA-15 materials in the absence and presence of methanol as an additive was studied by ^{15}N and ^{13}C CP/MAS NMR spectroscopy. It was the aim to clarify the adsorption and reaction behavior of reaction intermediates, products, by-products, and carbonaceous deposits. For this purpose, ^{13}C-methanol was added to the ^{15}N-oxime/silccalite-1, ^{15}N-oxime/H-ZSM-5, ^{15}N-oxime/SBA-15, and ^{15}N-oxime/[Al]SBA-15 mixtures, and, subsequently, the mixtures were heated at reaction temperatures between 393 K to 523 K.

In the case of the vapor-phase Beckmann rearrangement of cyclohexanone oxime on silicalite-1, it was found by *in situ* solid-state ^{15}N NMR spectroscopy, that the presence of methanol in the reaction system increases the selectivity towards ε-caprolactam by decreasing the energy barrier for the product desorption, and no side-reactions leading to the formation of amines occur. Upon loading and heating of ^{15}N-cyclohexanone oxime on H-ZSM-5 in the presence of methanol, water is formed *via* dehydration of methanol into dimethyether. These water molecules promote the conversion of O-protonated ε-caprolactam species into ε-aminocapric acid. In addition, on both silicalite-1 and H-ZSM-5 catalysts, partial conversion of methanol into hydrocarbons, such as isobutane, was observed. Furthermore, by ^{13}C MAS NMR spectroscopy, it was found that isopropylamine is formed on silicalite-1 by the reaction of isobutane and by-products of the Beckmann rearrangement, such as hydroxyl amine. In contrast, no influence and conversion of methanol during the Beckmann rearrangement of ^{15}N-cyclohexanone oxime on the mesoporous SBA-15 and [Al]SBA-15 materials were found.

References

[1] D.H. Everett, Pure Appl. Chem. 31 (1972) 577-638.

[2] K.S.W. Sing, D.H. Everett, R.A.W. Haul, L. Moscou, R.A. Pierotti, J. Rouquerol, T. Siemieniewska, Pure Appl. Chem. 57 (1985) 603-619.

[3] J. Weitkamp, Solid State Ionics 131 (2000) 175-188.

[4] A. Taguchi, F. Schüth, Microporous Mesoporous Mater. 77 (2005) 1-45.

[5] E.M. Flanigen, in: "Introduction to Zeolite Science and Practice", H. van Beckkum, E.M. Flanigen, P.A. Jacobs, J.C. Jansen (Eds.), Elsevier, Amsterdam, 2001, p. 11-35.

[6] M.E. Davis, R.F. Lobo, Chem. Mater. 4 (1992) 756-768.

[7] F. Schwochow, L. Puppe, Angew. Chem. Int. Edn. 14 (1975) 620-628.

[8] R.M. Barrer, J. Chem. Soc. (1948) 2158-2163.

[9] J.-L. Guth, H. Kessler, in: "Catalysis and Zeolites: Fundamentals and Applications", J. Weitkamp, L.Puppe (Eds.), Springer-Verlag, Berlin, Heidelberg, New York, 1999, p. 1-52.

[10] C.S. Cundy, P.A. Cox, Chem. Rev. 103 (2003) 663-701.

[11] C.S. Cundy, P.A. Cox, Microporous Mesoporous Mater. 82 (2005) 1-78.

[12] A. Pfenninger, in: "Molecular Sieves 2 - Science and Technology", H.G. Karge, J. Weitkamp (Eds.), Springer-Verlag, Berlin, Heidelberg, 1999, Vol. 2, p. 163-198.

[13] S.T. Sie in: "Advanced Zeolite Science and Applications", J.C. Jansen, M. Stöcker, H.G. Karge, J. Weitkamp (Eds.), Studies in Surface Science and Catalysis, Vol. 85, Elsevier, Amsterdam, 1994, p. 587-631.

[14] F. Fajula, D. Plee, in: "Advanced Zeolite Science and Applications", J.C. Jansen, M. Stöcker, H.G. Karge, J. Weitkamp (Eds.), Studies in Surface Science and Catalysis, Vol. 85, Elsevier, Amsterdam, 1994, p. 633-650.

[15] M.E. Davis, Science 300 (2003) 438-439.

[16] U. Dingerdissen, A. Martin, D. Herein, H.J. Wernicke, in: "Handbook of Heterogeneous Catalysis", 2nd Edn., G. Ertl, H. Knözinger, F. Schüth, J. Weitkamp (Eds.), WILEY-VCH Verlag, Weinheim, 2008, Vol. 1, p. 37-56.

[17] J.A. Johnson, A.R. Oroskar in: “Zeolites as catalysts, sorbents and detergents builders: Applications and Innovations”, H.G. Karge, J. Weitkamp (Eds.), Studies in Surface Science and Catalysis, Vol. 46, Elsevier, Amsterdam, 1989, p. 451-467.

[18] S.T. Wilson, B.M. Lok, C.A. Messina, T.R. Cannan, E.M. Flanigen, J. Am. Chem. Soc. 104 (1982) 1146-1147.

[19] M.E. Davis, C. Saldarriaga, C. Montes, J. Garces, C. Crowder, Nature 331 (1988) 698-699.

[20] J.A. Martens, M. Mertens, P.J. Grobet, P.A. Jacobs, in: “Innovation in Zeolite Material Science”, P.J. Grobet, W.J. Mortier, E.F. Vansant, G. Schulz-Ekloff (Eds.), Studies in Surface Science and Catalysis, Vol. 37, Elsevier, Amsterdam, 1988, p. 97-105.

[21] J.M. Bennet, B.K. Marcus, in: “Innovation in Zeolite Material Science”, P.J. Grobet, W.J. Mortier, E.F. Vansant, G. Schulz-Ekloff (Eds.), Studies in Surface Science and Catalysis, Vol. 37, Elsevier, Amsterdam, 1988, p. 269-279.

[22] http://www.iza-structure.org/databases/

[23] E.G. Derouane, Z. Gabelica, J. Catal. 65 (1980) 486-489.

[24] E.G. Derouane, J.C. Vedrine, J. Mol. Catal. 8 (1980) 479-483.

[25] L.B. Young, S.A. Butter, W.W. Kaeding, J. Catal. 76 (1982) 418-432.

[26] S.M. Csiscery, Zeolites 4 (1984) 202-213.

[27] G.T. Kokotalio, S.L. Lawton, D.H. Olson, Nature 272 (1978) 437-438.

[28] E.M. Flanigen, J.M. Bennet, R.W. Grose, J.P. Cohen, R.L. Patton, R.M. Kirchner, J.V. Smith, Nature 271 (1978) 512-516.

[29] T. Yanagisawa, T. Shimizu, K. Kuroda, C. Kato, Bull. Chem. Soc. Jpn. 63 (1990) 988-992.

[30] S. Inagaki, Y. Fukushima, K. Kuroda, J. Chem. Soc. Chem. Commun. (1993) 680-682.

[31] S. Inagaki, A. Koiwai, N. Suzuki, Y. Fukushima, K. Kuroda, Bull. Chem. Soc. Jpn. 69 (1996) 1449-1457.

[32] C.T. Kresge, M.E. Leonowicz, W.J. Roth, J.C. Vartuli, J.S. Beck, Nature 359 (1992) 710-712.

[33] J.S. Beck, J.C. Vartuli, W.J. Roth, M.E. Leonowicz, C.T. Kresge, K.D. Schmitt, C.T.-W. Chu, D.H. Olson, E.W. Sheppard, S.B. McCullen, J.B. Higgins, J.L. Schlenker, J. Am. Chem. Soc. 114 (1992) 10834-10843.

[34] Q. Huo, R. Leon, P.M. Petroff, G.D. Stucky, Science 268 (1995) 1324-1327.

[35] D. Zhao, J. Feng, Q. Huo, N. Melosh, G.H. Fredrickson, B.F. Chmelka, G.D. Stucky, Science 279 (1998) 548-552.

[36] D. Zhao, Q. Huo, J. Feng, B.F. Chmelka, G.D. Stucky, J. Am. Chem. Soc. 120 (1998) 6024-6036.

[37] P.T. Tanev, M. Chibwe, T.J. Pinnavaia, Nature 368 (1994) 321-323.

[38] P.T. Tanev, T.J. Pinnavaia, Science 267 (1995) 865-867.

[39] J.Y. Ying, C.P. Mehnert, M.S. Wong, Angew. Chem. Int. Edn. 38 (1999) 56-77.

[40] US Patent, 5 378 440, January 3, 1995, Mobil Oil Corp. (Inv.: J.A. Herbst, C.T. Kresge, D.H. Olson, K.D. Schmitt, J.C. Vartuli, D.C.I. Wang).

[41] US Patent 5 348 687, September 20, 1994, Mobil Oil Corp. (Inv.: J.S. Beck, G.H. Kühl, D.H. Olson, J.L. Schlenker, G.D. Stucky, J.C. Vartuli).

[42] US Patent 5 364 797, November 15, 1994, Mobil Oil Corp. (Inv.: D.H. Olson, G.D. Stucky, J.C. Vartuli).

[43] Y.-J. Han, J.M. Kim, G.D. Stucky, Chem. Mater. 12 (2000) 2068-2069.

[44] D. Zhao, J. Sun, Q. Li, G.D. Stucky, Chem. Mater. 12 (2000) 275-279.

[45] J. Weitkamp, M. Hunger, in: “Introduction to Zeolite Molecular Sieves”, H. van Bekkum, J. Cejka, A. Corma, F. Schüth (Eds.), Studies in Surface Science and Catalysis, Vol. 168, Elsevier, Amsterdam, 2007, p. 787-835.

[46] Y. Izumi, H. Ichihashi, Y. Shimazu, M. Kitamura, H. Sato, Bull. Chem. Soc. Jpn. 80 (2007) 1280-1287.

[47] W.F. Hölderich, J. Röseler, G. Heitmann, A.T. Liebens, Catal. Today 37 (1997) 353-366.

[48] W. Hu, Q. Luo, Y. Su, L. Chen, Y. Yue, C. Ye, F. Deng, Microporous Mesoporous Mater. 92 (2006) 22-30.

[49] H. Koch, A. Liepold, K. Roos, M. Stöcker, W. Reschetilowski, Chem. Eng. Technol. 22 (1999) 807-811.

[50] D. Freude, M. Hunger, H. Pfeifer, Chem. Phys. Lett. 91 (1982) 307-310.

[51] H. Pfeifer, D. Freude, M. Hunger, Zeolites 5 (1985) 274-286.

[52] G. Fisher, Fibers & Texttiles in Eastern Europe 11 (No.1(40)) (2003) 14-15.

[53] S. van der Linde, G. Fisher, Fibers & Texttiles in Eastern Europe 12 (No.1(45)) (2004) 17-18.

[54] Product focus: Caprolactam, Chemical Week, September 21, (2005) p. 45.

[55] Product focus: Caprolactam, Chemical Week, March 7, (2007) p. 26.

[56] E. Beckmann, Ber. 19 (1886) 988-993.

[57] A.H. Blatt, Chem. Rev. 12 (1933) 215-260.

[58] A. Lachman, J. Am. Chem. Soc. 46 (1924) 1477-1483.

[59] J.G. Korsloot, V.G. Keizer, Tetrahedron Lett. 10 (1969) 3517-3520.

[60] Kirk-Othmer, Encyclopedia of Chemical Technology, Vol. 19, 4th Edn., JOHN WILEY & SONS, Inc., New York, 1992, pp. 839.

[61] G. Dahlhoff, J.P.M. Niederer, W.F. Hölderich, Catal. Rev. Sci. Eng. 43 (2001) 381-441.

[62] H. Ichihashi, M. Ishida, A. Shiga. M. Kitamura, T. Suzuki, K. Suenobu, K. Sugita, Catal. Surv. Asia 7 (2003) 261-270.

[63] J. Ritz, H. Fuchs, H. Kieczka, W.C. Moran, in: "Ullmann's Encyclopedia of Industrial Chemistry", 6th Edn., W. Gerhartz, Y.S. Yamamoto, F.T. Campbell, R. Pfefferkorn, J.F. Rounsaville (Eds.), WILEY-VCH Verlag, Weinheim, Vol. A5, p. 31-50.

[64] J. Peng, Y. Deng, Tetrahedron Lett. 42 (2001) 403-405.

[65] B. Wang, Y. Gu, C. Luo, T. Yang, L. Yang, J. Suo, Tetrahedron Lett. 45 (2004) 3369-3372.

[66] S. Guo, Z. Du, S. Zhang, D. Li, Z. Li, Y. Deng, Green Chem. 8 (2006) 296-300.

[67] B. Thomas, U.R. Prabhu, S. Prathapan, S. Sugunan, Microporous Mesoporous Mater. 102 (2007) 138-150.

[68] Z. Tvarlžková, K. Habersberger, N. Žílkova, P. Jiru, Appl. Catal. A: General 79 (1991) 105-114.

[69] A. Thangaraj, S. Sivasanker, P. Ratnasamy, J. Catal. 131 (1991) 394-400.

[70] A. Zechina, G. Spoto, S. Bordiga, F. Geobaldo, G. Petrini, G. Leofanti, M. Padovan, M.A. Mantegazza, P. Rofia, in: "Proceedings of the 10th International

Congress on Catalysis", L. Guczi, F. Solymosi, P. Tétényi (Eds.), Studies in Surface Science and Catalysis, Vol. 75, Part A, Elsevier, Amsterdam, 1993, p. 719-729.

[71] A. Zechina, S. Bordiga, C. Lamberti, G. Ricchiardi, D. Scarano, G. Petrini, G. Leofanti, M.A. Mantegazza, Catal. Today 32 (1996) 97-106.

[72] US Patent 2 234 566, March 11, 1941, E.I. Du Pont de Nemours & Co. Inc., (Inv.: W. Lazier, G. Rigby).

[73] US Patent, 2 634 269, April 7, 1953, (Inv.: D. England).

[74] P.S. Landis, P.B. Venuto, J. Catal. 6 (1966) 245-252.

[75] A. Aucejo, M.C. Burguet, A. Corma, V. Fornes, Appl. Catal. 22 (1986) 187-200.

[76] A. Corma, H. Garcia, J. Primo, Zeolites 11 (1991) 593-597.

[77] L.-X. Dai, K. Koyama, M. Miyamoto, T. Tatsumi, Appl. Catal. A: General 189 (1999) 237-242.

[78] A. Thangaraj, S. Sivasanker, P. Ratnasamy, J. Catal. 137 (1992) 252-256.

[79] H. Sato, N. Ishi, K. Hirose, S. Nakamura, in: "Proceedings of the 7th International Zeolite Conference", Y. Murakami, A. Ijima, J.W. Ward (Eds.), Studies in Surfcae Science and Catalysis, Vol. 28, Elsevier, Amsterdam, 1986, p. 755-762.

[80] H. Sato, K.-i. Hirose, Y. Nakamura, Chem. Lett. 22 (1993) 1765-1766.

[81] H. Sato, K.-i. Hirose, Y. Nakamura, Chem. Lett. 22 (1993) 1987-1990.

[82] T. Yashima, K. Miura, T. Komatsu, in: "Proceedings of the 10th International Zeolite Conference", J. Weitkamp, H.G. Karge, H. Pfeifer, W. Hölderich (Eds.), Studies in Surfcae Science and Catalysis, Vol. 84, Part C, Elsevier, Amsterdam, 1994, p. 1897-1904.

[83] T. Yashima, N. Oka, T. Komatsu, Catal. Today 38 (1997) 249-253.

[84] T. Takahashi, M. Nishi, Y. Tagawa, T. Kai, Microporous Mater. 3 (1995) 467-471.

[85] H. Sato, Catal. Rev. Sci. Eng. 39 (1997) 395-424.

[86] J. Röseler, G. Heitmann, W.F. Hölderich, Appl. Catal. A: General 144 (1996) 319-333.

[87] P. Albers, K. Seibold, T. Haas, G. Prescher, W.F. Hölderich, J. Catal. 176 (1998) 561-568.

[88] G.P. Heitmann, G. Dahlhoff, W.F. Hölderich, J. Catal. 186 (1999) 12-19.

[89] G.P. Heitmann, G. Dahlhoff, J.P.M. Niederer, W.F. Hölderich, J. Catal. 194 (2000) 122-129.

[90] W.F. Hölderich, Catal. Today 62 (2000) 115-130.

[91] H. Ichihashi, H. Sato, Appl. Catal. A: General 221 (2001) 359-366.

[92] H. Kath, R. Gläser, J. Weitkamp, Chem. Eng. Technol. 24 (2001) 150-153.

[93] H. Ichihashi, M. Kitamura, Catal. Today 73 (2002) 23-28.

[94] C. Flego, L. Dalloro, Microporous Mesoporous Mater. 60 (2003) 263-271.

[95] L. Forni, G. Fornasari, C. Lucarelli, A. Katovic, F. Trifirò, C. Perri, J.B. Nagy, Phys. Chem. Chem. Phys. 6 (2004) 1842-1847.

[96] W. Tao, D. Mao, J. Xia, Q. Chen, Y. Hu, Chem. Lett. 34 (2005) 472-473.

[97] Y. Bu, Y. Wang, Y. Zhang, L. Wang, Z. Mi, W. Wu, E. Min, S. Fu, Catal. Commun. 8 (2007) 16-20.

[98] L. Forni, E. Patriarchi, G. Fornasari, F. Trifirò, A. Katovic, G. Giordano, J.B. Nagy, in: "Oxide Based Materials - New sources, novel phases, new applications", A. Gamba, C. Colella, S. Coluccia (Eds.), Studies in Surface Science and Catalysis, Vol. 155, Elsevier, Amsterdam, 2005, p. 281-290.

[99] J.S. Reddy, R. Ravishankar, S. Sivasanker, P. Ratnasamy, Catal. Lett. 11 (1993) 139-140.

[100] P.S. Singh, R. Bandyopadhyay, S.G. Hegde, B.S. Rao, Appl. Catal. A: General 136 (1996) 249-263.

[101] L.-X. Dai, R. Hayasaka, Y. Iwaki, K.A. Koyano, T. Tatsumi, Chem. Commun. 9 (1996) 1071-1072.

[102] M.A. Camblor, A. Corma, H. García, V. Semmer-Herlédan, S. Valencia, J. Catal. 177 (1998) 267-272.

[103] G.P. Heitmann, G. Dahlhoff, W.F. Hölderich, Appl. Catal. A: General 185 (1999) 99-108.

[104] L.-X. Dai, Y. Iwaki, K. Koyama, T. Tatsumi, Appl. Surf. Sci. 121/122 (1997) 335-338.

[105] G. Dahlhoff, U. Barsnick, W.F. Hölderich, Appl. Catal. A: General 210 (2001) 83-95.

[106] R. Anand, R.B. Khomane, B.S. Rao, B.D. Kulkarni, Catal. Lett. 78 (2002) 189-194.

[107] L.-X. Dai, K. Koyama, T. Tatsumi, Catal. Lett. 53 (1998) 211-214.

[108] D. Shouro, Y. Moriya, T. Nakajima, S. Mishima, Appl. Catal. A: General 198 (2000) 275-282.

[109] D. Shouro, Y. Ohya, S. Mishima, T. Nakajima, Appl. Catal. A: General 214 (2001) 59-67.

[110] K. Chaudhari, R. Bal, A.J. Chandwadkar, S. Sivasanker, J. Mol. Catal. A: Chemical 177 (2002) 247-253.

[111] R. Maheswari, K. Shanthi, T. Sivakumar, S. Narayanan, Appl. Catal. A: General 248 (2003) 291-301.

[112] L. Forni, C. Tosi, G. Fornasari, F. Trifirò, A. Vaccari, J.B. Nagy, J. Mol. Catal. A: Chemical 221 (2004) 97-103.

[113] C. Ngamcharussrivichai, P. Wu, T. Tatsumi, J. Catal. 227 (2004) 448-458.

[114] J.-C. Chang, A.-N. Ko, React. Kinet. Catal. Lett. 83 (2004) 283-290.

[115] J.-C. Chang, A.-N. Ko, Catal. Today 97 (2004) 241-247.

[116] T.D. Conesa, J.M. Hidalgo, R. Luque, J.M. Campelo, A.A. Romero, Appl. Catal. A: General 299 (2006) 224-234.

[117] T.D. Conesa, R. Mokaya, Z. Yang, R. Luque, J.M. Campelo, A.A. Romero, J. Catal. 252 (2007) 1-10.

[118] R. Palkovits, C.-M. Yang, S. Olejnik, F. Schüth, J. Catal. 243 (2006) 93-98.

[119] S. Sato, K. Urabe, Y. Izumi, J. Catal. 102 (1986) 99-108.

[120] H. Sato, K. Hirose, M. Kitamura, Y. Nakamura, in: "Proceedings of the 8th International Zeolite Conference**",** P.A. Jacobs, R.A. van Santen (Eds.), Studies in Surface Science and Catalysis, Vol. 49, Part B, Elsevier, Amsterdam, 1989, p. 1213-1222.

[121] W.F. Hölderich, G. Heitmann, Catal. Today 38 (1997) 227-233.

[122] P. O'Sullivan, L. Forni, B. K. Hodnett, Ind. Eng. Chem. Res. 40 (2001) 1471-1475.

[123] M. Ishida, T. Suzuki, H. Ichihashi, A. Shiga, Catal. Today 87 (2003) 187-194.

[124] A.B. Fernández, A. Marinas, T. Blasco, V. Fornés, A. Corma, J. Catal. 243 (2006) 270-277.

[125] A.B. Fernández, I. Lezcano-Gonzalez, M. Boronat, T. Blasco, A. Corma, J. Catal. 249 (2007) 116-119.

[126] Y. Murakami, S. Saeki, K. Ito, Nippon Kagaku Kaishi (1978) 21-26.

[127] M.T. Nguyen, L.G. Vanquickenborne, J. Chem. Soc. Perkin Trans. 2, (1993) 1969-1973.

[128] M.T. Nguyen, G. Raspoet, L.G. Vanquickenborne, J. Chem. Soc. Perkin Trans. 2, (1995) 1791-1795.

[129] M.T. Nguyen, G. Raspoet, L.G. Vanquickenborne, J. Am. Chem. Soc. 119 (1997) 2552-2562.

[130] Y. Shinohara, S. Mae, D. Shouro, T. Nakajima, J. Mol. Struct. 497 (2000) 1-9.

[131] J. Sirijaraensre, T.N. Truong, J. Limtrakul, J. Phys. Chem. B 109 (2005) 12099-12106.

[132] V. Šimunić-Mežnarić, Z. Mihalić, H. Vačik, J. Chem. Soc. Perkin Trans. 2, (2002) 2154-2158.

[133] A.B. Fernández, M. Boronat, T. Blasco, A. Corma, Angew. Chem. Int. Edn. 44 (2005) 2370-2373.

[134] V.R.R. Marthala, Y. Jiang, J. Huang, W. Wang, R. Gläser, M. Hunger, J. Am. Chem. Soc. 128 (2006) 14812-14813.

[135] M. Kitamura, H. Ichihashi, in: "Proceedings of the International Symposium on Acid-Base Catalysis II", H. Hattori, M. Misono, Y. Ono (Eds.), Studies in Surface Science and Catalysis, Vol. 90, Elsevier, Amsterdam, 1994, p. 67-70.

[136] T. Komatsu, T. Maeda, T. Yashima, Microporous Mesoporous Mater. 35-36 (2000) 173-180.

[137] D. Mao, Q. Chen, G. Lu, Appl. Catal. A: General 244 (2003) 273-282.

[138] N. Kob, R.S. Drago, Catal. Lett. 49 (1997) 229-234.

[139] C. Fild, D.F. Shantz, R.F. Lobo, H. Koller, Phys. Chem. Chem. Phys. 2 (2000) 3091-3098.

[140] http://www.iza-online.org/synthesis/default.htm.

[141] S. Wu, Y. Han, Y.-C. Zou, J.-W. Song, L. Zhao, Y. Di, S.-Z. Liu, F.-S. Xiao, Chem. Mater. 16 (2004) 486-492.

[142] Y. Li, W. Zhang, L. Zhang, Q. Yang, Z. Wie, Z. Feng, C. Li, J. Phys. Chem. B 108 (2004) 9739-9744.

[143] K. Chaudhari, T.K. Chandwadkar, S. Sivasanker, J. Catal. 186 (1999) 81-90.

[144] L.B. McCusker, in: "Verified Synthesis of Zeolitic Materials", 2nd Revised Edn., H. Robson, K.P. Lillerud (Eds.), Elsevier, Amsterdam, 2001, p. 47-49.

[145] A. Abragam, "The Principles of Nuclear Magnetism", Oxford University Press, London, 1961, pp. 599.

[146] F.A. Bovey, "Nuclear Magnetic Resonance Spectroscopy", 2nd Edn., Academic Press, San Diego, 1988, pp. 653.

[147] C.P. Slichter, "Principles of Magnetic Resonance", 3rd Edn., Springer-Verlag, Heidelberg, 1996, pp. 655.

[148] M. Hunger, E. Brunner, in: "Molecular Sieves 4 - Science and Technology", H.G. Karge, J. Weitkamp (Eds.), Springer- Verlag, Berlin, Heidelberg, 2004, p. 201-293.

[149] J.M. Thomas, J. Klinowski, Adv. Catal. 33 (1985) 199-374.

[150] J.F. Haw, T. Xu, Adv. Catal. 42 (1998) 115-180.

[151] M. Hunger, W. Wang, Adv. Catal. 50 (2006) 149-225.

[152] S.R. Hartmann, E.L. Hahn, Phys. Rev. 128 (1962) 2042-2053.

[153] M. Hunger, T. Horvath, J. Chem. Soc. Chem. Commun. (1995) 1423-1424.

[154] M. Hunger, M. Seiler, T. Horvath, Catal. Lett. 57 (1999) 199-204.

[155] H. Knicker, P.G. Hatcher, F.J. González-Vila, J. Environ. Qual. 31 (2002) 444-449.

[156] European Patent 0162387, November 27, 1985, BASF AG, (Inv.: W. Hölderich, F. Merger, W.D. Mross, R. Fischer).

[157] V. Sundaramurthy, N. Lingappan, Microporous Mesoporous Mater. 65 (2003) 243-255.

[158] L. Brabec, J. Nováková, L. Kubelková, J. Mol. Catal. 94 (1994) 117-130.

[159] R.A. van Santen, G.J. Kramer, Chem. Rev. 95 (1995) 637-660.

[160] H. Koller, G. Engelhardt, R.A. van Santen, Top. Catal. 9 (1999) 163-180.

[161] J. Sauer, in: "Modelling of Structure and Reactivity in Zeolites", C.R.A. Catlow (Ed.), Academic Press, London, 1992, p. 183.

[162] M.S. Stave, J.B. Nicholas, J. Phys. Chem. 99 (1995) 15046-15061.

[163] C. Fild, H. Eckert, H. Koller, Angew. Chem. Int. Edn. 37 (1998) 2505-2507.

[164] K.F.M.G.J. Scholle, W.S. Veeman, Zeolites 5 (1985) 118-122.

[165] S.A. Axon, J. Klinowski, J. Phys. Chem. 98 (1994) 1929-1932.

[166] S.-J. Hwang, C.-Y. Chen, S.I. Zones, J. Phys. Chem. B 108 (2004) 18535-18546.

[167] H. Koller, C. Fild, R.F. Lobo, Microporous Mesoporous Mater. 79 (2005) 215-224.

[168] H. Meier, in: "Spektroskopische Methoden in der organischen Chemie", M. Hesse, H. Meier, B. Zeeh (Eds.), Georg Thieme Verlag, Stuttgart, New York, 1987, p. 67.

[169] M. Hunger, Solid State Nucl. Magn. Reson. 6 (1996) 1-29.

[170] http://webbook.nist.gov/chemistry.

[171] L.A. Clark, M. Sierka, J. Sauer, J. Am. Chem. Soc. 125 (2003) 2136-2141.

[172] M. Bjørgen, F. Bonino, B. Arstad, S. Kolboe, K-.P. Lillerud, A. Zecchina, S. Bordiga, ChemPhysChem. 6 (2005) 232-235.

[173] T. Tatsumi, in: "Fine Chemicals through Heterogeneous Catalysis", R.A. Sheldon, H. van Bekkum (Eds.), WILEY-VCH Verlag, Weinheim, 2001, p. 185-204.

[174] T. Takahashi, M.N.A. Nasution, T. Kai, Appl. Catal. A: General 210 (2001) 339-344.

[175] T. Takahashi, M. Nakanishi, T. Kai, J. Jpn. Petrol. Inst. 49 (2006) 301-307.

[176] M. Hunger, Catal. Rev. Sci. Eng. 39 (1997) 345-393.

[177] H. Ernst, D. Freude, I. Wolf, Chem. Phys. Lett. 212 (1993) 588-596.

[178] H. Ernst, D. Freude, H. Pfeifer, I. Wolf, in: "Proceedings of the 10th International Zeolite Conference", J. Weitkamp, H.G. Karge, H. Pfeifer, W. Hölderich (Eds.), Studies in Surfcae Science and Catalysis, Vol. 84, Part A, Elsevier, Amsterdam, 1994, p. 381-385.

[179] D. Freude, H. Ernst, I. Wolf, Solid State Nucl. Magn. Reson. 3 (1994) 271-286.

[180] J.M. Kobe, T.J. Gluszak, J.A. Dumesik, T.W. Root, J. Phys. Chem. 99 (1995) 5485-5491.

[181] A.G. Stepanov, T.O. Shegai, M.V. Luzgin, N. Essayem, H. Jobic, J. Phys. Chem. B 107 (2003) 12438-12443.

[182] HNMR predictor & dB 9.0, Advanced Chemistry Development, Inc., Toronto, Ontario, Canada.

[183] T. Bucko, J. Hafner, L. Benco, J. Phys. Chem. A 108 (2004) 11388-11397.

[184] NNMR predictor & dB 9.0, Advanced Chemistry Development, Inc., Toronto, Ontario, Canada.

[185] P.P. Nechaev, Y.U. Moiseev, G.E. Zaikov, T.E. Petrova, Russ. Chem. Bull. 21 (1972) 29-33.

[186] J.M. Rosenholm, T. Czuryszkiewicz, F. Kleitz, J.B. Rosenholm, M. Linden, Langmuir 23 (2007) 4315-4323.

[187] H.R. Kricheldorf, Org. Magn. Reson. 12 (1979) 414-417.

[188] V. Bosáček, R. Klik, F. Genoni, G. Spano, F. Rivetti, F. Figueras, Magn. Reson. Chem. 37 (1999) S135-S141.

[189] W. Wang, A. Buchholz, M. Seiler, M. Hunger, J. Am. Chem. Soc. 125 (2003) 15260-15267.

[190] H.O. Kalinowski, S. Berger, S. Braun, ^{13}C-NMR-Spektroskopie, Georg Thieme Verlag, Stuttgart, New York, 1984, pp. 685.

[191] M. Seiler, U. Schenk, M. Hunger, Catal. Lett. 62 (1999) 139-145.

[192] D. Zeng, J. Yang, J. Wang, J. Xu, Y. Yang, C. Ye, F. Deng, Microporous Mesoporous Mater. 98 (2007) 214-219.

[193] A. Thursfield, M.W. Anderson, J. Dwyer, G.J. Hutchings, D. Lee, J. Chem. Soc., Faraday Trans. 94 (1998) 1119-1122.

[194] C.M. Zicovich-Wilson, A. Corma, J. Phys. Chem. 98 (1994) 10863-10870.

Publications

J. Huang, Y. Jiang, **V.R.R. Marthala**, M. Hunger, *Insight into the mechanisms of the ethylbenzene disproportionation: Transition state shape selectivity on zeolites*, J. Am. Chem. Soc. 130 (2008) 12642-12644.

V.R.R. Marthala, S. Rabl, J. Huang, B. Thomas, M. Hunger, *In situ solid-state NMR investigations of the vapor-phase Beckmann rearrangement of ^{15}N-cyclohexanone oxime on MFI-type zeolites and mesoporous SBA-15 materials in the absence and presence of the additive ^{13}C-methanol*, J. Catal. 257 (2008) 134-141.

J. Huang, Y. Jiang, **V.R.R. Marthala**, Y.S. Ooi, M. Hunger, *Regioselective H/D exchange at the side-chain of ethylbenzene on dealuminated zeolite Y studied by in situ pulsed-flow ^{1}H MAS NMR-UV/Vis spectroscopy*, ChemPhysChem 9 (2008) 1107-1109.

J. Huang, Y. Jiang, **V.R.R. Marthala**, B. Thomas, E. Romanova, M. Hunger, *Characterization and acidic properties of aluminum-exchanged zeolites X and Y*, J. Phys. Chem. C 112 (2008) 3811-3818.

Y. Jiang, J. Huang, **V.R.R. Marthala**, Y.S. Ooi, J. Weitkamp, M. Hunger, *In situ MAS NMR-UV/Vis investigation of H-SAPO-34 catalysts partially coked in the methanol-to-olefin conversion under continuous-flow conditions and of their regeneration*, Microporous Mesoporous Mater. 105 (2007) 132-139.

J. Huang, Y. Jiang, **V.R.R. Marthala**, Y.S. Ooi, J. Weitkamp, M. Hunger, *Concentration and acid strength of hydroxyl groups in zeolites La,Na-X and La,Na-Y with different lanthanum exchange degrees studied by solid-state NMR spectroscopy*, Microporous Mesoporous Mater. 104 (2007) 129-136.

V.R.R. Marthala, W. Wang, J. Jiao, Y. Jiang, J. Huang, M. Hunger, *Effect of probe molecules with different proton affinities on the coordination of boron atoms in dehydrated zeolite H-[B]ZSM-5*, Microporous Mesoporous Mater. 99 (2007) 91-97.

J. Huang, Y. Jiang, **V.R.R. Marthala**, W. Wang, B. Sulikowski, M. Hunger, *In situ ^{1}H MAS NMR investigations of the H/D exchange of alkylaromatic hydrocarbons on zeolites H-Y, La,Na-Y, and H-ZSM-5*, Microporous Mesoporous Mater. 99 (2007) 86-90.

V.R.R. Marthala, Y. Jiang, J. Huang, W. Wang, R. Glaser, M. Hunger, *Beckmann rearrangement of ^{15}N-cyclohexanone oxime on zeolites silicalite-1, H-ZSM-5, and H-[B]ZSM-5 studied by solid-state NMR spectroscopy*, J. Am. Chem. Soc. 128 (2006) 14812-14813.

J. Jiao, J. Kanellopoulos, B. Behera, Y. Jiang, J. Huang, **V.R.R. Marthala**, S.S. Ray, W. Wang, M. Hunger, *Effects of adsorbate molecules on the quadrupolar interaction of framework aluminum atoms in dehydrated zeolite H,Na-Y*, J. Phys. Chem. B 110 (2006) 13812-13818.

Y. Jiang, W. Wang, **V.R.R. Marthala**, J. Huang, B. Sulikowski, M. Hunger, *Effect of organic impurities on the hydrocarbon formation via the decomposition of surface methoxy groups on acidic zeolite catalysts*, J. Catal. 238 (2006) 21-27.

T. Selvam, **V.R.R. Marthala,** R. Hermann, W. Schwieger, N. Pfänder, R. Schlögl, H. Ernst, D. Freude, *Al-rich mesoporous FSM-16 materials: Synthesis, characterization, and catalytic properties*, Stud. Surf. Sci. Catal. 158 (2005) 501-508.

Conference contributions

V.R.R. Marthala, S. Rabl, M. Hunger, *Solid-state NMR studies on the vapor-phase Beckmann rearrangement of ^{15}N-cyclohexanone oxime*, 20. Deutsche Zeolith-Tagung, Halle, Germany, March 5 to 7, 2008, Poster presentation.

V.R.R. Marthala, M. Hunger, *The influence of methanol as an additive in the vapor-phase Beckmann rearrangement on MFI-type zeolites*, INSIDE PORes, 3rd International workshop "New challenges for nanoporous materials", Alicante, Spain, September 24 to 26, 2007, Poster presentation.

S. Rabl, **V.R.R. Marthala**, M. Hunger, *Solid-state NMR investigations on the mechanism of Beckmann rearrangement of ^{15}N-cyclohexanone oxime on mesoporous catalysts*, INSIDE PORes, 3rd International workshop "New challenges for nanoporous materials", Alicante, Spain, September 24 to 26, 2007, Poster presentation.

V.R.R. Marthala, W. Wang, R. Gläser, M. Hunger, *Beckmann rearrangement of ^{15}N-cyclohexanone oxime into ε-caprolactam on silicalite-1, H-ZSM-5, and H-[B]ZSM-5 studied by solid-state NMR spectroscopy*, 40. Jahrestreffen Deutscher Katalytiker, Weimar, Germany, March 14 to 16, 2007, Poster presentation.

V.R.R. Marthala, W. Wang, J. Jiao, M. Hunger, *Coordination transformation of boron atoms in zeolite H-[B]ZSM-5 upon the adsorption of probe molecules studied by solid-state NMR spectroscopy*, First International Workshop on In situ Studies and Development of Processes Involving Nanoporous Solids, La Grande Motte, France, March 19 to 23, 2006, Poster presentation.

Curriculum vitae

Personal details:

Name:	Venkata Ramana Reddy Marthala
Born:	on June 1, 1978, India
Nationality:	Indian
Marital status:	married

Education:

02/2005 – 11/2008	Ph.D. (Chemistry), Institute of Chemical Technology, University of Stuttgart, Stuttgart, Germany.
09/1997 - 07/2004	M.Sc. (Chemical Engineering), Friedrich-Alexander University, Erlangen-Nürnberg, Germany.
09/1997 - 07/2001	B.Tech. (Chemical Engineering), Jawaharlal Nehru Technological University, Hyderabad, India.